



Plains CO₂ Reduction (PCOR) Partnership
Energy & Environmental Research Center (EERC)

REGIONAL SUBSURFACE STRESS ASSESSMENT FOR CO₂ STORAGE IN CANDIDATE BASAL RESERVOIRS IN THE PCOR REGION

Plains CO₂ Reduction (PCOR) Partnership
Subtask 2.1 – Deliverable (D) 11

Prepared for:

AAD Document Control

National Energy Technology Laboratory
U.S. Department of Energy
626 Cochran Mill Road
PO Box 10940, MS 921-107
Pittsburgh, PA 15236-0940

DOE Cooperative Agreement No. DE-FE0031838

Prepared by:

Bret J. Fossum
Thomas H. Jo
Wesley D. Peck

Energy & Environmental Research Center
University of North Dakota
15 North 23rd Street, Stop 9018
Grand Forks, ND 58202-9018

2024-EERC-03-02

November 2023
Revised February 2024
Approved March 2024

EERC DISCLAIMER

LEGAL NOTICE: This research report was prepared by the Energy & Environmental Research Center of the University of North Dakota (UND EERC) as an account of work sponsored by the U.S. Department of Energy (DOE) National Energy Technology Laboratory and the North Dakota Industrial Commission (NDIC) (SPONSORS). To the best of UND EERC's knowledge and belief, this report is true, complete, and accurate; however, because of the research nature of the work performed, neither UND EERC, nor any of their directors, officers, or employees, makes any warranty, express or implied, or assumes any legal liability or responsibility for the use of any information, apparatus, product, method, process, or similar item disclosed or represents that its use would not infringe privately owned rights. Reference herein to any specific commercial product, process, or service by trade name, trademark, manufacturer, or otherwise does not necessarily constitute or imply its endorsement or recommendation by UND EERC. SPONSORS understand and accept that this research report and any associated deliverables are intended for a specific project. Any reuse, extensions, or modifications of the report or any associated deliverables by SPONSORS or others will be at such party's sole risk and without liability or legal exposure to UND EERC or to their directors, officers, and employees.

ACKNOWLEDGMENTS

This material is based upon work supported by DOE's National Energy Technology Laboratory under Award No. DE-FE0031838 and the North Dakota Industrial Commission under Contract Nos. FY20-XCI-226 and G-050-96.

The EERC wishes to thank Plains CO₂ Reduction (PCOR) Partnership member Dr. Craig Schneider of ConocoPhillips for his timely and critical review of this document.

DOE DISCLAIMER

This report was prepared as an account of work sponsored by an agency of the United States Government. Neither the United States Government, nor any agency thereof, nor any of their employees, makes any warranty, express or implied, or assumes any legal liability or responsibility for the accuracy, completeness, or usefulness of any information, apparatus, product, or process disclosed, or represents that its use would not infringe privately owned rights. Reference herein to any specific commercial product, process, or service by trade name, trademark, manufacturer, or otherwise does not necessarily constitute or imply its endorsement, recommendation, or favoring by the United States Government or any agency thereof. The views and opinions of authors expressed herein do not necessarily state or reflect those of the United States Government or any agency thereof.

NDIC DISCLAIMER

LEGAL NOTICE: This research report was prepared by the Energy & Environmental Research Center of the University of North Dakota (UND EERC) as an account of work sponsored by the North Dakota Industrial Commission (NDIC) through the Lignite Research and Oil and Gas Research Programs. To the best of UND EERC's knowledge and belief, this report is true, complete, and accurate; however, because of the research nature of the work performed, neither UND EERC, NDIC, nor any of their directors, officers, or employees makes any warranty, express or implied, or assumes any legal liability or responsibility for the use of any information, apparatus, product, method, process, or similar item disclosed or represents that its use would not infringe privately owned rights. Reference herein to any specific commercial product, process, or service by trade name, trademark, manufacturer, or otherwise does not necessarily constitute or imply its endorsement or recommendation by UND EERC or NDIC. NDIC understands and accepts that this research report and any associated deliverables are intended for a specific project. Any reuse, extensions, or modifications of the report or any associated deliverables by NDIC or others will be at such party's sole risk and without liability or legal exposure to UND EERC or to their directors, officers, and employees.

TABLE OF CONTENTS

LIST OF FIGURES	ii
LIST OF TABLES	v
DEFINITIONS.....	vi
EXECUTIVE SUMMARY	ix
INTRODUCTION AND WORKFLOW	1
AREA OF INTEREST AND STRATIGRAPHY.....	2
SOURCES OF STRESS IN NORTH AMERICA.....	5
MOHR–COULOMB CRITICAL STRESS FAULT HYPOTHESIS	7
A _φ PARAMETER TO DESCRIBE FAULT REGIME.....	11
TECTONIC FRAMEWORK.....	14
BASEMENT FAULTING	20
A _φ FAULT REGIME AND MAXIMUM HORIZONTAL STRESS DIRECTION.....	22
DEPTH TO BASEMENT AND BASAL RESERVOIRS.....	23
BASEMENT STRESS STUDY AREAS	25
INDUSTRY ACTIVITY AND BASEMENT STRESS STUDY AREAS.....	28
PCOR REGION RECENT EARTHQUAKE ACTIVITY	29
GEOMECHANICS ANALYSIS OF PRIMARY STRESS FOCUS AREAS	33
Williston Basin Stress Focus Area	38
Greater Green River Stress Focus Area	42
South Central Alberta Stress Focus Area	46
Northern Cook Inlet Stress Focus Area.....	49
GEOMECHANICS OBSERVATIONS OF SECONDARY STRESS FOCUS AREAS	54
Alberta Central and Alberta South Stress Focus Areas.....	54
Powder River and Wind River Stress Focus Areas.....	54
SITE-SPECIFIC WORKFLOW – GEOMECHANICS ANALYSIS OF FAULTS	55
KEY MESSAGES – CO ₂ STORAGE IN BASAL RESERVOIRS	56
REFERENCES	57
PCOR REGION INDUSTRY CARBON CAPTURE AND STORAGE PROJECTS	Appendix A

LIST OF FIGURES

1	PCOR study area, with major cities, sedimentary basin outlines, and Precambrian basement outcrops	3
2	GSA geologic time scale	4
3	Cross section of the lithosphere and upper asthenosphere depicting three categories of sources of crustal stress	7
4	Faulting regime based on A_{Φ} method vs. North America glacial maximum during last ice age, approximately 18,000 years before present	8
5	Mechanisms for inducing slip on faults due to wastewater injection, hydraulic fracturing operations, or CO ₂ injection	9
6	Slip in basement layer due to pressure transmission along permeable fault zone	10
7	Schematic Mohr circle diagram depicting pressure to slip for three example faults	11
8	Relationship of vertical stress, maximum horizontal stress, and minimum horizontal stress to determine main faulting regime	12
9	Fault styles and corresponding values of A_{Φ}	13
10	PCOR region A_{Φ} map of present-day fault regime and major sedimentary basins	14
11	Basement tectonic domain names and major basement faults within the PCOR region	15
12	Basement tectonic setting and major basement faults within the PCOR region	16
13	Basement tectonic domains, accretion young age in color, ranges of published accretion ages labeled, and major basement faulting within the PCOR study area	18
14	Last orogen age across PCOR study area	19
15	PCOR region age of last orogen and western margin of the North America plate boundary vs. USGS recent earthquake activity with magnitudes greater than M2.5	20
16	Major basement faults and type across PCOR region	21
17	PCOR area A_{Φ} fault regime and maximum horizontal stress direction	23
18	Estimated depth from surface to top basement in feet across the PCOR area, based on Muehlberger in Canada and U.S	24
19	Map of basement stress study areas, sedimentary basin outlines, and distribution of available subsurface stress data	26

LIST OF FIGURES (continued)

20	PCOR region basement stress study areas with CCS facility industry type project locations and major basement faults	27
21	PCOR region earthquake magnitude activity in last 10 years greater than M2.5, major basement faults, and basement stress study areas	29
22	PCOR region earthquake activity in the last 10 years showing estimated epicenter depth	30
23	USGS earthquake Modified Mercalli intensity scale	31
24	Relationships among various scaling parameters for earthquakes	32
25	FSP model areas of interest for the four high-graded stress focus areas and locations of stress data points illustrated in Figure 19	34
26	Williston Basin stress focus area FSP model input faults, stress data, and injection well locations	39
27	Williston Basin deterministic FSP model geomechanical critical stress analysis results ...	39
28	Williston Basin deterministic Mohr–Coulomb analysis of faults	40
29	Williston Basin probability of slip for each fault assuming variability in inputs depicted in Figure 30	40
30	Williston Basin tornado plot of percent variability in base case parameter inputs for geomechanics sensitivity analysis	40
31	Probability distribution of pressure exceedance on all faults due to hydrological factors in blue vs. pressure needed to slip each fault due to geomechanical factors in green after 20 years of CO ₂ injection in the Williston Basin stress focus area	41
32	Greater Green River stress focus area FSP model input faults, stress data, and injection well locations.....	42
33	Greater Green River deterministic FSP model geomechanical critical stress analysis results	43
34	Greater Green River deterministic Mohr–Coulomb analysis of faults.....	43
35	Greater Green River probability of fault slip assuming variability in inputs depicted in Figure 36	44
36	Greater Green River tornado plot showing percent variability in base case parameter inputs for geomechanics sensitivity analysis	44

Continued . . .

LIST OF FIGURES (continued)

37	Probability distribution of pressure exceedance on all faults due to hydrological factors in blue vs. pressure needed to slip each fault due to geomechanical factors in green after 20 years of CO ₂ injection in the Greater Green River stress focus area	44
38	South Central Alberta stress focus area FSP model input faults, stress data, and injection well locations.....	46
39	South Central Alberta deterministic FSP model geomechanical critical stress analysis results	47
40	South Central Alberta deterministic Mohr–Coulomb analysis of faults	47
41	South Central Alberta probability of fault slip assuming variability in inputs depicted in Figure 42	48
42	South Central Alberta tornado plot showing percent variability in base case parameter inputs for geomechanics sensitivity analysis	48
43	Probability distribution of pressure exceedance on all faults due to hydrological factors in blue vs. pressure needed to slip each fault due to geomechanical factors in green after 20 years of CO ₂ injection in the South Central Alberta stress focus area	48
44	Northern Cook Inlet stress focus area FSP model input faults and stress data locations....	50
45	Northern Cook Inlet deterministic FSP model geomechanical critical stress analysis results	51
46	The probability of geomechanical fault slip as a function of pore pressure increases on each fault segment for Case 1 on left and Case 2 on right for the northern Cook Inlet	52
47	Northern Cook Inlet tornado plot showing percent variability in geomechanical base case parameter inputs for sensitivity analysis	52
48	Northern Cook Inlet probability distribution of pressure exceedance for faults after 30 years of CO ₂ injection due to hydrological factors	53

LIST OF TABLES

1	Regional Stratigraphic Correlation Charts Applicable to PCOR Region	5
2	Main Sources of Subsurface Stress Across PCOR Study Area	6
3	Stratigraphically Deepest Candidate CO ₂ Storage Reservoir Formation and Age Overlying Basement and Approximate Maximum Depth to Basement or Sediment Fill for Major Basins Within PCOR Area	25
4	Summary of Basement Stress Study Areas Depicted in Figure 19	28
5	Summarized FSP Base Case Input Data for Modeled Stress Focus Areas	36
6	FSP Model Base Case Input Data Sensitivity Analysis Variable Range in Percent	37
7	Williston Basin FSP Stress Focus Area Geomechanical Model Sensitivity Analysis Results by Sorted Rank	40
8	Greater Green River Stress Focus Area FSP Geomechanical Model Sensitivity Analysis Results by Sorted Rank	45
9	South Central Alberta Stress Focus Area FSP Geomechanical Model Sensitivity Analysis Results by Sorted Rank	49

DEFINITIONS

Allostratigraphic – The packaging of rocks bounded by stratigraphic discontinuities within a time-stratigraphic framework.

A ϕ parameter – Value that represents the relative magnitude of the principal stresses (SHmax, Shmin, and Sv) and is used to show the relative direction of slip on a fault.

Asthenosphere – The upper layer of the earth's mantle below the lithosphere, which is weak and in which isostatic adjustments take place, magma may be generated, and seismic waves are strongly attenuated.

Basal reservoir – Candidate CO₂ injection zone that lies directly over basement.

Basal traction – Convection in the mantle leads to basal traction or basal drag of the lithosphere over the asthenosphere. This is one of the primary forces of plate tectonics, the other two being ridge push or convergent and slab pull or divergent.

Compressibility – The capacity of something to be flattened or reduced in size by pressure.

Critical stress analysis – A geomechanical methodology to determine the differential stress (pressure) or pore pressure change required to cause slip on a fault in response to CO₂ injection into a storage reservoir.

Deterministic – A model or result based on one set of assumptions and data.

Earthquake moment magnitude – Estimation of total energy released by an earthquake event; abbreviated “Mw.” In this document, “Mw” and “M” are used interchangeably.

Effective stress – Defined as the total subsurface stress minus the pore pressure.

Fault cohesion – The innate shear strength of a fault that is independent of friction. Mineralization along a fault plane can provide cohesive strength. Movement along a fault will occur when the shear stress on a fault exceeds the fault cohesion.

Friction angle – A measurement to determine the shear strength of a rock material; used in calibration of the mechanical earth model.

Glacial maximum – Refers to the North America Laurentide ice sheet that was present during the Pleistocene Epoch. The glacial maximum or southernmost extent of the ice sheet occurred approximately 18,000 years before present (B.P.).

Lithosphere – The rigid outer part of the earth, consisting of the crust and upper mantle.

Lithostratigraphic – Classification of bodies of rocks based on the lithological properties of the strata and their relative stratigraphic positions.

Mohr–Coulomb failure theory – A set of linear equations that describe how an isotropic material will exhibit shear failure in response to principal stresses, e.g., vertical overburden stress (S_v), maximum horizontal stress (SH_{max}), and minimum horizontal stress (SH_{min}).

Neotectonics – Recent tectonic activity due to natural factors.

Normal (extensional) fault regime – Vertical stress (S_v) > maximum horizontal stress (SH_{max}) > minimum horizontal stress (SH_{min}).

Plane of weakness – Synonym for fault.

Poisson's ratio – An elastic constant that is a measure of the compressibility of material perpendicular to applied stress. Poisson's ratio is symbolized by ν . The static (vs. dynamic) value is required for MEM calibration and characterization of rock strength, e.g., lower Poisson's ratio values indicate the material is more resistant to deformation and is stronger.

Pore pressure – The pressure of fluids within the pores of a reservoir. Normal pore pressure is the pressure exerted by a column of water from sea level to the formation's depth (hydrostatic pressure). Pore pressures above or below normal pressure are referred to as overpressure or underpressure, respectively.

Probabilistic – A statistical approach that uses the effect of random occurrences or actions to forecast a range of future occurrences, foundation of sensitivity analysis.

Sediment fill – Thickness of sediment fill is measured from surface to top of basement.

SH_{max} – Maximum horizontal stress, perpendicular to vertical stress.

SH_{min} – Minimum horizontal stress, perpendicular to vertical stress.

Stress – The force applied to a body that can result in deformation or strain, usually described in terms of magnitude per unit of area or intensity. Stress is characterized vertically and horizontally.

Stress focus area – Study area where more detailed evaluation of subsurface stress was carried out in the PCOR study area.

Stress tensor – Relative dominant stress direction of a geological area, e.g., vertical vs. maximum horizontal vs. minimum horizontal stress.

Strike slip fault regime – Maximum horizontal stress (SH_{max}) > vertical stress (S_v) > minimum horizontal stress (SH_{min}).

S_v – Vertical stress.

Tectonic domain or terrane – A mappable region of the earth with a similar tectonic history and/or tectonic type, e.g., rift, craton, foredeep, etc.

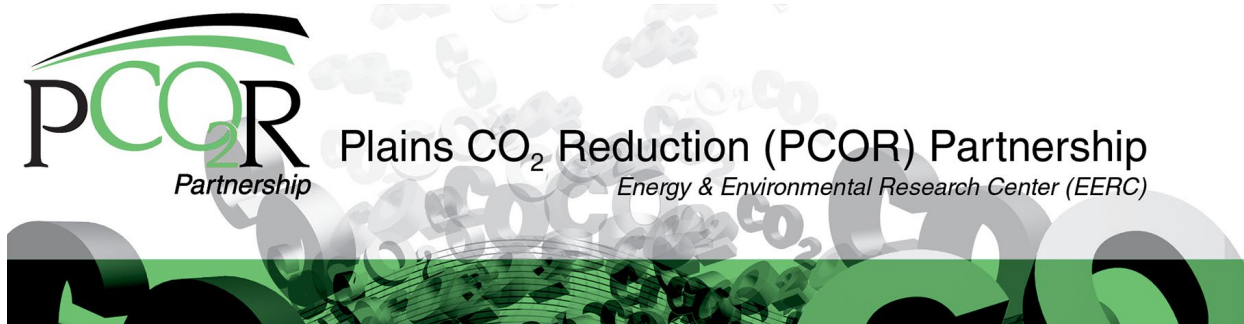
Thrust fault regime – Maximum horizontal stress (S_{Hmax}) > minimum horizontal stress (S_{Hmin}) > vertical stress (S_v).

Unconfined compressive strength – The maximum axial compressive strength that a cylindrical core sample can bear before failure under zero confining (around the core) stress; used in calibration of the MEM.

Vertical stress – Combined stress on the earth due to the total weight of rock and fluids above a specific depth.

Viscosity – A quantity reflecting the magnitude of internal friction of a fluid.

Young's modulus – An elastic constant that is the ratio of longitudinal stress to longitudinal strain and is symbolized by E. The static (vs. dynamic) value is required for MEM calibration and characterization of rock strength, e.g., higher Young's modulus values indicate a stronger, more brittle material vs. a material that is more ductile.



REGIONAL SUBSURFACE STRESS ASSESSMENT FOR CO₂ STORAGE IN CANDIDATE BASAL RESERVOIRS IN THE PCOR REGION

EXECUTIVE SUMMARY

The Plains CO₂ Reduction (PCOR) Partnership Initiative, funded by the U.S. Department of Energy's (DOE) National Energy Technology Laboratory (NETL), the North Dakota Industrial Commission's Oil and Gas Research Program and Lignite Research Program, and more than 250 public and private partners, is accelerating the deployment of carbon capture, utilization, and storage (CCUS) technology. The PCOR Partnership (hereinafter "PCOR") is focused on a region comprising ten U.S. states and four Canadian provinces in the upper Great Plains and northwestern regions of North America and is led by the University of North Dakota Energy & Environmental Research Center (EERC), with support from the University of Wyoming and the University of Alaska Fairbanks.

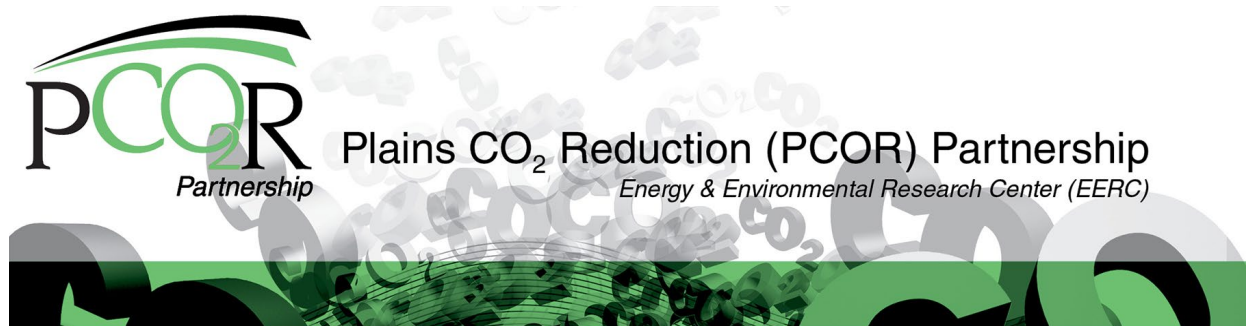
A screening-level regional evaluation of basement and mechanical overburden stress across the geologically diverse PCOR region was carried out by the EERC. The main objective of the project was to assess potential basement fault reactivation and to better understand technical uncertainties pertaining to carbon dioxide (CO₂) storage in candidate basal reservoirs.

The tectonic framework, tectonic history, and associated main basement faulting were characterized along with present-day stress regime and dominant maximum horizontal stress across the study area. Tectonic or plate-level to subregional or local sources of subsurface stress have been summarized and captured. Basal reservoirs situated directly above basement have been identified and used in geomechanics modeling. The estimated depth to basement from surface has been characterized and mapped to determine potential maximum CO₂ storage depths in each of the main sedimentary basins across the PCOR region and to screen out basins that are too shallow for storage of CO₂ because of the lack of subsurface conditions supporting the occurrence of supercritical CO₂ fluids. Recent "felt" earthquake activity (greater than magnitude 2.5) in the past 10 years has been characterized and integrated to determine the relationship to PCOR tectonic history and structural framework and to determine areas that have a higher or lower risk profile of natural earthquakes or induced seismicity activity.

Eight "stress focus areas" were identified across the PCOR study area based on elevated industry carbon capture and storage (CCS) activity, presence of basement faulting, and availability of subsurface stress and reservoir characterization data to carry out screening-level geomechanics analyses. Based on the availability of subsurface stress and reservoir characterization calibration

data, a deterministic and probabilistic critical stress analysis of published basement faults assuming storage of injected CO₂ in a basal reservoir was carried out in four of the eight stress focus areas using geomechanical and hydrological criteria and regional calibration data that were adapted for use in the modeling. The critical stress geomechanics analysis models were completed in active and emerging CCS areas across the PCOR region within the Alberta Basin (Canada), Williston Basin (North Dakota, USA), Greater Green River Basin (Wyoming, USA), and Cook Inlet (Alaska, USA).

Key conclusions include that faulting and fracturing associated with reactivated basement faults in tectonically active regions can occur in basal reservoirs, particularly the geomechanically stronger intervals, leading to a higher risk of fault slippage and related induced seismicity in response to fluid injection (CO₂, produced water disposal, fracture fluids, etc.). Thermally induced subsurface stress in response to CO₂ injection was not considered in this study because of the lack of calibration data and coupled flow modeling resources; however, it is generally agreed in the literature that lower-temperature CO₂ injected into a storage reservoir reduces fracture gradient, hence potentially reducing storage capacity. This is an active, developing, and complex area of research within industry and academia. Additionally, a scalable and integrated site-specific structural interpretation and geomechanics workflow to characterize and carry out a critical stress analysis of identified faults and associated fractures has been captured.



REGIONAL SUBSURFACE STRESS ASSESSMENT FOR CO₂ STORAGE IN CANDIDATE BASAL RESERVOIRS IN THE PCOR REGION

INTRODUCTION AND WORKFLOW

The Plains CO₂ Reduction (PCOR) Partnership, funded by the U.S. Department of Energy's (DOE) National Energy Technology Laboratory (NETL), the North Dakota Industrial Commission's Oil and Gas Research Program and Lignite Research Program, and more than 250 public and private partners, is accelerating the deployment of carbon capture, utilization, and storage (CCUS) technology. The PCOR Partnership (hereinafter "PCOR") is focused on a region comprising ten U.S. states and four Canadian provinces in the upper Great Plains and northwestern regions of North America and is led by the University of North Dakota Energy & Environmental Research Center (EERC), with support from the University of Wyoming and the University of Alaska Fairbanks.

A screening-level regional evaluation of basement and mechanical overburden stress across the geologically diverse PCOR region was carried out by the EERC. The main objective of the project was to assess potential for carbon dioxide (CO₂) storage in candidate basal reservoirs by characterizing the likelihood of basement fault reactivation technical uncertainties.

The following workflow was carried out to achieve the objectives of the project, and corresponding observations, results, and path forward recommendations are documented in this report:

1. Review, capture, and integrate public studies, literature, and associated data.
2. Develop and capture key project elements in an ArcGIS project along with robust data and information attribution for map elements.
3. Map published basement terranes and basement domains and integrate with basement faulting.
4. Consider the impact of published accretion ages and most recent orogenic activity of tectonic domains on stress regimes and basement faulting.
5. Identify basement-rooted faults based on available literature and spatial data resources.
6. Map published present-day stress field and maximum horizontal stress direction. Consider U.S. Geological Survey (USGS) earthquake data greater than magnitude (M) 2.5 for the past ~10 years; consider the more recent and shallow events potentially related to induced or triggered seismicity.

7. Develop and apply criteria to select representative stress focus areas within the PCOR region for more detailed critical stress analysis of basement faults using Mohr–Coulomb fault theory. The publicly available Stanford University Fault Slip Potential (FSP) screening tool was used.
8. Characterize the likelihood of fault slip in response to pore pressure increases, stress conditions, and fault regime, with the assumption that Mohr–Coulomb fault theory is the main control of fault slippage.
9. Use results to develop a site-specific workflow to evaluate the risk of critically stressed faults.
10. Summarize main learnings and path forward recommendations.

AREA OF INTEREST AND STRATIGRAPHY

The PCOR study area includes ten U.S. states and four Canadian provinces (Figure 1) and encompasses ~2.4 million square miles. The PCOR region extends from Alaska in the north through central and western Canada and into the north central United States. The geologically diverse area encompasses ~55 sedimentary basins greater than 1000 square miles, ranging from divergent to convergent tectonic history and outside of the sedimentary basins, exhibits outcrops of Precambrian basement based on the geologic map of North America (GMNA) (Garritty and Soller, 2005). Sedimentary fill for each basin across the PCOR region varies widely as well, with maximum sedimentary fill from surface to basement ranging from ~800 to 25,000 feet while representing geological ages from Holocene to Cambrian.

The most recent (v. 6.0) Geological Society of America (GSA) geologic time scale (Figure 2, Walker and Geissman, 2022) was selected to represent the regional stratigraphy across the region. Additionally, basin-specific stratigraphy and formation names can be found in the series of American Association of Petroleum Geologists COSUNA (Correlation of Stratigraphic Units of North America) correlation charts for the Lower 48 and Alaska, and the Canadian Society of Petroleum Geologists and Alberta Research Council Western Canada Sedimentary Basin atlas for Canada. The pertinent regional stratigraphic correlation charts applicable to the PCOR region are listed in Table 1. Both the COSUNA and Western Canada Sedimentary Basin¹ stratigraphic charts were constructed mainly using a lithostratigraphic and allostratigraphic framework, and formation names and stratigraphic equivalents represented on the charts are largely still applicable. Although these stratigraphic frameworks may not capture local details within each basin, we feel it is accurate for the purposes of this study.

¹ The Western Canada Sedimentary Basin is also referred to as the Alberta Basin in the literature.

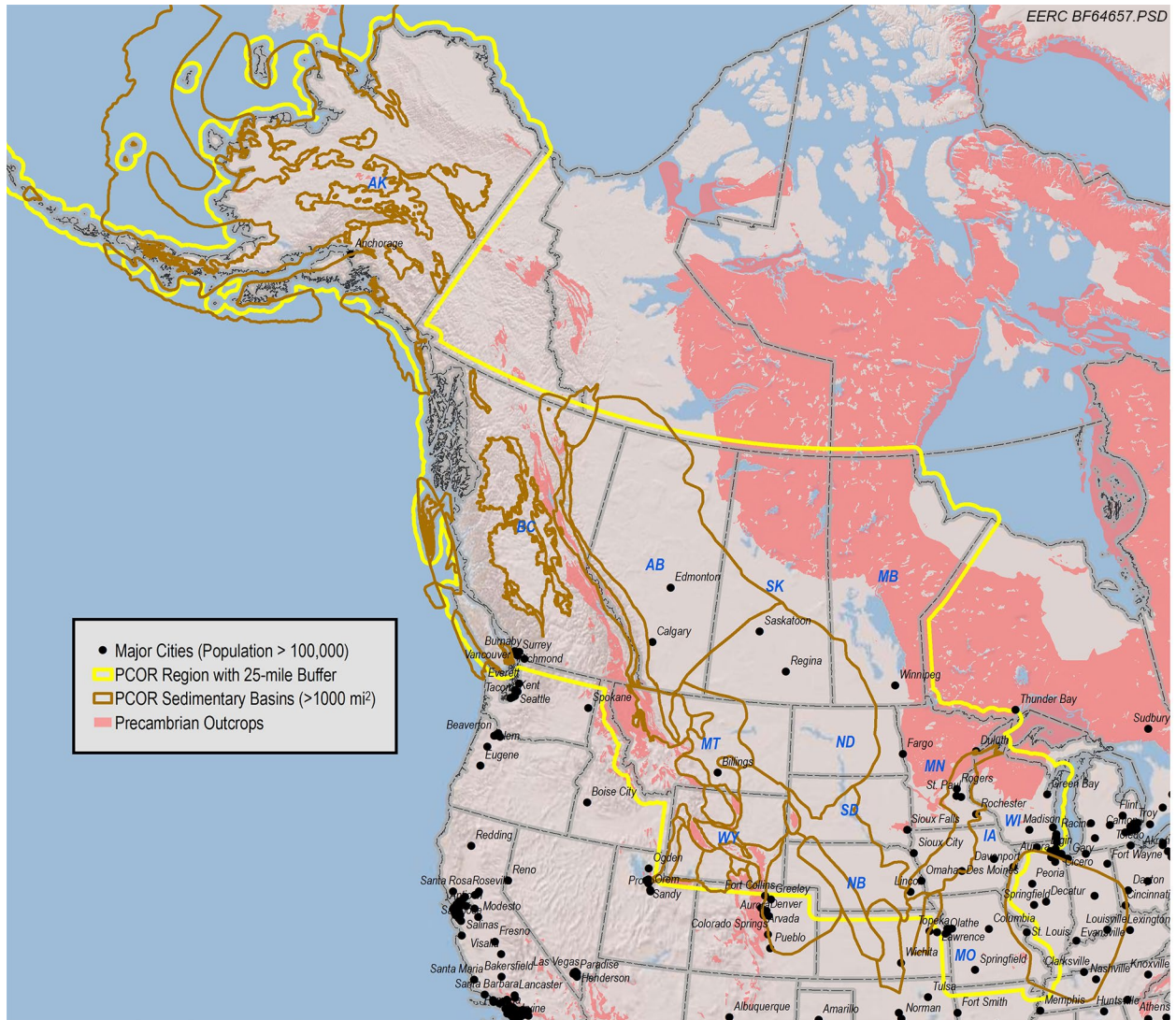


Figure 1. PCOR study area (yellow outline), with major cities, sedimentary basin outlines, and Precambrian basement outcrops (Garrity and Soller, 2005).

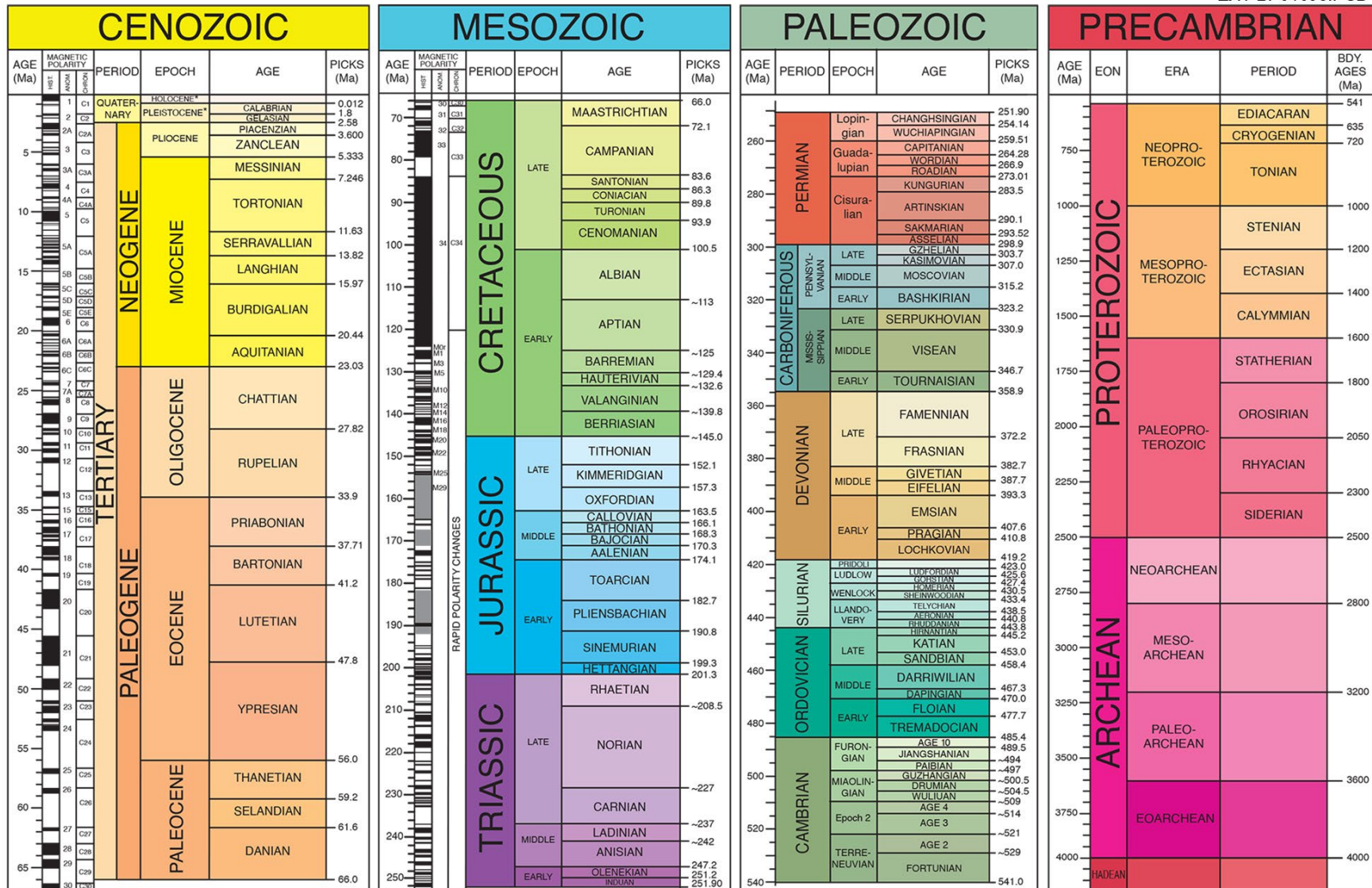


Figure 2. GSA geologic time scale (Walker and Geissman, 2022).

Table 1. Regional Stratigraphic Correlation Charts Applicable to PCOR Region

Region	Regional Coordinators and Year Published
Lower 48 Mid-Continent	Adler (1987)
Lower 48 Northern Rockies and Williston Basin	Ballard and others (1983)
Lower 48 Northern Mid-Continent	Bergstrom and others (1985)
Lower 48 Midwestern Basins and Arches	Shaver (1985)
Lower 48 Central and Southern Rockies	Kent and others (1988)
Northern Alaska	Schaff and Gilbert (1987)
Southern Alaska	Schaff and Gilbert (1987)
Western and Central Canada	Mossop and Shetsen (1994)

SOURCES OF STRESS IN NORTH AMERICA

Sources of stress across the PCOR region can be considered at two levels of scale – regional/tectonic plate scale and local scale (Lund-Snee, 2020). Regional and plate level and local sources of stress considered in the study are captured in Table 2.

Regional and plate-level sources of stress in North America are depicted in Figures 3 and 4 and detailed in Table 2. Figure 3 is a diagram showing the three general sources of plate/regional stress: plate boundary interactions, gravitational potential energy, and basal tractions. Although beyond the scope of this project, it is still important to illustrate these large-scale impacts on stress in the subsurface. Figure 4 illustrates the last glacial maximum (University of Koeln, 2022) versus faulting regime (Lund-Snee and Zoback, 2020) in the North America and PCOR region. It should be noted that the elevated stresses exist north of the Laurentide glacial maximum, where higher $A\phi$ (discussed later in this document) values associated with reverse and strike-slip faulting regimes are dominant, versus south of the glacial maximum, where normal fault regimes are dominant. Because of the relatively short period of geologic time since the Laurentide ice sheets have melted, there appears to be a strong correlation between the location of the glacial maximum and residual regional stress. Additionally, the stress change may also be related to the proximity to the transtensional North America versus Pacific plate margin (Table 2). Characterization of fault stability, or the likelihood of fault reactivation due to pore pressure changes associated with CO₂ injection, requires an understanding of the present-day stress regime as well as the geometry and orientation of faults.

Table 2. Main Sources of Subsurface Stress Across PCOR Study Area (adapted from Lund-Snee, 2020)

Scale	Category	Mechanism	Effect	Source
Regional/ Tectonic Plates	Plate interactions	Ridge push	Compression perpendicular to ridge.	Orowan (1964) Jacoby (1970) Richardson (1992)
		Subduction zone convergence	Orientations and magnitudes vary systematically inboard.	Nakamura and Uyeda (1980)
		Boundary shear traction	Rotates SHmax and can apply compression or extension.	
	Surface loading or unloading	Glacial rebound	Compressive outside former margin and extensional within.	Stein and others (1979, 1989) Stewart and others (2000)
		Sedimentary or glacial loading	Compressive under load, extensional at margins.	Stein and others (1979) Nunn (1985)
Sub- Regional/ Local	Elevated pore pressure in sedimentary basins	Decrease in differential stress over a volume	More isotropic principal stress, which aids in rotation of SHmax and changes in faulting regime for a given applied force.	Jaeger and others (2009)
		Increase or decrease in pore pressure restricted to one side of a fault	SHmax rotation and change in magnitude.	Zoback (2010)
	Recent, large-magnitude fault slip		Transient change in SHmax orientations and relative magnitudes, including possibility of 90-degree rotation.	Castillo and Zoback (1994)

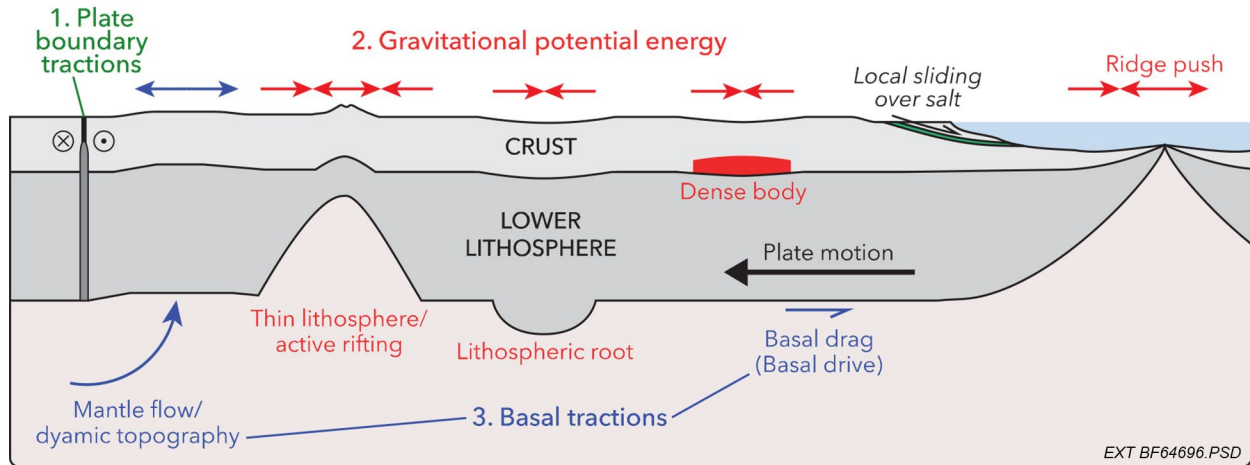


Figure 3. Cross section of the lithosphere and upper asthenosphere depicting three categories of sources of crustal stress (Lund-Snee, 2020). Inward-pointing arrows indicate superimposed upper crustal compression and outward-pointing arrows represent extension. Table 2 provides additional details and sources.

MOHR-COULOMB CRITICAL STRESS FAULT HYPOTHESIS

Faults that intersect a CO₂ injection zone (Figure 5) or the upper or lower confining zone have the potential to slip and leak in response to increases in pore pressure resulting from CO₂ injection. The Mohr–Coulomb theory of fault failure states that faults slip when the shear stress acting on a fault exceeds the effective normal stress, or the stress acting perpendicular to the fault, times the coefficient of internal friction plus the cohesion of the fault (Zoback, 2010). Injection of CO₂ can increase the pore pressure thus reducing the effective normal stress acting on a fault allowing the fault to move. The shear and normal stresses acting on a fault depends upon the orientation of the fault to the maximum horizontal stresses. A fault that is optimally oriented, such that very little or no pore pressure is required to cause the fault to move is called a critically stressed fault. Later in this document, various PCOR stress study areas are identified based on elevated CO₂ storage industry activity, presence of basement faults, and availability of stress and pore pressure data. Depending on data availability, basement faults within the stress study areas were evaluated using Mohr–Coulomb fault theory, while other stress study areas are only discussed in the context of regional geology and stress.

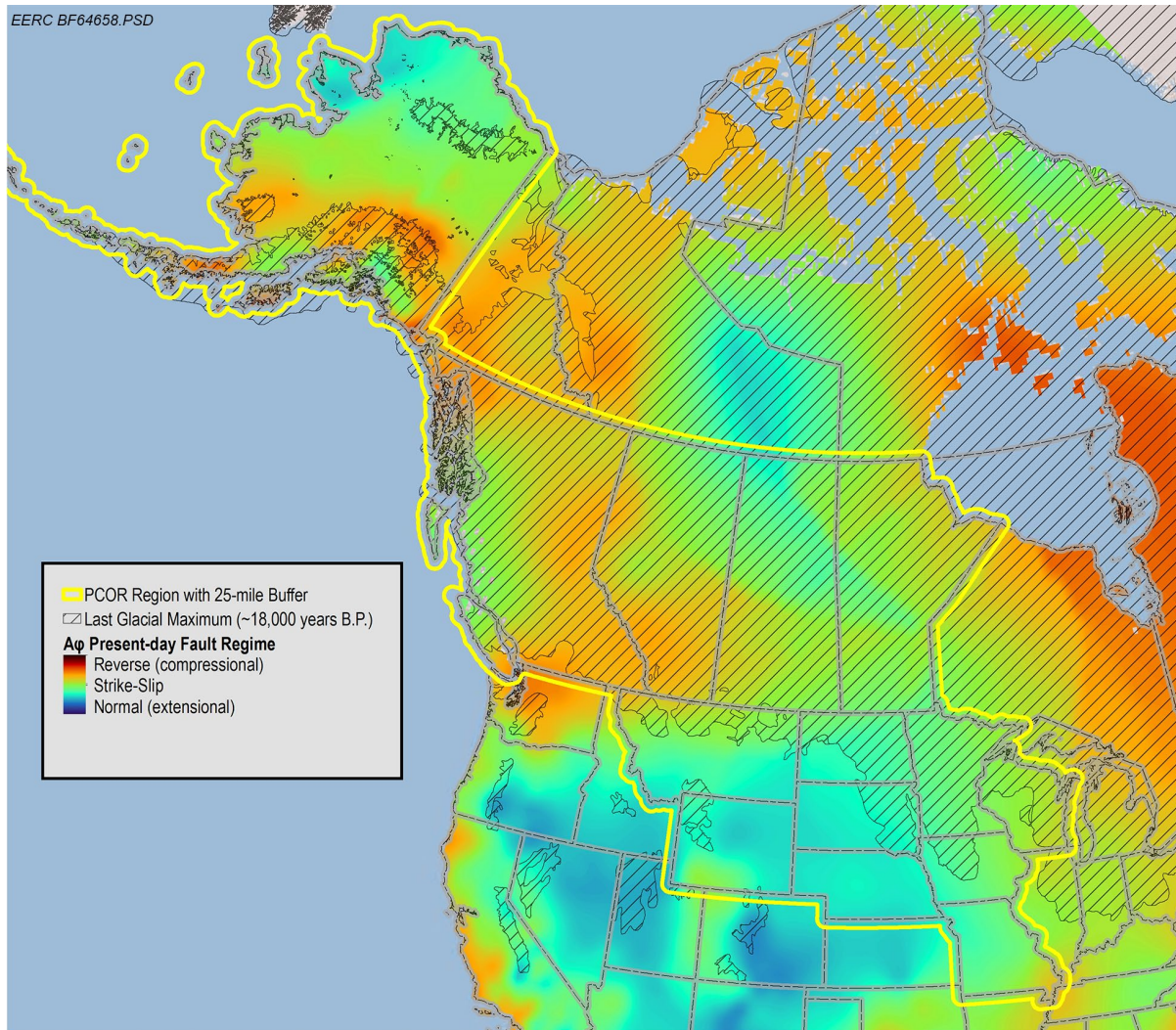


Figure 4. Faulting regime (Lund-Snee and Zoback, 2020) based on $A\phi$ method vs. North America glacial maximum during last ice age, approximately 18,000 years before present (B.P.), (University of Koeln, 2022).

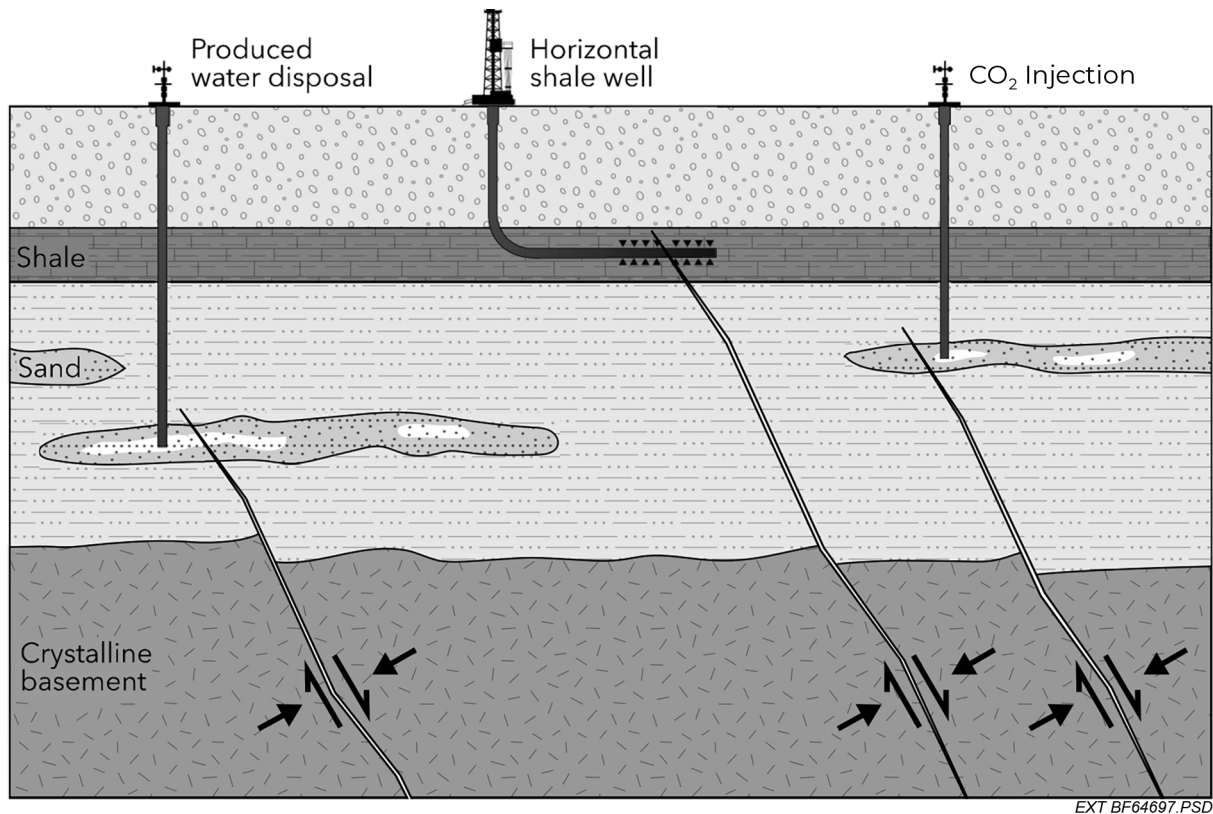


Figure 5. Mechanisms for inducing slip on faults due to wastewater injection, hydraulic fracturing operations, or CO₂ injection (modified from Lund-Snee [2020] based on an original by Southwest Energy).

When available data allowed, Mohr–Coulomb-based critical stress analysis of faults in stress study areas was carried out using the Stanford University FSP screening tool (v2) (Walsh and others, 2018). The FSP tool allows for screening-level analysis to identify faults that might be prone to slip using a deterministic method, followed by a sensitivity analysis and probability approach. Heterogeneities in fault geometries, resolved stresses, pore pressure, and material properties at fine scales are not considered. Specifically, the FSP tool calculates the probability that planar fault segments will be critically stressed within the ambient stress field at a specified or modeled pore pressure (Lund-Snee, 2020). The FSP tool uses a linearized Mohr–Coulomb failure criterion for faults within the specified stress field and pore pressure conditions, with critically stressed conditions occurring when the ratio of resolved shear stress to normal stress reaches or exceeds the failure envelope. In practice, uncertainties are associated with all input parameters, including fault strike and dip, ambient stress field, fault properties, and initial fluid pressure. Hence, the probabilistic geomechanics function in the FSP program is utilized, which is made by a Monte Carlo-type analysis to randomly sample values of each input parameter from specified, uniform uncertainty distributions (Lund-Snee, 2020).

The FSP program is based on Mohr–Coulomb fault theory, where pore pressure increase in an injection layer leads to changes in vertical and horizontal stresses in that layer. However, for the low-permeability basement layer, pressure changes and associated effective stress changes are

limited primarily to the fault zone because of minimal permeability outside of the fault zone, preventing fluid flow. The pressure increases in the fault zone reduces effective normal stress in the fault plane, which makes slip more likely (Walsh and others [2018]; Figure 6).

To carry out the analyses using the FSP tool, the Mohr circle diagram based on vertical and horizontal stresses is plotted and location of the stress state of each fault plane is plotted on the diagram. Figure 7 provides an example, where three faults are plotted (red, orange, and green). As pore pressure increases because of injection, the effective stresses decrease and the Mohr circles move to the left on the plot toward the frictional slip line (in this example, the same friction coefficient is used for all faults). Hence, the horizontal distance from fault stress state point to frictional slip line indicates the pore pressure to slip for that fault, as depicted in Figure 7. It should be noted that this predicted pressure corresponds to the pressure to slip for the basement seismicity scenario; the pressure to slip in the injection layer itself is generally higher (for normal and strike-slip faulting regimes) because of effective stress changes in that layer leading to changes in sizes of Mohr circle due to Poisson's ratio effect. Consequently, the FSP tool focuses on the conservative (lower) pressure to slip estimate corresponding to slip in basement (Walsh and others, 2018).

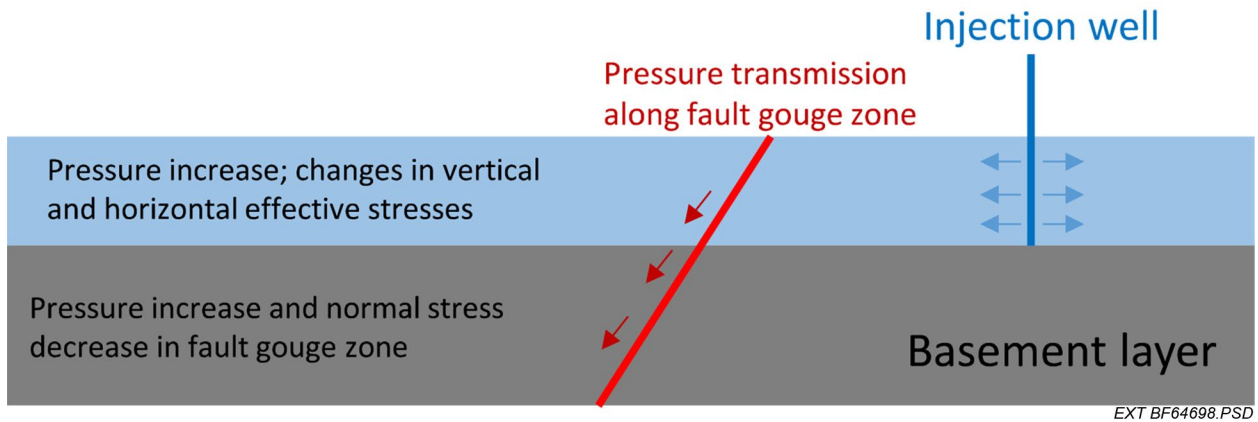


Figure 6. Slip in basement layer due to pressure transmission along permeable fault zone.

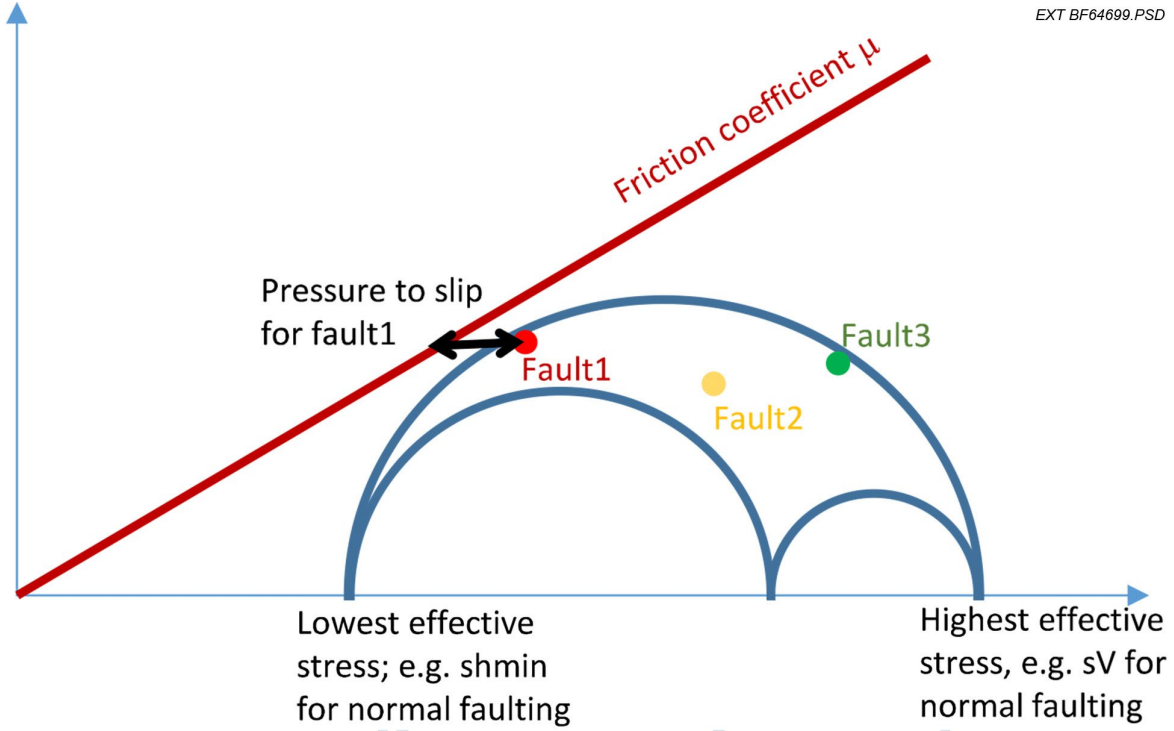


Figure 7. Schematic Mohr circle diagram depicting pressure to slip for three example faults. The red Fault 1 requires a lower pressure increase to slip versus Faults 2 or 3.

A_φ PARAMETER TO DESCRIBE FAULT REGIME

The state of stress at any location can be simply described by the orientations and magnitudes of three mutually perpendicular principal stresses (Lund-Snee and Zoback, 2022). It is convenient to represent the stress field in terms of the three principal stresses (Figure 8), which are generally horizontal and vertical in the earth's brittle upper crust (Anderson, 1951) (Figure 3). Several studies have confirmed this assumption (Zoback and Zoback, 1980, 1989; Zoback, 1992; Peska and Zoback, 1995; Heidbach and others, 2018; Lund-Snee and Zoback, 2018, 2020; Lund-Snee, 2020).

As originally depicted by Anderson (1951), the style of faulting active in an area is determined by the relative magnitudes of the principal stresses. Normal (extensional) faulting occurs when S_v (vertical stress) $>$ S_{Hmax} (maximum horizontal stress) $>$ S_{Hmin} (minimum horizontal stress), strike-slip faulting occurs when $S_{Hmax} > S_v > S_{Hmin}$, and reverse (compressional) faulting occurs when $S_{Hmax} > S_{Hmin} > S_v$. Because the relative magnitude of three values cannot be expressed using a simple ratio, Simpson (1997) developed the A_ϕ calculation to express their relationship (Equation 1):

$$A_\phi = (n + 0.5) + (-1)^n (\phi - 0.5) \quad [\text{Eq. 1}]$$

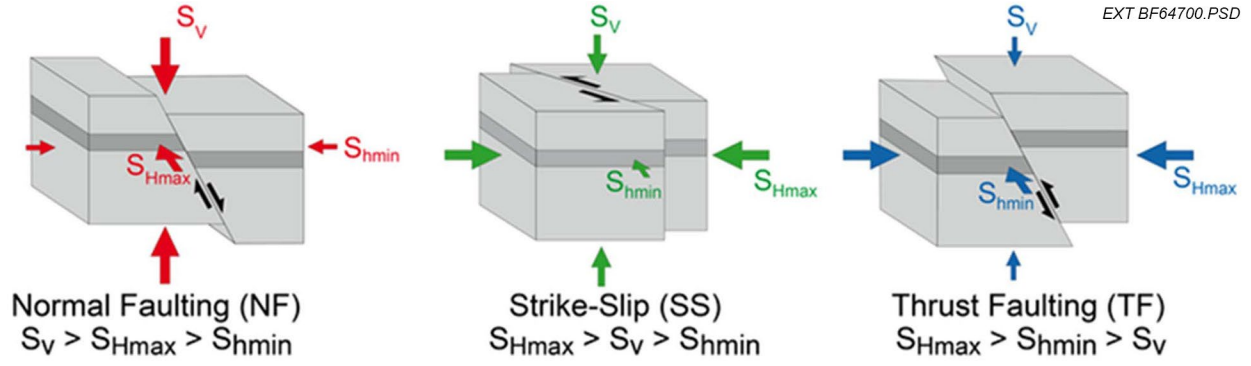


Figure 8. Relationship of vertical stress, maximum horizontal stress, and minimum horizontal stress to determine main faulting regime (Anderson, 1951).

The shape parameter calculation conveys relative magnitudes of stress tensors (Equation 2), where:

$$\phi = \frac{S_2 - S_3}{S_1 - S_3} \quad [\text{Eq. 2}]$$

and where S_1 , S_2 , and S_3 are the maximum, intermediate, and minimum principal stresses, respectively, with $n = 0$ for normal (extensional) faulting, $n = 1$ for strike-slip faulting, and $n = 2$ for reverse (compressional) faulting. The ϕ parameter, which ranges between 0 and 1, was originally defined by Angelier (1979) to indicate the relative magnitude of S_2 with respect to S_1 and S_3 . Its value controls the relative direction of slip on a given fault (Lund-Snee and Zoback, 2020).

Figure 9 depicts the styles of faulting that can be active in the earth and their corresponding values of A_ϕ (Lund-Snee and Zoback, 2018).

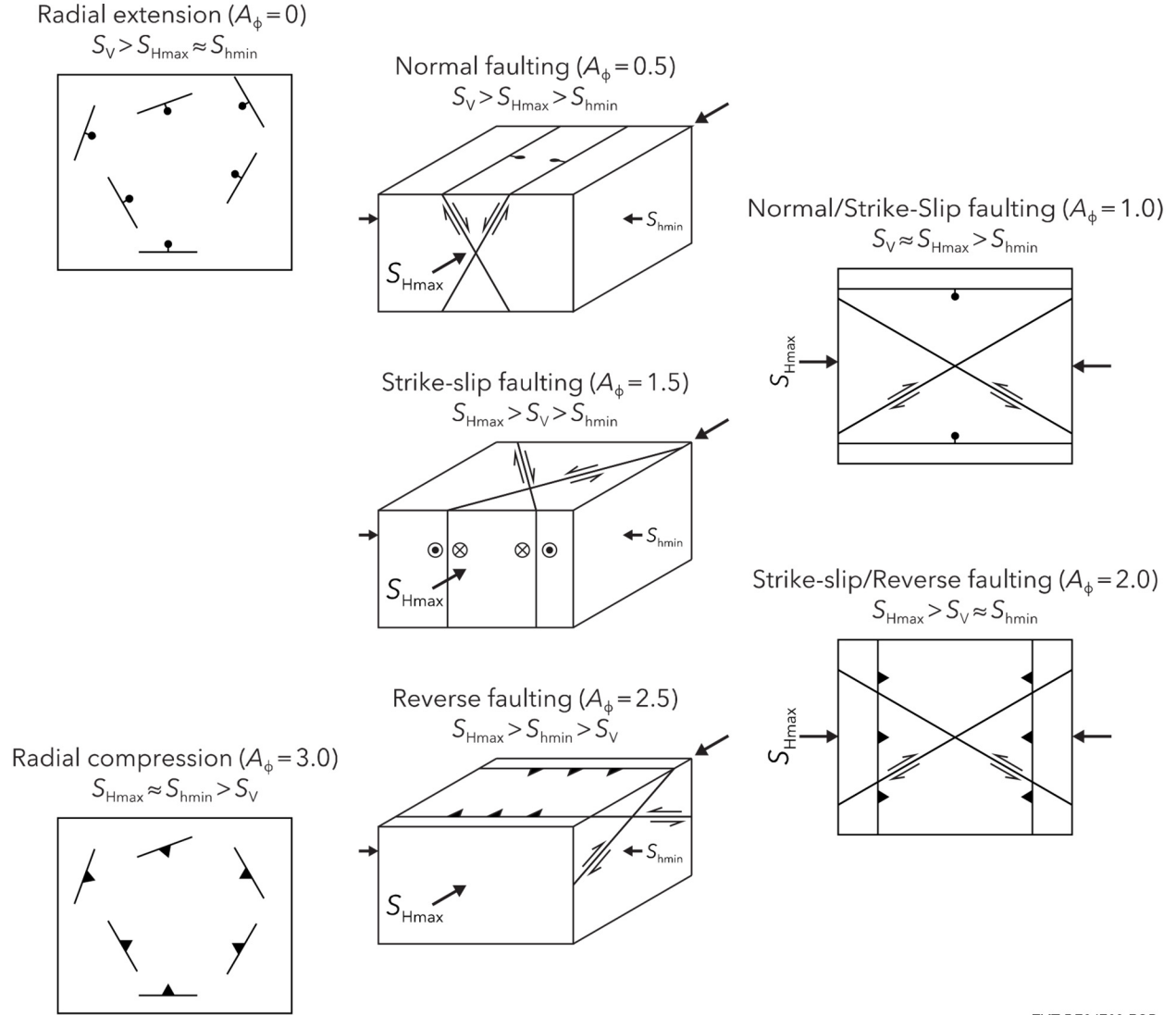


Figure 9. Fault styles and corresponding values of A_ϕ (Lund-Snee and Zoback, 2018).

A multiyear study by Lund-Snee and Zoback (2020) resulted in the interpretation of numerous stress data points across North America, which includes the PCOR region, resulting in preparation of the A_ϕ fault regime map in Figure 10. The map is based on 2,020 data points across the PCOR region, which are sourced from image log data (wellbore breakouts, drilling-induced tensile fractures), literature, the world stress map (Heidbach and others, 2018; Zoback, 1992), and focal mechanism inversions. In the absence of site-specific stress measurements, the A_ϕ fault regime information is critical for understanding dominant present-day relative stress directions, important for modeling and carrying out critical stress analysis of subsurface faults.

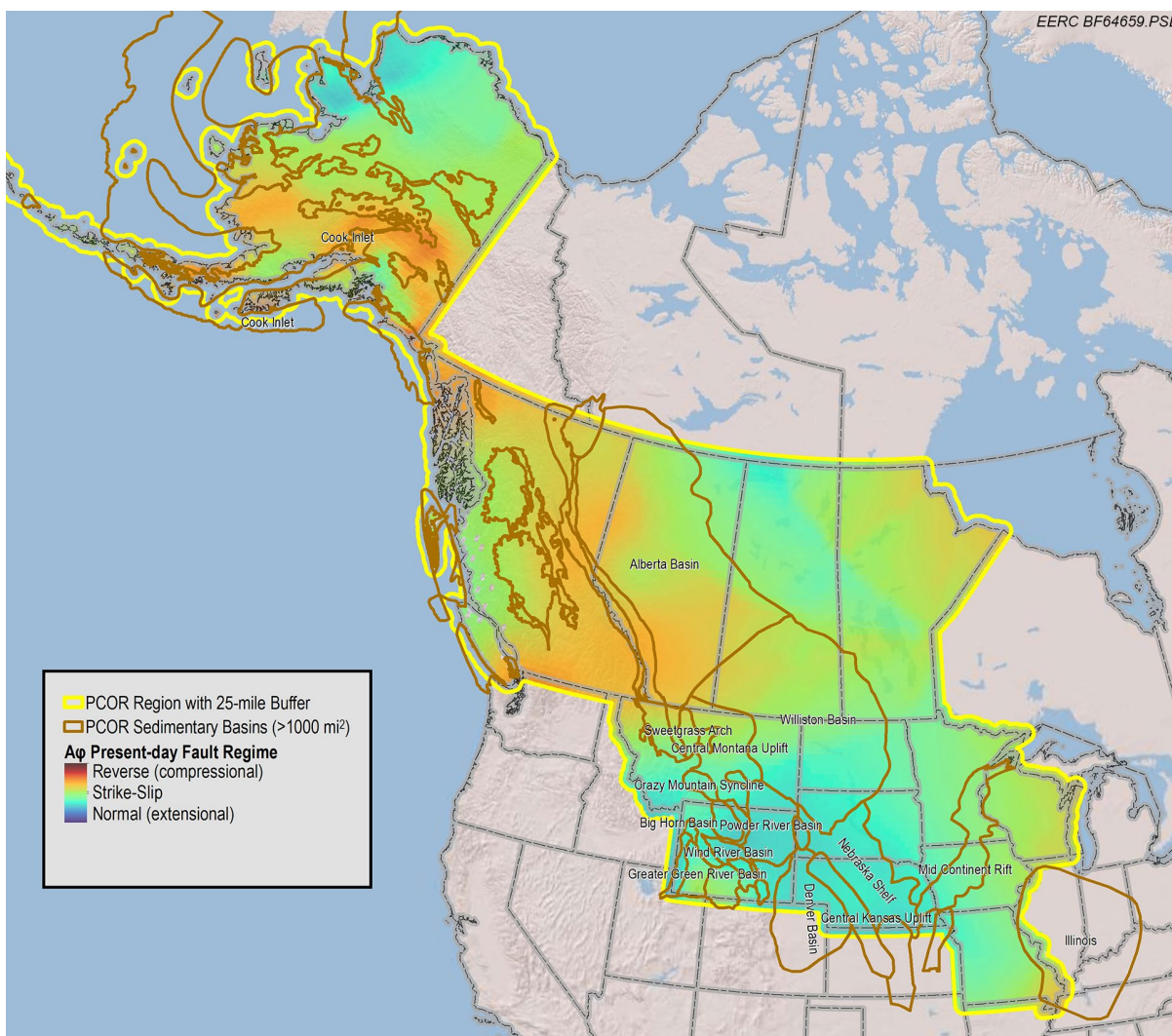


Figure 10. PCOR region A_0 map of present-day fault regime (Lund-Snee and Zoback, 2020) and major sedimentary basins.

TECTONIC FRAMEWORK

Tectonic maps including domain (Figure 11), setting (Figure 12), accretion age (Figure 13), and age of last orogenic activity (Figure 14) were prepared across the PCOR study area to provide a framework for basement faulting and test hypotheses related to regional stress distribution and present-day maximum horizontal stress direction. Major basement faults depicted in the maps (discussed later in this document) are used here for reference and to portray the spatial relationship between fault populations and tectonic domains and settings.

Tectonic domains are defined as distinct regions or subregions with similar tectonic history and setting. Tectonic domain and tectonic setting regions in this study are based largely on the work of Hasterok and others (2022), while accretion ages and confirmation of various tectonic

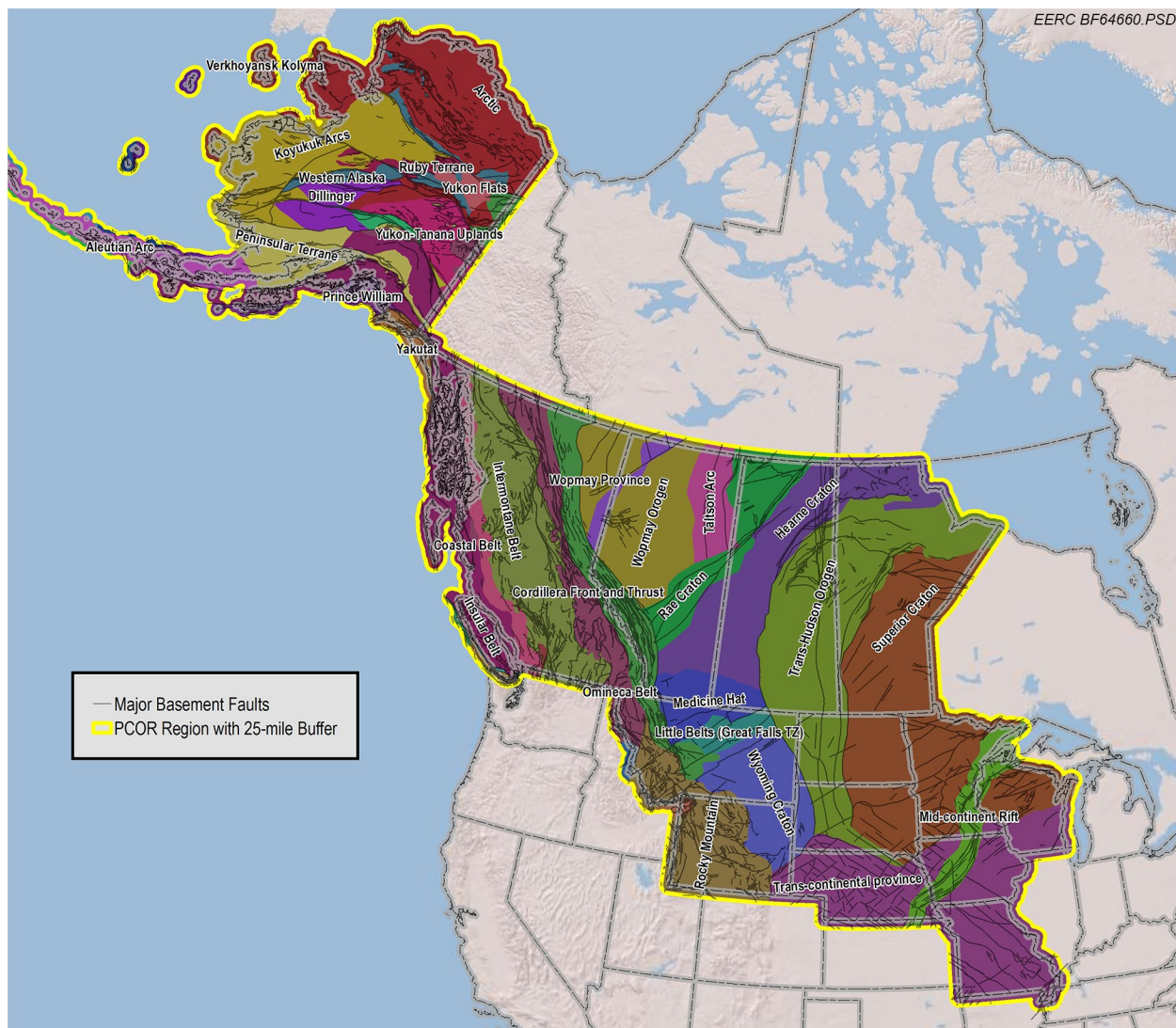


Figure 11. Basement tectonic domain names (Hasterok and others, 2022) and major basement faults within the PCOR region.

domain boundaries are based on several sources (Bayley and Muehlberger, 1968; Brown and Brown, 1987; Carlson and Anderson, 1965; Chorlton, 2007; Dicken and others, 2001; Domrois, 2013; Hasterok and others, 2022; Gerhard and others, 1990; Gifford and others, 2020; Heck, 1988; Hoffman, 1988; Lund and others, 2015; Marshak and others, 2017, 2016; Ross and others, 2003; Shultz, 2019; Sims and others, 2008; and Whitmeyer and Karlstrom, 2007).

Interpreted tectonic boundaries can be inconsistent between publications, especially when boundaries are buried or data to determine boundaries are sparse or poor. The Hasterok and others (2022) data set for tectonic boundaries across the PCOR region is internally consistent, as the boundaries are interpreted by one group using the same method, which lowers overall interpretation uncertainty. Details regarding the interpretation method of tectonic boundaries and the extensive list of global references are captured in Hasterok and others (2022).



Figure 12. Basement tectonic setting (Hasterok and others, 2022) and major basement faults within the PCOR region.

Tectonic domain settings (Figure 12) vary widely across the PCOR study area and include the following (Hasterok and others, 2022):

- **Craton** – Predominantly Archean core and contains granite–greenstone belts and other undifferentiated terranes with relatively small area.
- **Shield** – Like a craton, predominantly Meso- to Paleoproterozoic lithosphere, undifferentiated.
- **Passive margin** – Sediment accumulation built on transitional crust between continental and oceanic crust marking half of a tectonically inactive fossil rift.

- **Accretionary complex** – Active/subduction margin consisting of sedimentary wedges built on oceanic or continental crust.
- **Basin** – Intracontinental sedimentary cover built on preexisting continental crust with uncertain or unknown basement provenance.
- **Foredeep basin** (foreland basin) – Thick intracontinental sedimentary basin created during continent collision; basement uncertain.
- **Orogenic belt** – Fold and thrust belts created during accretionary, collisional, and intracontinental settings that may incorporate a variety of preexisting terrane types, often commingled, making them difficult to differentiate at the regional scale.
- **Narrow rift** – Focused extensional terrane with continental basement.
- **Wide rift** – Distributed extensional terrane with continental basement.
- **Volcanic arc** – Predominantly magmatic arc crust related to subduction but may contain crust predating the arc and/or interspersed accretionary material in island arcs and in seaward-migrating arcs due to retreating trenches.
- **Oceanic back-arc basin** – A back-arc basin where seafloor spreading has been sustained, creating enriched basaltic compositions relative to mid-ocean ridge basalt.
- **Ophiolite complex** – Obducted oceanic crust of some variety, excluding volcanic arc-type, but including suprasubduction zone oceanic crust.
- **Magmatic province** – A large intraplate magmatic terrane not clearly associated with subduction or extension processes.
- **Oceanic crust** – Typical oceanic crust not created in a back-arc setting.

Published tectonic accretion ages (Figure 13) were reviewed and captured to investigate the potential relationship of basement faulting and basement stress. Using Hasterok and others (2022) tectonic domains as the basis, accretion ages based on published information were assigned to the tectonic domains. When possible, both “young age” and “old age” were captured, which represents the uncertainty in the interpretation of accretion age. Uncertainty in the accretion age is driven by several factors, but the main reasons include data density, data type, and sample availability. In general, a higher density of identified basement faulting is associated with basement terranes that are younger, interpreted to be due to overall shallower depths and reduced mapping uncertainty.

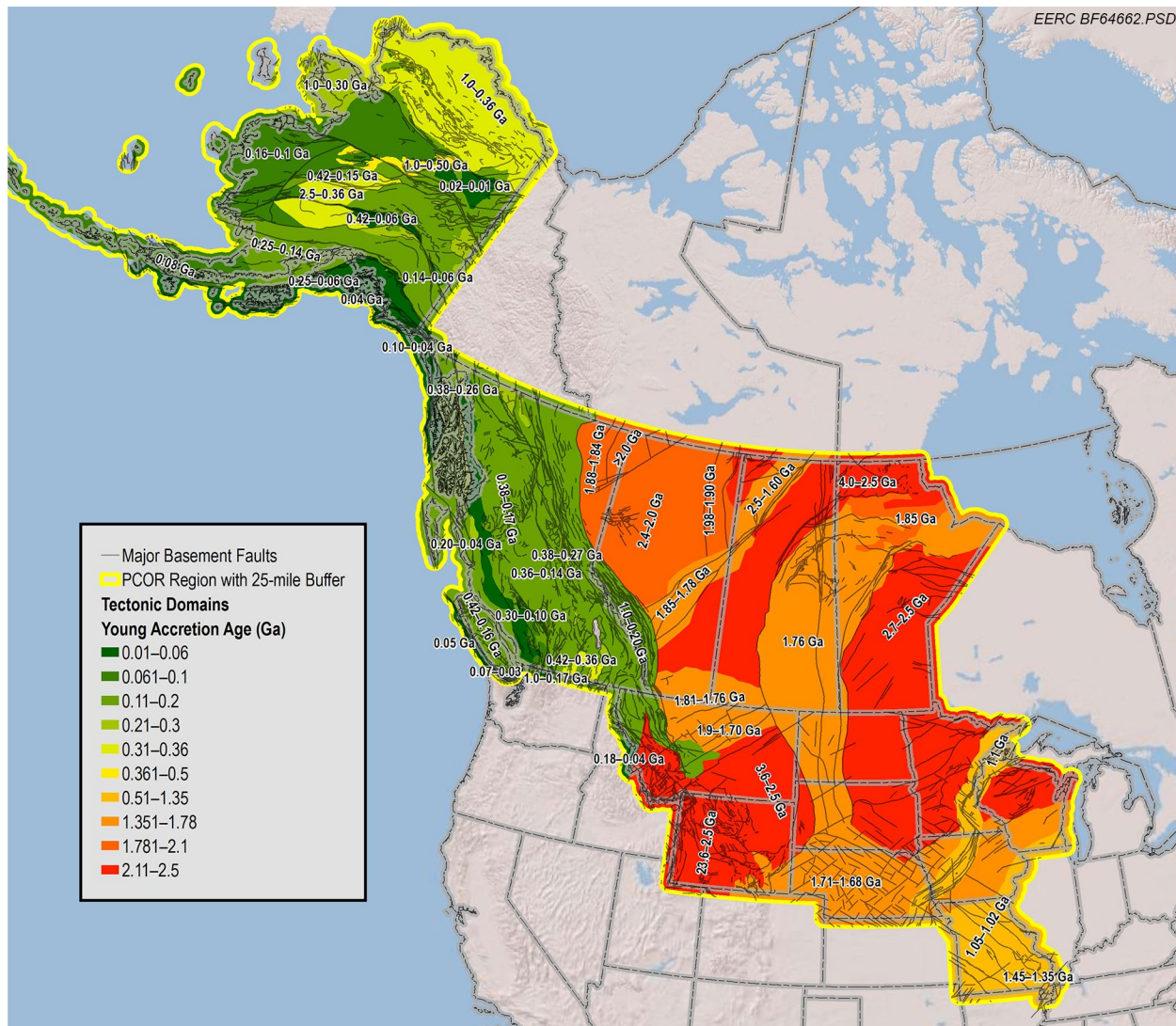


Figure 13. Basement tectonic domains (Hasterok and others, 2022), accretion young age (Ga) in color, ranges of published accretion ages (numerous sources) labeled, and major basement faulting within the PCOR study area.

Additionally, the published age of the last orogenic activity (Hasterok and others, 2022) was mapped (Figure 14) to investigate the relationship to basement faulting and stress. In general, craton tectonic settings are interpreted to have identical accretion ages and last orogeny ages, while older basement terranes that accreted earlier may have been subject to a later orogenic event. Like the basement terrane accretion age map in Figure 13, the more recent orogenic events tend to be associated with a higher density of basement faults, particularly the western (southern Alaska, British Columbia, and western Montana and Wyoming) Cordilleran and northern Caledonian regions (Alaska) of the PCOR region. The regions with more recent orogenic activity tend also to be related to areas with increased present-day seismicity, depicted in Figure 15 and discussed later in this report. Figure 15 shows

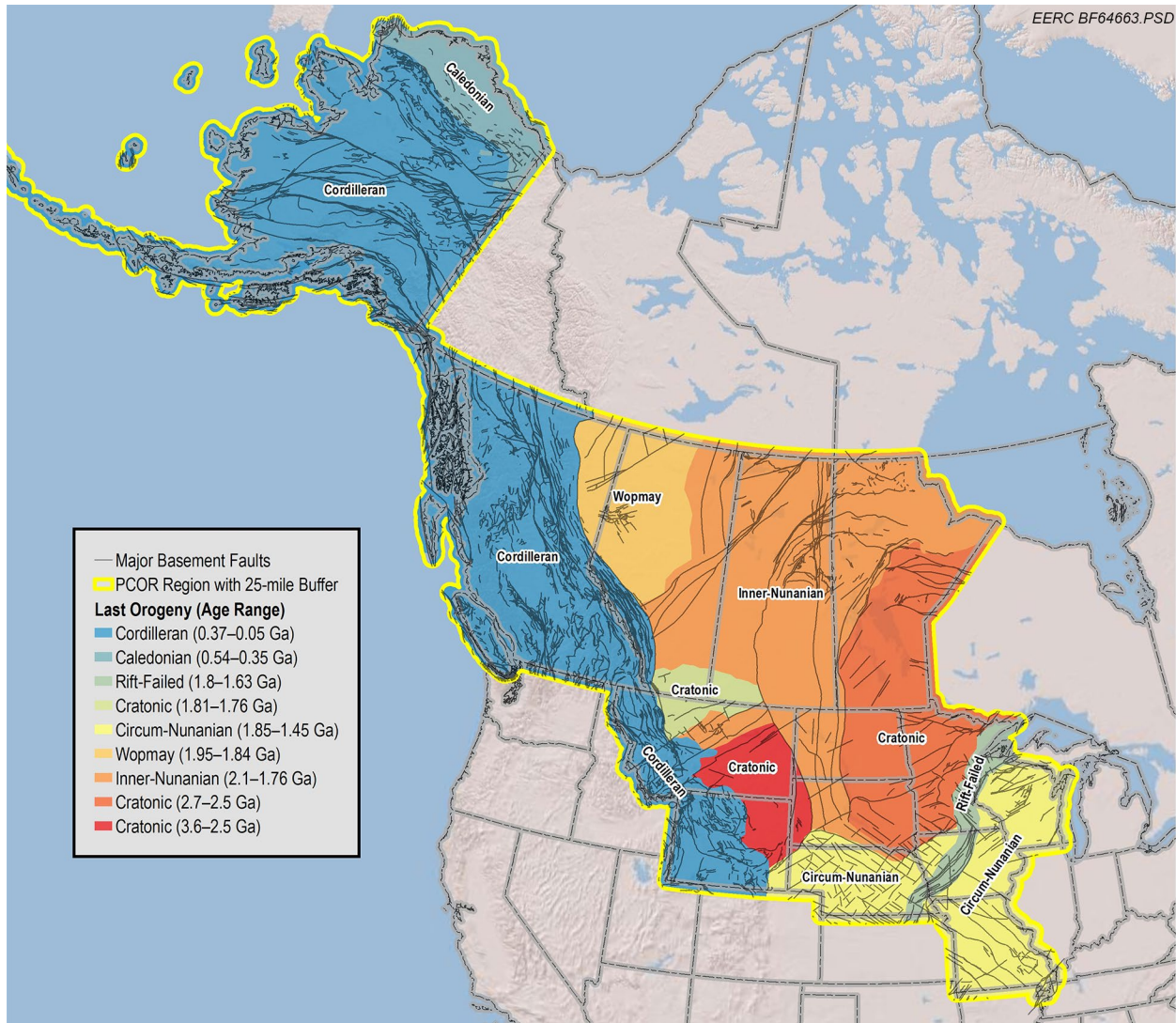


Figure 14. Last orogen age (Hasterok and others, 2022) across PCOR study area. Younger “last orogeny” ages are in blue green colors, and older “last orogeny” ages are in orange red colors. Labels denote the age range (Ga) of orogenic events.

seismic events reported by USGS in the past ~10 years that are greater than Richter scale magnitude 2.5 (M2.5). Earthquakes greater than M2.5 are generally considered to be “felt by humans” who are situated in the general vicinity of the earthquake epicenter. Important to note is the increased density of recent earthquakes associated with the tectonic regions with more recent orogenic activity throughout the PCOR region and with the western edge of the North American tectonic plate boundary (Figure 15). Since earthquakes are a result of fault slip and fault dilation (opening) can be associated with fault slip, earthquake seismicity can be associated with a higher risk profile for a leaky fault (Zoback and Gorelick, 2012), but not in all cases (Vilarrasa and Carrera, 2015).

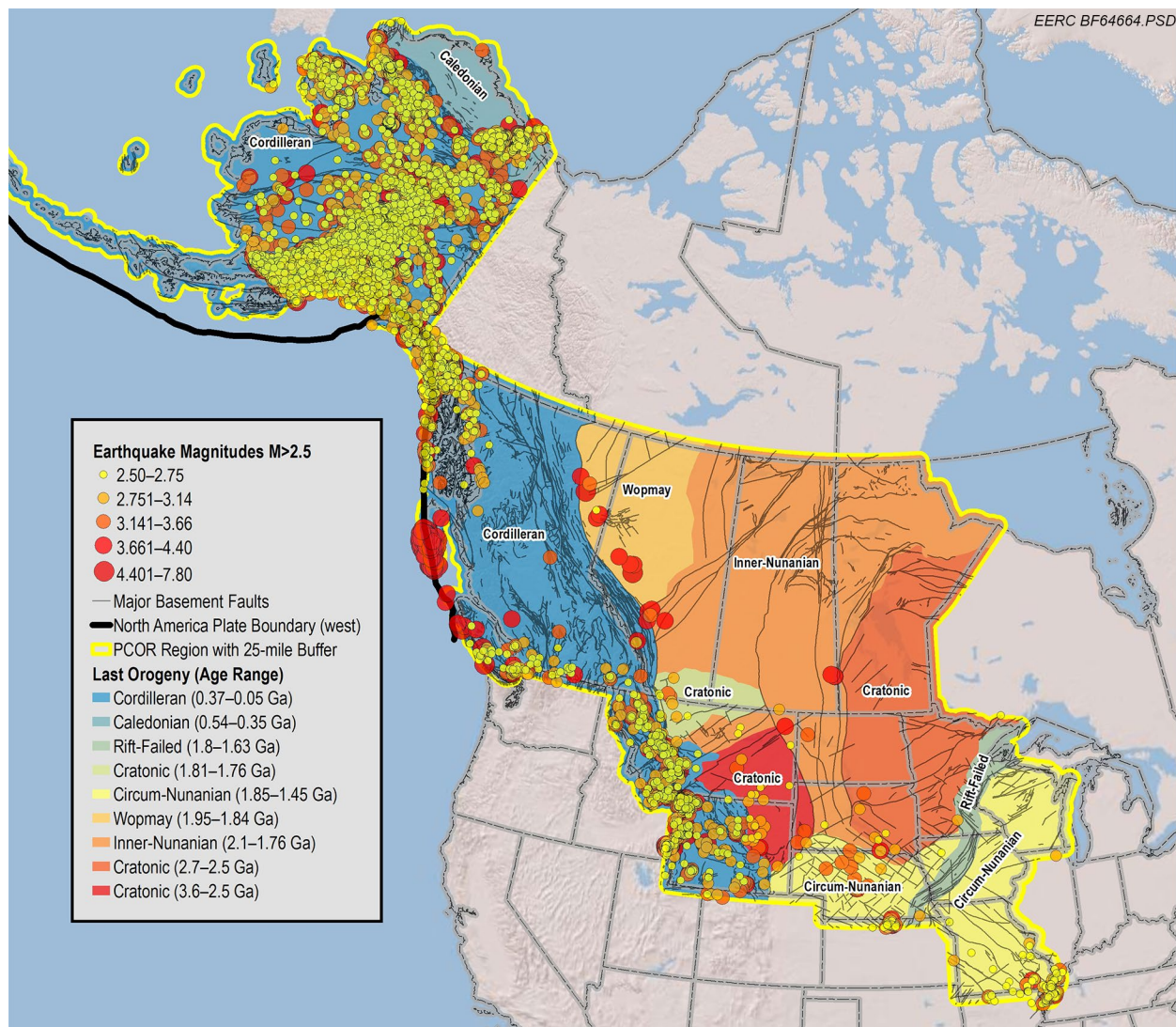


Figure 15. PCOR region age of last orogen (Figure 14) and western margin of the North America plate boundary (Hasterok and others, 2022) vs. USGS recent earthquake activity with magnitudes greater than $M2.5$.

BASEMENT FAULTING

Major basement faults were captured and integrated within the ArcGIS environment based on a series of shapefile, geodatabase, and georeferenced raster image sources from publications, USGS, Canadian province geological surveys, and U.S. state geological surveys. Because of the complex tectonic, structural, and geologic history, a vast array of different basement fault populations exists across the PCOR region (Figure 16). As previously mentioned, fault traces without relative motion have been depicted in Figures 11–15 for reference. Sources of basement faults in this study include Alberta Geological Survey (2023), Anderson (2016), Bartos and others (2021), British Columbia Geological Survey (2022), Burberry and others (2018), Chorlton (2007),



Figure 16. Major basement faults and type across PCOR region.

Cui and others (2017), Ekpo and others (2017), Filina and others (2018), Garrity and Soller (2005), Gregersen and Shellenbaum (2016), Guthrie (2018), LeFever and others (2011), Manitoba Geological Survey (2023), McCormick (2010), Mossop and Shetson (1994), Saskatchewan Ministry of Energy and Resources (2023), Sims and others (2004), Sims and Peterman (1986), U.S. Geological Survey (2023b), Wheeler and others (1997), Wyoming State Geological Survey (2022), and Yukon Geological Survey – Government of Yukon (2020).

The interpretation, compilation, and capture of basement faults across the PCOR study area was carried out using the following methodology:

1. Merged pertinent digital basement fault data sources using ArcGIS.
2. Georeferenced pertinent raster images and digitized faults of importance.

3. Integrated captured faults to align with tectonic domains and ensure faults were geologically reasonable.
4. Clipped fault shapefiles 25 km outside of PCOR boundary to minimize edge effects of data set.
5. Assigned fault type, e.g., normal, reverse, strike-slip, where data were available while considering tectonic and reactivation history.
6. Assigned fault dip, e.g., 25 degrees for reverse, 55 degrees for normal, and vertical (90 degrees) for strike-slip, high-angle, shear, and unspecified fault types (Miller, 2023).
7. Calculated fault azimuth and strike based on starting and ending points of each fault segment.
8. Created and populated a consistent ArcGIS attribute table for all captured faults that included the following information: data source, fault name (if available), fault type, confidence, age (if available), strike, dip, tectonic domain, tectonic province type, and sedimentary basin.

Because of the diverse nature of basement fault data sources, care was taken to ensure that the faults selected for the study were considered “basement-rooted” faults versus faults that only exist in the sedimentary section above the top of basement. Main data sets used to constrain basement faults captured in the study include potential fields, i.e., magnetics and gravity, extrapolation from surface outcrops, and regional 2D seismic lines. To that end, basement fault data in this study should be considered a regional data set and only as a starting point for site-specific evaluations, where additional data (such as 2D or 3D seismic, potential fields) may be available to better constrain and characterize the nature of potential basement and associated sedimentary section faulting.

A_Φ FAULT REGIME AND MAXIMUM HORIZONTAL STRESS DIRECTION

Data to characterize the maximum horizontal stress direction are shown in Figure 17, along with the A_Φ fault regime distribution discussed earlier in this report. The interpreted maximum horizontal stress direction data points are based on two sources: Lund-Snee (2020) and Levandowski and others (2022). The Lund-Snee (2020) data set in blue is based on four data type sources: drilling-induced tensile fracture and wellbore breakout orientation from wellbore images, focal mechanism inversion solutions from earthquake events, hydraulic fracture orientations from wellbores interpreted from microseismic data, and shear velocity anisotropy interpreted from wellbore cross-dipole electric logs. Lund-Snee (2020) also assigned four levels of data quality; however, in Figure 17, all data quality points are depicted. The Levandowski and others (2022) data set in purple is based primarily on moment tensors and focal mechanism inversion solutions from earthquake events. Within the PCOR region, the Lund-Snee (2020) data set comprises

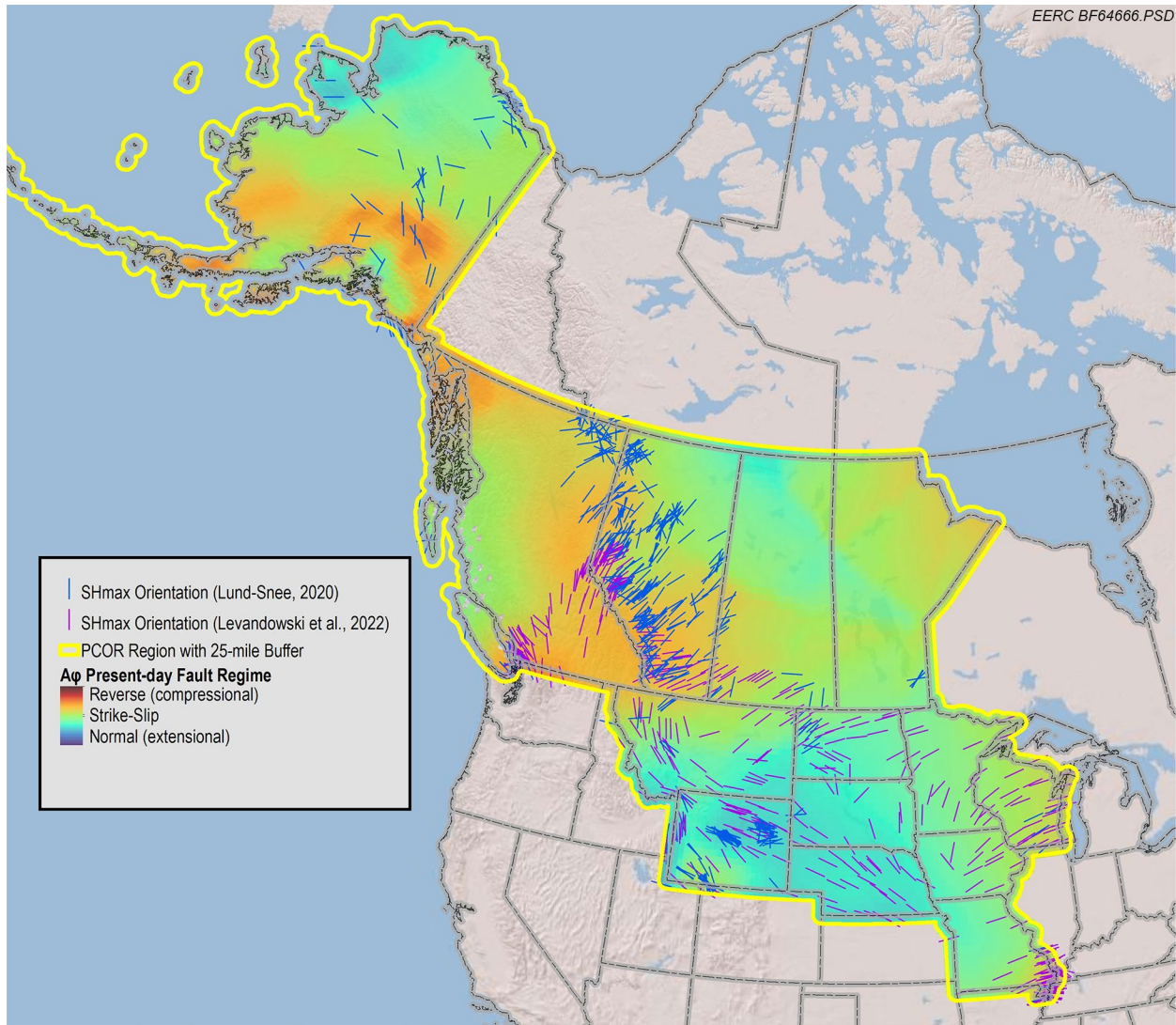


Figure 17. PCOR area $A\Phi$ fault regime (Lund-Snee and Zoback, 2020) and maximum horizontal stress direction (Lund-Snee, 2020; Levandowski and others, 2022).

535 data points, while the Levandowski and others (2022) data set comprises 474 data points, for a total of 1009 data points. The interpreted maximum horizontal stress direction data are used to assess the variability of crustal stress and are a key element in calibration of critical stress analysis modeling, as discussed below.

DEPTH TO BASEMENT AND BASAL RESERVOIRS

Determination of maximum sediment fill by basin was carried out based on Muehlberger (1996) in Canada and the Lower 48 and Gregersen and Shellenbaum (2016) in the Alaska northern Cook Inlet Basin. Muehlberger (1996) is comprised of four maps across North America that show major basement features, tectonic elements, and the depth of basement from the surface within

major sedimentary basins. The maps were georeferenced, and a series of depth to basement data points (in feet) were captured across all basins and adjacent areas within the PCOR region (Figure 18) to represent the sediment fill depth range. For reference, Precambrian basement outcrops (Garrity and Soller, 2005) are displayed on the map, along with sedimentary basin outlines.

Table 3 captures the oldest prospective or potential storage reservoir just above basement based on stratigraphic correlation charts (Table 1), along with the maximum sediment fill (after Muehlberger, 1996; and Gregersen and Shellenbaum, 2016). All values in Table 3 are inclusive of the PCOR region.

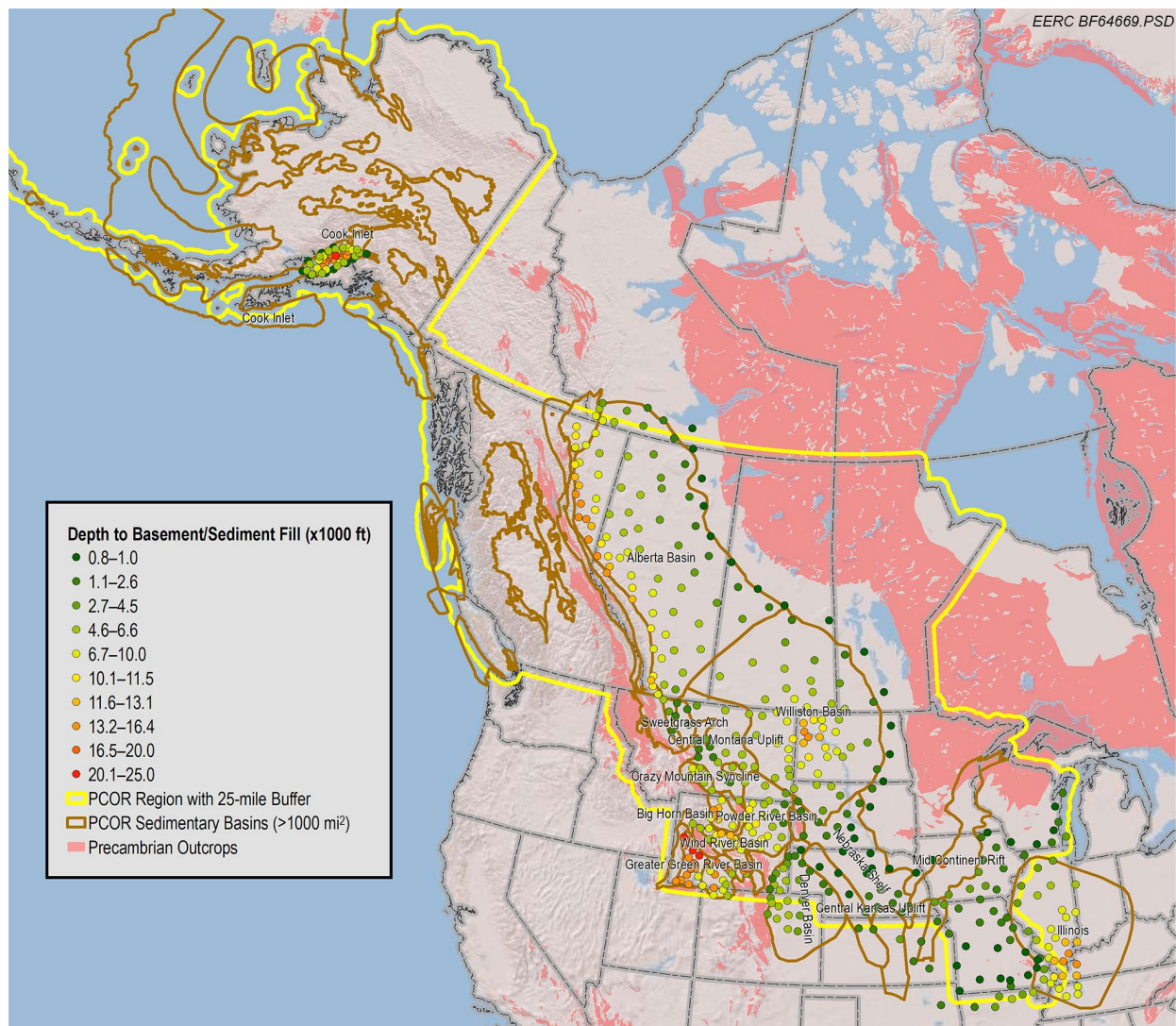


Figure 18. Estimated depth from surface to top basement (sediment fill) in feet across the PCOR area, based on Muehlberger (1996) in Canada and U.S. Lower 48 and Gregersen and Shellenbaum (2016) in the Alaska northern Cook Inlet Basin.

Table 3. Stratigraphically Deepest Candidate CO₂ Storage Reservoir Formation and Age Overlying Basement and Approximate Maximum Depth to Basement or Sediment Fill for Major Basins Within PCOR Area (Figure 18)

Basin Name	Deepest Potential Storage Reservoir Formation	Deepest Potential Storage Reservoir Age	Approximate Maximum Sediment Fill, feet
Green River Basin	Flathead	Cambrian	24,600
Wind River Basin	Flathead	Cambrian	12,300
Willison Basin	Deadwood	Cambrian	14,000
Powder River Basin	Flathead	Cambrian	11,500
Big Horn Basin	Flathead	Cambrian	14,800
Central Montana Uplift	Flathead	Cambrian	7000
Crazy Mountain Syncline	Flathead	Cambrian	9800
Denver Basin	Sawatch	Cambrian	5700
Alberta Basin	Pika/Earlie	Cambrian	15,000
Illinois Basin	Mt. Simon	Cambrian	11,500
Mid-Continent Rift (flank)	Copper Harbor	Cambrian (?)	17,700
Cook Inlet (north)	Kamishak	Late Triassic	25,000

BASEMENT STRESS STUDY AREAS

A series of eight representative basement stress study areas were identified across the PCOR study area based on the identification of basement faults/fault segments (Figure 16) existence of adequate subsurface stress and supporting reservoir quality data (Figure 19) pertinent to basal reservoirs for critical stress analyses using the Stanford FSP tool and occurrence of elevated carbon capture and storage (CCS) industry activity (Figure 20). A summary of each basement stress study area is captured in Table 4.

The available stress and reservoir quality data across the PCOR study area (Figure 19) vary and were sourced from Class VI permit applications from the Wyoming Department of Environmental Quality (2023), the North Dakota Division of Mineral Resources (2023), U.S. Environmental Protection Agency (EPA) monitoring, reporting and verification (MRV) plans in the United States (2023b), carbon capture project operating documents in Canada, Mossop and Shetson, 1994; Weides and others, 2014; Ozkan, 2001; Chalaturnyk, 2007; Miskimins and others, 2001; Cipolla and others, 1994; Pantaleone, 2020. The North Dakota Williston Basin basement stress focus study area holds the largest stress database in the PCOR region, with 24 data points that range in age from the Cretaceous to the Cambrian. Data types captured for calibration



Figure 19. Map of basement stress study areas, sedimentary basin outlines, and distribution of available subsurface stress data. Circles are Paleozoic-aged data, triangles are Mesozoic-aged data, diamonds are Cenozoic-aged data, and squares indicate geologic age of data not known.

of fault slip analysis (Walsh and others, 2018) critical stress models include pore pressure, fracture gradient, vertical stress, maximum and horizontal stress, unconfined compressive strength (UCS), fault cohesion, friction angle, porosity, and permeability. Available data types of formation-specific data across each study area vary widely, so to carry out geomechanical FSP modeling, assumptions were made in some cases that were reflected in uncertainty ranges of results. Maximum horizontal stress azimuth data, also used to calibrate the FSP models, are captured in Figure 17 and were sourced primarily from image log wellbore data and earthquake focal mechanism stress inversion data (Lund-Snee, 2020; Levandowski and others, 2022).



Figure 20. PCOR region basement stress study areas with CCS facility industry type project locations and major basement faults. All facilities are either a CCS sink or CCS combination source and sink.

Table 4. Summary of Basement Stress Study Areas Depicted in Figure 19

Name	Primary State or Province	Number of Basement Fault Segments	Number of Stress Data Points	Stress Data Age Range	Critical Stress Analysis Modeling Carried Out
Greater Green River Basin	Wyoming, USA	116	4	Jurassic–Triassic	Yes
Wind River Basin	Wyoming, USA	17	0	NA ¹	No
Powder River Basin	Wyoming, USA	5	0	NA	No
Williston Basin	North Dakota, USA	14	24	Cretaceous to Cambrian	Yes
Alberta South	Alberta, Canada	7	2	Unknown	No
Alberta South Central	Alberta, Canada	11	13	Unknown/Cambrian	Yes
Alberta Central	Alberta, Canada	21	1	Unknown	No
Northern Cook Inlet	Alaska, USA	167	4	Mesozoic to Miocene	Yes (publication)

¹ Not available.

INDUSTRY ACTIVITY AND BASEMENT STRESS STUDY AREAS

A map showing existing and under development CCS projects across the PCOR region is depicted in Figure 20. Each project indicated on the map is either a CCS sink or combination source and sink. Given the rapid development of the CCS industry across the PCOR region in recent years, the map should be considered a “snapshot in time” and an information source to illustrate the state of the industry, areas of existing and developing CCS activity, and the relationship of facility locations to identified major basement faults. Figure 20 depicts the primary industry associated with existing or proposed CCS facilities, which includes ethanol production, fertilizer production, fuel and methanol production, hydrogen production, oil and gas production and processing, synthetic natural gas production, power generation, or technology R&D.

The areas of highest CCS project activity were one of the criteria to select stress study areas, discussed below, which are depicted on the map.

Detailed information for each facility is available in Appendix A, Table A-1, and is based on numerous sources including the Global CCS Institute facilities database (2023), EPA Facility Level Information on Greenhouse gases Tool (FLIGHT) database (2023a), various Class VI permit applications, a CO₂ enhanced oil recovery (EOR) in Wyoming report (Robertson, 2022), and unpublished information from the EERC.

PCOR REGION RECENT EARTHQUAKE ACTIVITY

Significant earthquake activity greater than M2.5 over the past 10 years across the PCOR region is shown in Figures 21 (U.S. Geological Survey, 2023) and Figure 22 (Muehlberger, 1996; Gregersen and Shellenbaum, 2016). M2.5 was selected as a cutoff, as that is the earthquake magnitude that is generally felt by humans, as characterized in the Modified Mercalli Scale in Figure 23 (U.S. Geological Survey, 2021b) and in Figure 24 (Zoback and Gorelick, 2012). The Modified Mercalli Scale is based on observable earthquake damage while the moment magnitude scale is based on seismic records. The earthquake activity data were extracted from the USGS earthquake catalog associated with the Earthquake Hazards Program (U.S. Geological Survey, 2021a).

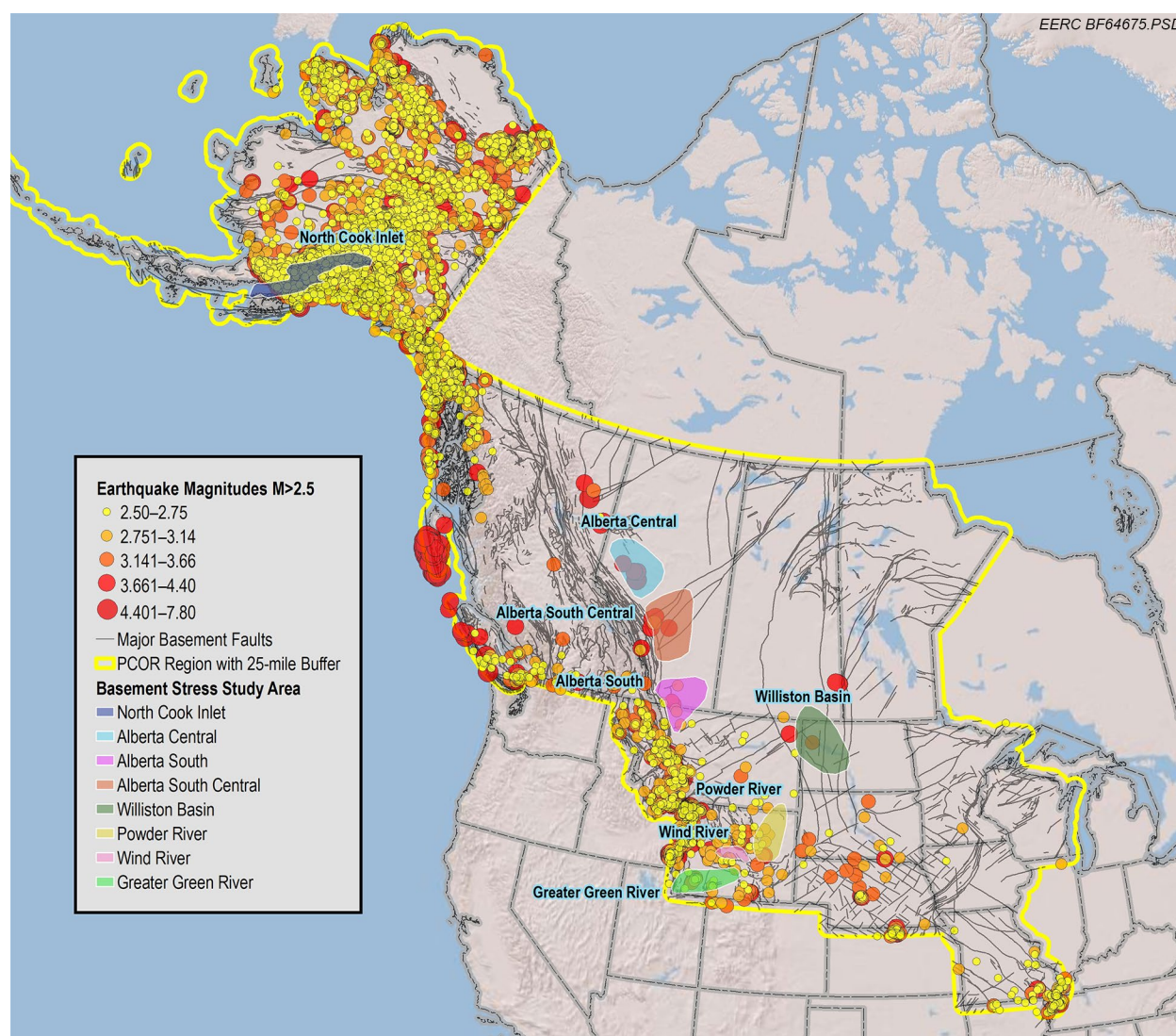


Figure 21. PCOR region earthquake magnitude activity in last 10 years greater than M2.5, major basement faults, and basement stress study areas (U.S. Geological Survey, 2023).

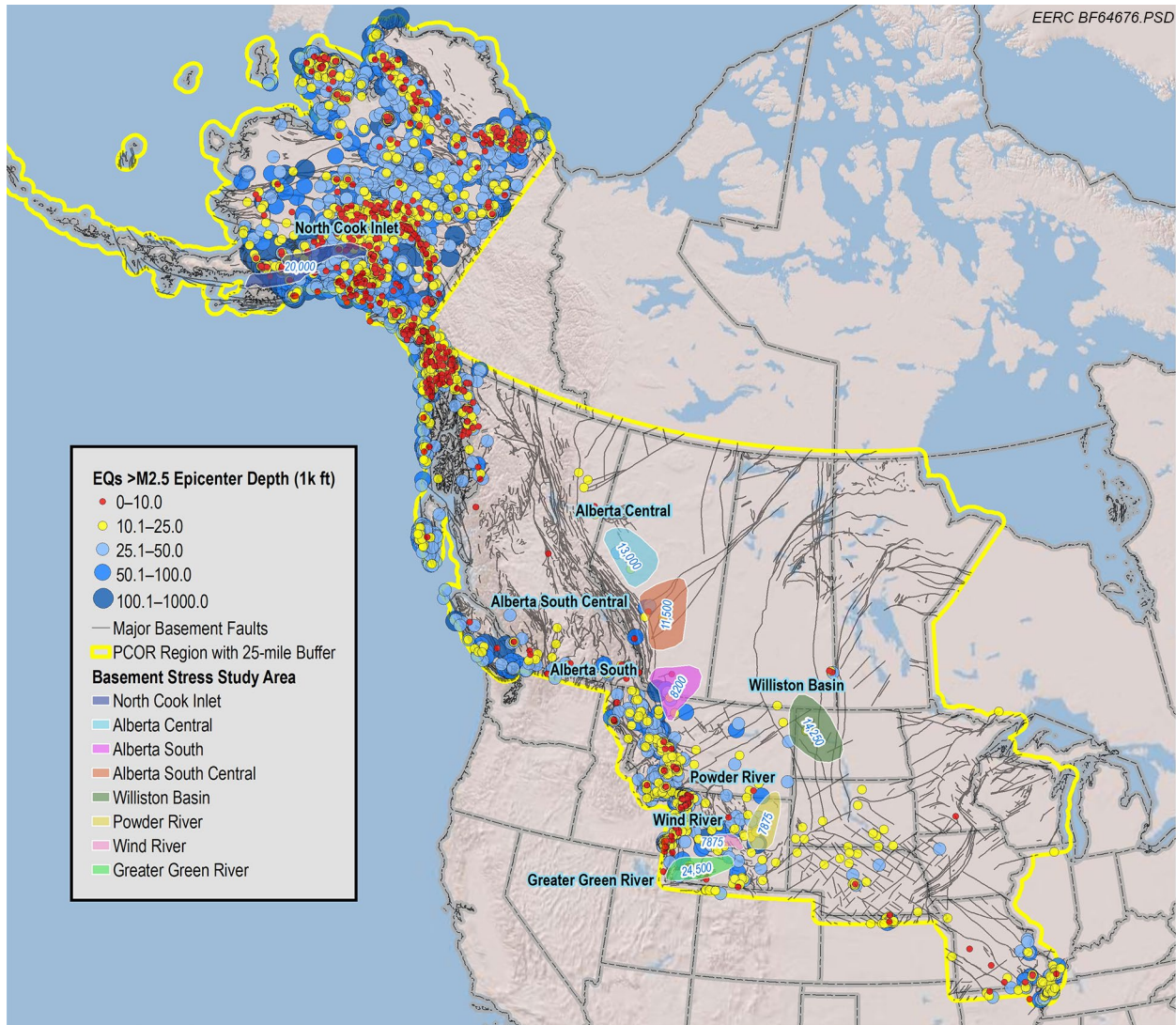












Figure 22. PCOR region earthquake activity in the last 10 years showing estimated epicenter depth (USGS, 2021a). Maximum depth to basement in feet is labeled in blue for each basement stress study area based on Muehlberger (1996) in Canada and U.S. Lower 48 and Gregersen and Shellenbaum (2016) in the Alaska northern Cook Inlet Basin.

Zoback and Gorelick (2012) provide general guidelines to illustrate how the magnitude of an earthquake is related to the size of the fault that slipped and the amount of fault slip that occurred, using well-established seismological relationships. As shown in Figure 24, faults capable of producing magnitude $\sim M6$ earthquakes are at least tens of kilometers in extent (x-axis, size of slip patch). The fault size indicated along the x-axis is a lower bound of fault size, as it refers to the size of the fault segment that slips in each earthquake. The fault on which an earthquake occurs is larger than the part of the fault that slips in an individual event. In most cases, such faults should be easily identified during geophysical site characterization studies and thus should be avoided at any site chosen for a CO₂ storage site (Zoback and Gorelick, 2012). Figure 24 also depicts that the

Earthquake Intensity Scale

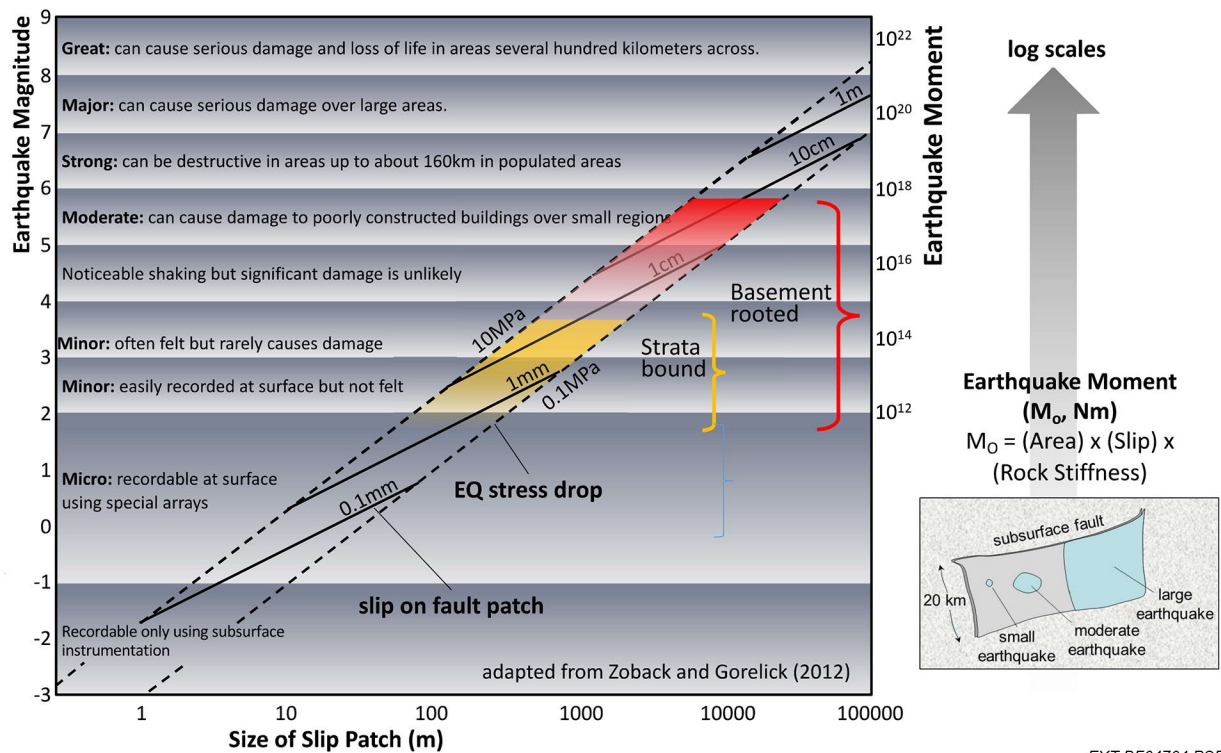
Modified Mercalli Intensity (MMI)

	INTENSITY	SHAKING	DESCRIPTION
	I	Not Felt	Not felt except by a very few under especially favorable conditions.
	II	Weak	Felt only by a few persons at rest, especially on upper floors of buildings.
	III	Weak	Felt quite noticeable by persons indoors. Many people do not recognize it as an earthquake. Standing cars may rock slightly, vibrations are similar to a passing truck.
	IV	Light	Felt indoors by many, outdoors by few. At night, some are awakened. Dishes, windows, and doors are disturbed. Sensation like a heavy truck striking a building. Standing cars rock noticeably.
	V	Moderate	Felt by nearly everyone; many awakened. Dishes and windows are broken. Unstable objects are overturned. Pendulum clocks may stop.
	VI	Strong	Felt by all; many frightened. Some heavy furniture moved. A few instances of fallen plaster. Damage is slight.
	VII	Very Strong	Negligible damage to buildings of good design/construction. Slight to moderate damage in well-built/ordinary construction. Considerable damage in poorly built/designed structures. Some chimneys broken.
	VIII	Severe	Slight damage to specially designed structures. Considerable damage to ordinary construction, including partial collapse. Damage is great in poorly built structures. Fall of chimneys, columns, monuments, and walls. Heavy furniture overturned.
	IX	Violent	Considerable damage to specially designed structures; well-designed frame structures are thrown out of plumb. Damage is great in substantial buildings, with partial collapse. Buildings shifted off foundations.
	X+	Extreme	Some well-built wooden structures destroyed; most masonry and frame structures with foundations are destroyed. Rails are bent.

EXT BF64703.PSD

Figure 23. USGS earthquake Modified Mercalli intensity scale (2021). Approximate Richter scale moment magnitude equivalents are: I: Mw 1.0-2.9; II-III: Mw 3.0-3.9; IV-V: Mw 4.0-4.9; VI-VII: 5.0-5.9; VIII-IX; 6.0-6.9; X+: Mw 7.0 and higher.

Shallow (Strata-bound) vs Basement-Rooted Faults



EXT BF64704.PSD

Figure 24. Relationships among various scaling parameters for earthquakes. The larger the earthquake, the larger the fault and amount of slip, depending on the stress drop in a particular earthquake event (Zoback and Gorelick, 2012).

concept of moment magnitude is a physical quantity proportional to the slip on the fault multiplied by the area of the fault surface that slips. The moment magnitude is related to the total energy released in the earthquake.

As shown in Figure 22, elevated earthquake activity is associated with the western portion of the PCOR region, associated with the more recent tectonic orogenic events (Figure 14), boundaries between major tectonic domains, and the western margin of the North America plate boundary (Figure 15). The basement stress study areas most impacted by elevated earthquake activity are the northern Cook Inlet in Alaska, the Wind River area in central Wyoming, and the Greater Green River area in southwest Wyoming. Additionally, the western edges of the Alberta Central, Alberta South Central, Alberta South, and Powder River (northeast Wyoming) regions are situated close to or on tectonic domain boundaries, which also have experienced elevated earthquake activity. In contrast, the Williston Basin region in North Dakota has experienced very little earthquake activity in the past 10 years, largely due to the region being situated on the tectonically old and stable Superior and Trans-Hudson terranes (Figure 11) associated with accretion ages in the Precambrian. (Figure 13).

The data shown in Figure 21, which are also sourced from the USGS Earthquake Hazards Program, illustrate recent (approximately last 10 years) earthquake activity and moment magnitudes greater than M2.5 across the PCOR region. In contrast to Figure 22 where the earthquake moment magnitude and estimated epicenter depth are depicted, along with the basement stress focus areas and associated maximum depth to basement within the focus area (white label). Because of the lack of velocity data across the PCOR region, in many cases the epicenter depth is considered a best effort estimate, but given this uncertainty, regional trends of relative depths of earthquake epicenters can be determined. For the purposes of this study and for generalized comparisons to the maximum basement depth value, the estimated earthquake epicenter depths of less than 10,000 feet have been highlighted on the map with a red dot and estimated earthquake epicenter depths of 10,000–25,000 feet have been highlighted on the map with a yellow dot. Figure 18 compares in greater detail the earthquake epicenter depth to basement depth.

The shallower epicenter depths associated with earthquake events (e.g., red and yellow dots) can be candidates for triggered or induced seismicity events associated with injection of fluids into zones above top of basement where fault slip was induced (Figure 5). Shallow seismicity can also be associated with areas of neotectonics, such as the active tectonic boundaries on the western margin of the North American plate boundary (Figure 15). Following the occurrence of an earthquake event, it may be necessary to carry out a systematic technical analysis to determine if the event is a naturally occurring earthquake or man-made triggered or induced seismicity.

GEOMECHANICS ANALYSIS OF PRIMARY STRESS FOCUS AREAS

Deterministic and probabilistic geomechanics critical stress analyses for four of the eight stress focus areas (Figures 19–22) were carried out to determine the sensitivities regarding basement faults for injecting CO₂ in basal reservoirs situated adjacent to basement. The Stanford FSP tool was utilized for the Williston Basin, Greater Green River, and South Central Alberta stress focus areas, and FSP results from Pantaleone (2020) were used for the northern Cook Inlet stress focus area, where a study of the Nicolai Field Hemlock Formation was carried out. The Hemlock Formation is situated stratigraphically above the Late Triassic Kamishak Formation basal reservoir in the Cook Inlet study area and represents the available stress and reservoir quality data in the focus study area. Figure 25 depicts the area of interest for each FSP model carried out and listed above. The absence of available stress calibration data in the remaining four areas prevented the use of FSP tool; however general observations for these four areas are captured below to characterize potential regional geological and geomechanical implications of CO₂ storage in basal reservoirs within those areas.

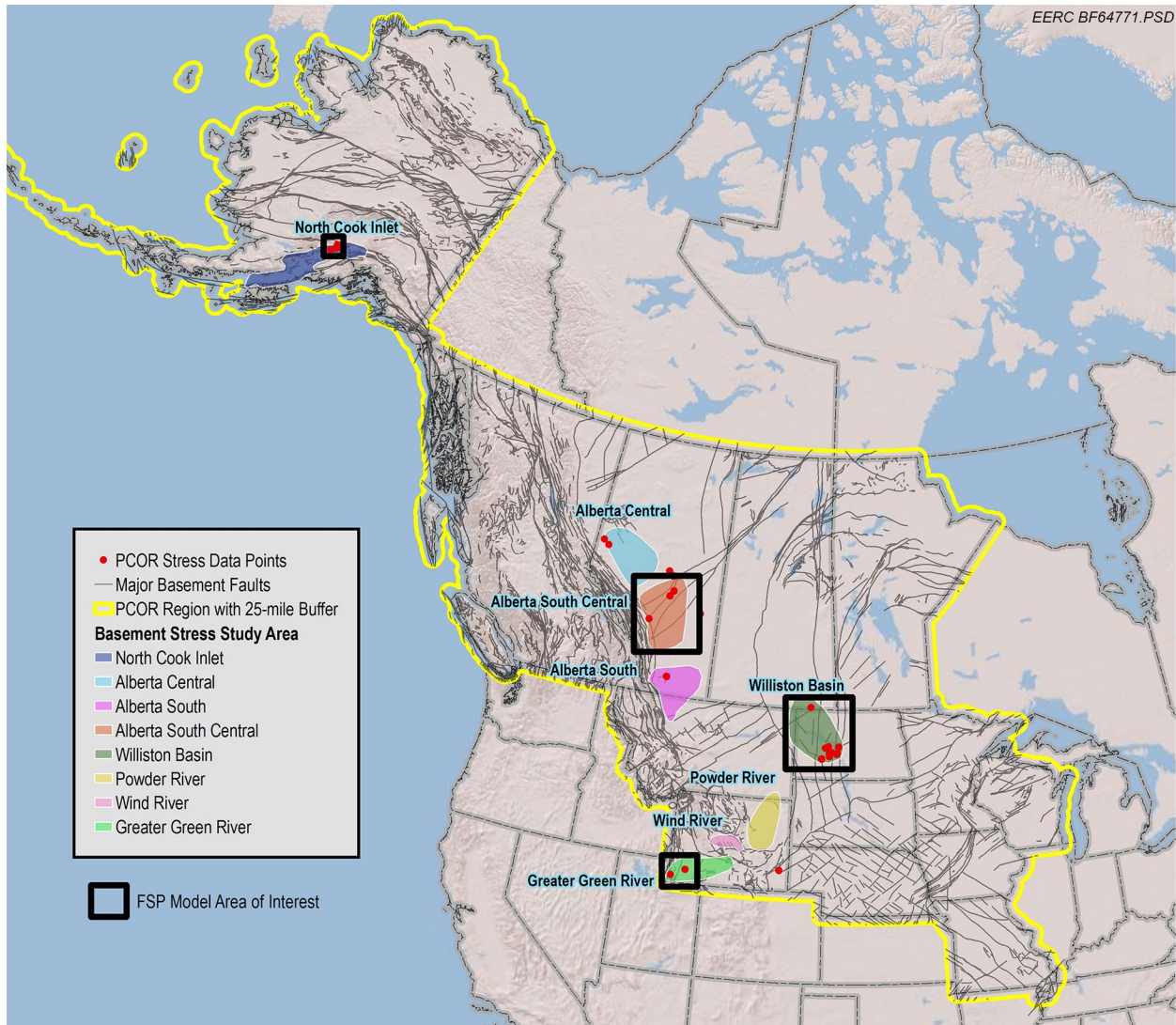


Figure 25. FSP model areas of interest (black rectangles) for the four high-graded stress focus areas and locations of stress data points illustrated in Figure 19.

Base case FSP input data and assumptions for each stress focus area model are summarized in Table 5. A sensitivity analysis to determine the relative importance of each base case input value for each area was carried out, based on ranges of uncertainty appropriate for each base case input parameter in Table 6, where the variability for each input parameter is captured.

Given the importance of selecting an appropriate friction coefficient (Table 5) for the FSP modeling as it pertains to shear failure and the relationship to internal friction angle (Table 5), we assume that shear failure in most rocks can be described by a linearized Mohr–Coulomb failure envelope with two parameters: internal friction angle (FA, μ_i) and UCS. The data set is plotted to fit a linearized Mohr–Coulomb failure line by using the peak stress and the confining stress at the failure onset. FA is related to the slope of the linear line, while UCS is related to the y-intercept.

Therefore, FA is one of the main strength parameters for rock matrix (Zoback, 2010). The linearized Mohr failure line can be written as:

$$\tau = S_0 + \mu_i \sigma_n \quad [\text{Eq. 3}]$$

where τ is the shear stress, σ_n is the effective normal stress, and S_0 is the cohesion.

On the other hand, the coefficient of friction was introduced to explain the relationship between two sliding rock surfaces. That is, frictional sliding on a plane will occur when the ratio of shear to normal stress reaches a material property of the material, μ , the coefficient of friction (Zoback 2010).

$$\mu = \frac{\tau}{\sigma_n} \quad [\text{Eq. 4}]$$

where τ is the shear stress resolved onto the sliding plane and σ_n is the effective normal stress resolved onto the sliding plane.

The coefficient of friction describes slip on a preexisting fault whereas FA is defined to describe the increase in strength of intact rock with pressure in the context of failure of an initially intact rock mass using the linearized Mohr–Coulomb failure criterion. Thus, the coefficient of friction and FA are explicitly different (Zoback 2010). However, when the cohesion is zero, Equations 3 and 4 become identical and the two coefficients have the same form. Although the relationship between the coefficient of friction and FA has not been clearly described in the literature, we assume that they have correlations to certain degrees. Additionally, data to measure the coefficient of friction are rarely available as compared to FA. Therefore, the coefficient of friction is often assumed to be 0.6. However, Byerlee (1967) demonstrates that the coefficient of friction value is between 0.6 and 0.85 and is dependent on loading conditions, e.g., high loading conditions tend to drive a linear trend versus low loading conditions, which drive data scatter.

This study uses FA values obtained from lab measurements instead of the generic value of 0.6 for the coefficient of friction for the reasons mentioned. The values (~ 0.94) from Table 5 might appear larger than the generic value of 0.6. However, it is important to note that real faults have non-zero cohesion, which makes these values plausible.

Table 5. Summarized FSP Base Case Input Data for Modeled Stress Focus Areas

Stress Focus Area → Input Data ↓	Williston Basin	Greater Green River	South Central Alberta	Northern Cook Inlet
Location	North Dakota, USA	Wyoming, USA	Alberta, Canada	Alaska, USA
Target Interval	Deadwood Formation	Flathead Formation	Basal Marine Sands Formation	Hemlock Formation
Target Interval Geologic Age	Cambrian	Cambrian	Cambrian	Eocene– Oligocene
Dominant Fault Regime	Normal	Strike-Slip	Strike-Slip	Strike-Slip
Vertical Stress Gradient, psi/foot	1.07	1.07	1.07	1.01
Maximum Horizontal Stress Gradient, psi/foot	0.94	1.69	1.07	1.47
Minimum Horizontal Stress Gradient, psi/foot	0.79	0.80	0.89	0.95
Maximum Horizontal Stress Azimuth, degrees from north	50	136	52	161
Initial Reservoir Pressure Gradient, psi/foot	0.45	0.45	0.52	Case 1: 0.71 Case 2: 0.43
Reference Depth, feet	10825	24850	6773	9771
Injection Zone Thickness, feet	180	200	154	305
Porosity, %	6.6	5.4	10.1	11.9
Permeability, mD	19.0	0.6	2.2	212.2
Number of Injection Wells	10	2	2	4
CO ₂ Injection Rate per Well, MTPA	1.0	1.0	1.0	2.32
Total CO ₂ Injection Rate, MTPA	10.0	2.0	2.0	9.3
Injection Period, year	2023–2043 (20 years)	2023–2043 (20 years)	2023–2043 (20 years)	2020–2050 (30 years)
Number of Fault Segments	14	77	13	2
Friction Coefficient	0.94	0.94	0.96	0.67
Average Friction Angle, deg	43.1	43.1	43.8	33.9
Fluid Density, kg/m ³	753.1	753.1	753.1	900
Fluid Dynamic Viscosity, Pa s	6.62e-05	6.62e-05	6.62e-05	9.5e-05
Fluid Compressibility, 1/Pa	1.0e-08	1.0e-08	1.0e-08	5.0e10-8
Rock Compressibility, 1/Pa	3.33e-11	3.33e-11	1.07e-10	Not reported

Table 6. FSP Model Base Case Input Data Sensitivity Analysis Variable Range (+ and -) in Percent

Stress Focus Area → Input Data ↓	Williston Basin	Greater Green River	South Central Alberta	Northern Cook Inlet
Vertical Stress Gradient, psi/foot	2.2	2.6	5.0	4.0
Maximum Horizontal Stress Gradient, psi/foot	3.8	36.1	10	1.0
Minimum Horizontal Stress Gradient, psi/foot	4.5	12.1	10	0.7
Maximum Horizontal Stress Direction, degrees from north	20	8.4	19.3	16
Initial Reservoir Pressure Gradient, psi/foot	5.8	5.8	10	1.4
Injection Zone Thickness, feet	100	100	100	17.8
Porosity, %	100	100	100	69.5
Permeability, mD	100	100	100	33.0
Friction Coefficient	3	3	8	1.7
Fluid Density, kg/m ³	10	10	10	Not reported
Fluid Dynamic Viscosity, Pa s	10	10	10	Not reported
Fluid Compressibility, 1/Pa	10	10	10	Not reported
Rock Compressibility, 1/Pa	10	10	10	Not reported
Fault Segment Strike	10	10	10	3
Fault Segment Dip	10	10	10	11

The Mohr–Coulomb sensitivity analysis study for each modeled stress focus area in Table 5 focused on two elements: the probabilistic geomechanical analysis of pore pressure to fault slip and the probabilistic hydrological analysis of pressure on faults. The geomechanical analysis addressed the key question of what differential pore pressure (CO₂ injection pressure) is required to slip a fault due to variable geomechanical base case input parameters, while the hydrological analysis addressed the key question of what differential pore pressure (CO₂ injection pressure) increases a fault would experience due to variable hydrological (CO₂ injection) inputs for each scenario.

Assumptions and technical basis common to each FSP Mohr–Coulomb critical stress analysis model included the following:

- Faults for each modeled stress focus area extracted from PCOR basement fault distribution (Figure 16).

- Simple faults or planes of weakness (POWs).
- Cohesion values of faults or POWs are zero (conservative).
- Internal friction angle values of faults (POWs) are based on offset analog data.
- The fluid phase of the supercritical CO₂ injection fluid remains constant during injection.
- All wells within each FSP model area are used for CO₂ injection.
- CO₂ injection rates are constant for the duration of the modeled time frame.
- Because of the limited availability of data for calibration, all injection wells have similar rock properties, pore pressure, and in situ stress conditions.
- Fault segments are input into the FSP model using coordinates of the starting and ending point, so each fault segment will be displayed and modeled as a straight line.
- Maximum horizontal stress direction is based on Lund-Snee (2020) and Levandowski and others (2022) (Figure 17).
- Summarized input stress data for each stress focus area (Tables 5 and 6) are based on available data.

Williston Basin Stress Focus Area (North Dakota, USA)

Figure 26 shows the 14 modeled basement fault segments and stress data locations, along with the base case maximum horizontal stress direction assumed for the model. The range in azimuths for basement faults across the area should be noted, which reflects multiple tectonic events throughout geologic time. Summarized stress calibration data and injection well locations (Table 5) are shown on the map. Figures 27–31 summarize the geomechanical and hydrological critical stress analysis of basement faults within the study area.

Figures 27 and 28 summarize the deterministic Mohr–Coulomb critical stress analysis of mapped faults using the FSP tool. Green indicates faults that are more stable (higher effective stress to failure), while orange and red indicate faults that are less stable (lower effective stress to failure) given geomechanical data inputs and assumptions.

A geomechanical sensitivity analysis was carried out to determine the probability of slip for each fault, reflected in Figures 29–31 and to determine which input parameters (Table 5) are most sensitive to fault slippage. Data input ranges for the sensitivity analysis are captured in Table 6 and depicted in Figure 30. Based on model inputs, the faults that are the most susceptible to slip (orange faults) have a 10% chance to slip with ~2800 psi of differential stress or a 90% chance to slip with ~3900 psi of differential stress (Figure 29). Table 7 summarizes ranked results of the geomechanical fault slip sensitivity analysis for the Williston Basin stress study area.

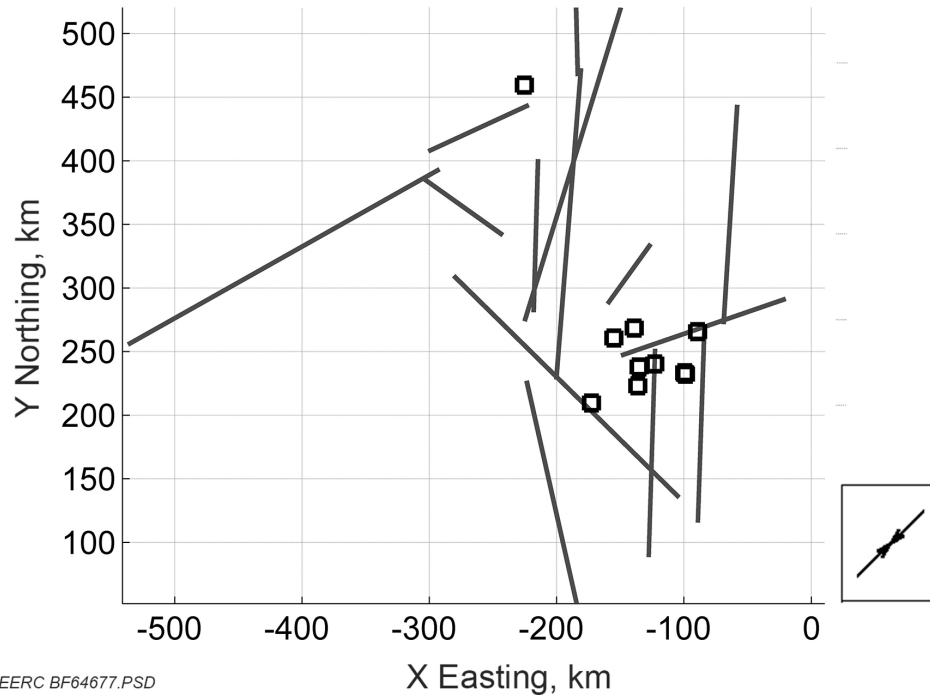


Figure 26. Williston Basin stress focus area FSP model input faults, stress data, and injection well locations. Well labels removed because of high density of well control. The maximum horizontal stress direction is northeast–southwest for the modeled area. Figure 25 depicts the area of interest.

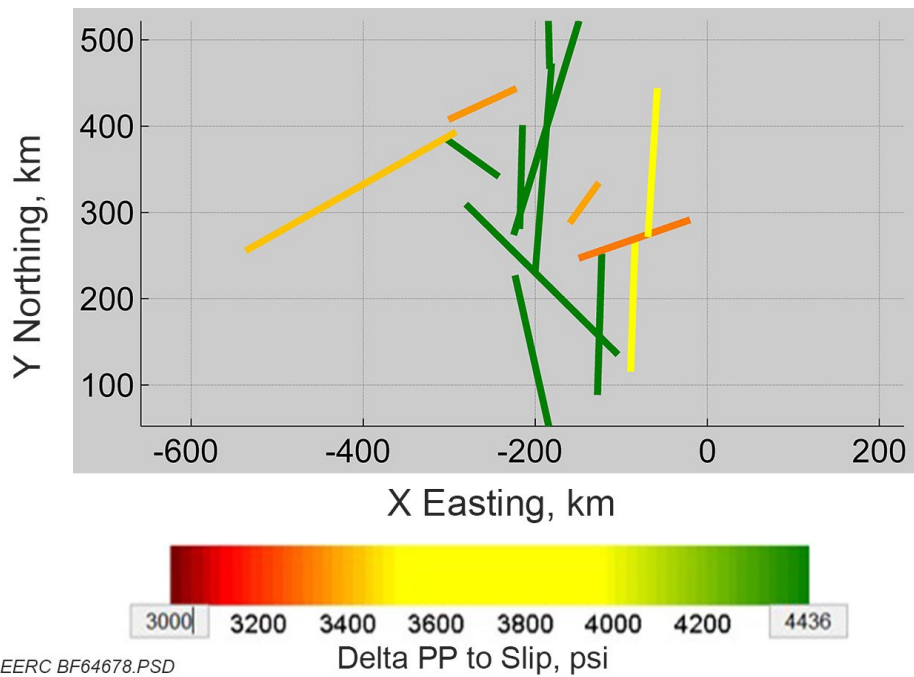


Figure 27. Williston Basin deterministic FSP model geomechanical critical stress analysis results. Green values indicate the fault is more stable, while red and orange values are less stable given geomechanical data inputs and assumptions. See Figure 25 for area of interest.

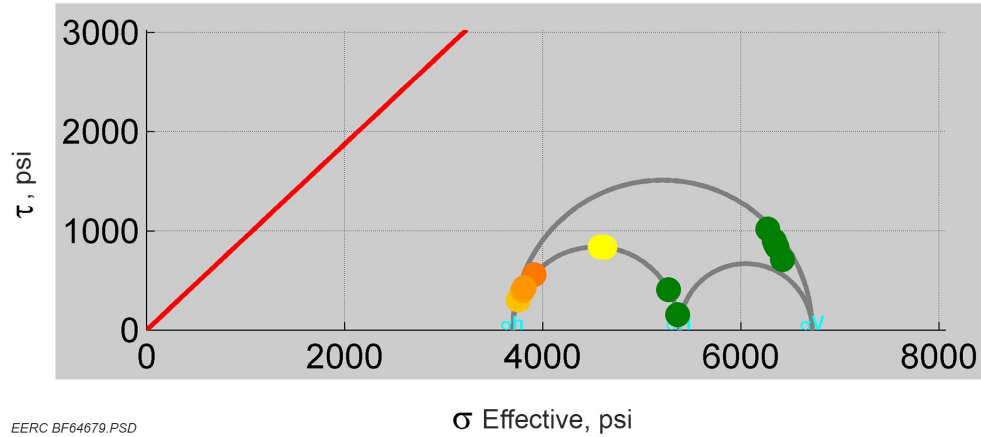


Figure 28. Williston Basin deterministic Mohr–Coulomb analysis of faults. The red line on the left indicates the edge of the fault failure envelope. Green dots indicate faults that are more stable vs. orange dots which indicate faults that are less stable.

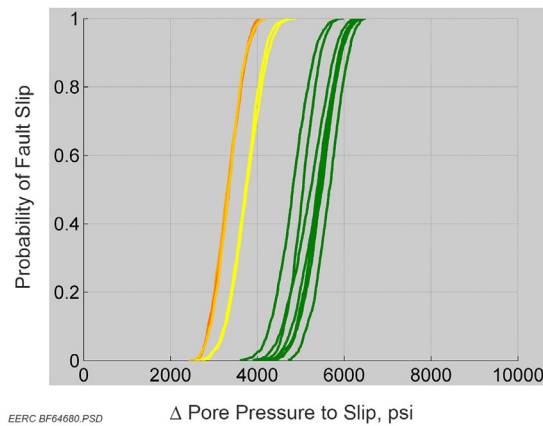


Figure 29. Williston Basin probability of slip for each fault assuming variability in inputs depicted in Figure 30.

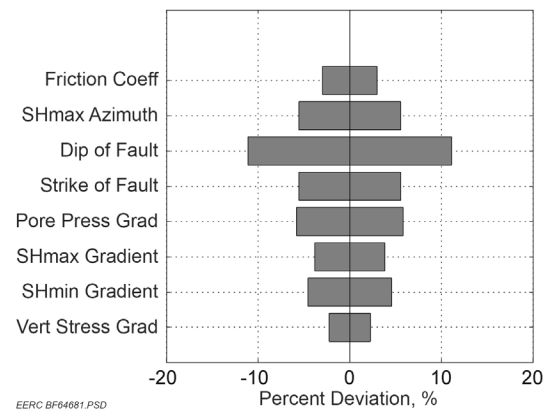


Figure 30. Williston Basin tornado plot of percent variability in base case parameter inputs for geomechanics sensitivity analysis.

Table 7. Williston Basin FSP Stress Focus Area Geomechanical Model Sensitivity Analysis Results by Sorted Rank

Sorted Rank	Base Case Input Parameters
1	Pore pressure gradient
2	Maximum horizontal stress azimuth
3	Minimum horizontal stress gradient
4	Fault strike
5	Fault dip
6	Maximum horizontal stress gradient
7	Friction coefficient
8	Vertical stress gradient

Figure 31 depicts the probability of pressure exceedance (e.g., pressure increase at the fault face) on all faults due to hydrological (CO₂ injection) factors in blue versus the pressure needed to slip each fault due to geomechanical factors in green. The width of each probability curve family (geomechanical vs. hydrological) reflects overall uncertainty for each factor. Results indicate that there is a 10% chance that one fault has achieved a maximum ~500-psi pressure response due to hydrological factors (blue) and a 90% chance that one fault requires a pressure of at least ~3800 psi to slip due to geomechanical factors (green). The probability distributions reflect the modeled project after 20 years of CO₂ injection.

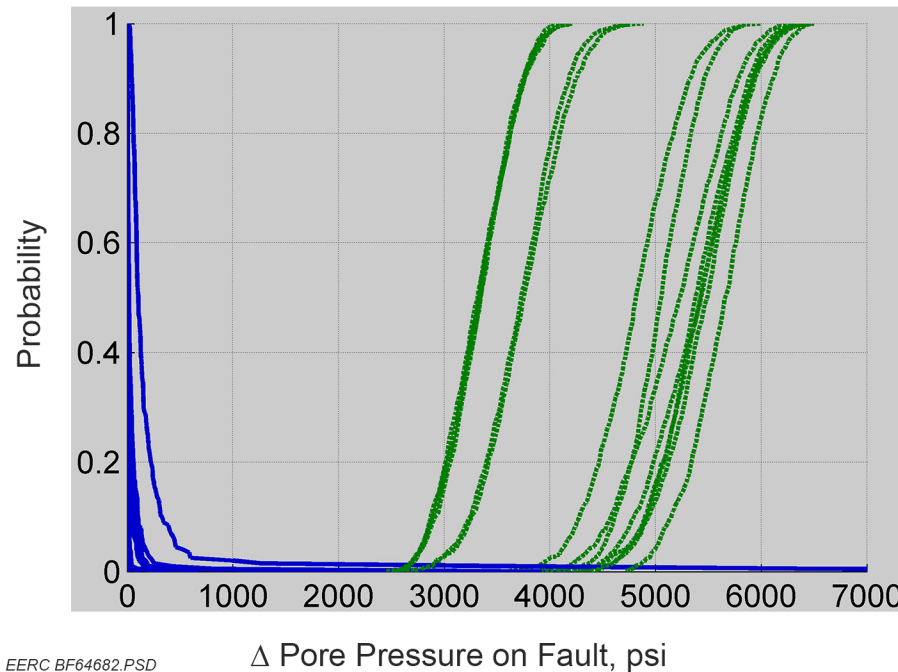


Figure 31. Probability distribution of pressure exceedance on all faults due to hydrological (CO₂ injection) factors in blue vs. pressure needed to slip each fault due to geomechanical factors in green after 20 years of CO₂ injection in the Williston Basin stress focus area.

The main results of geomechanical and hydrological deterministic and probabilistic critical stress analysis of basement faults within the Williston Basin FSP stress focus area are as follows:

- Pore pressure to slip each fault under given geomechanical inputs is higher (10% probability of ~2800 psi vs. 90% probability of ~6500 psi) than pore pressure increases due to hydrological (CO₂ injection) inputs.
- Uncertainties due to geomechanical input data are larger (i.e., wider, or more influential) than uncertainties due to hydrological (injection) input data (Figure 31).
- Given the base case CO₂ injection rate of 1 million tonnes per annum (MTPA) per well, the potential to slip faults is not determined by injection well location or the number of

injection wells (hydrological input or human-controlled factors); however, it is determined predominantly by the geomechanical factors pore pressure, maximum horizontal stress azimuth, and minimum horizontal stress gradient (natural factors).

- Increased CO₂ injection rates above base case values used in the model may impact results.

Greater Green River Stress Focus Area (Wyoming, USA)

Figure 32 shows the 77 modeled basement fault segments and stress data locations along with the maximum horizontal stress direction assumed for the model. The range in azimuths for basement faults across the area are relatively consistent, which reflects the dominant and most recent Laramide orogeny thick-skinned tectonic deformation event (Schwartz and others, 2023) that impacted this region. Summarized stress calibration data and injection well locations are identified sequentially, W1, W2, etc. Figures 33–37 summarize the geomechanical and hydrological critical stress analysis of basement faults within the study area.

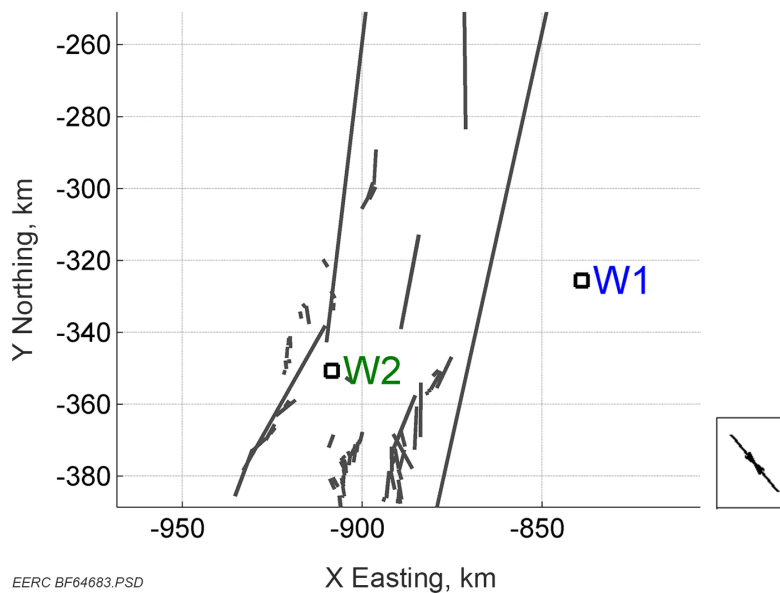


Figure 32. Greater Green River stress focus area FSP model input faults, stress data, and injection well locations. The maximum horizontal stress direction is northwest–southeast for the modeled area. See Figure 25 for area of interest.

Figures 33 and 34 summarize the deterministic Mohr–Coulomb critical stress analysis of mapped faults, using the FSP tool. Green indicates faults that are more stable (higher effective stress to failure), while orange and yellow indicate faults that are less stable (lower effective stress to failure) given geomechanical data inputs and assumptions.

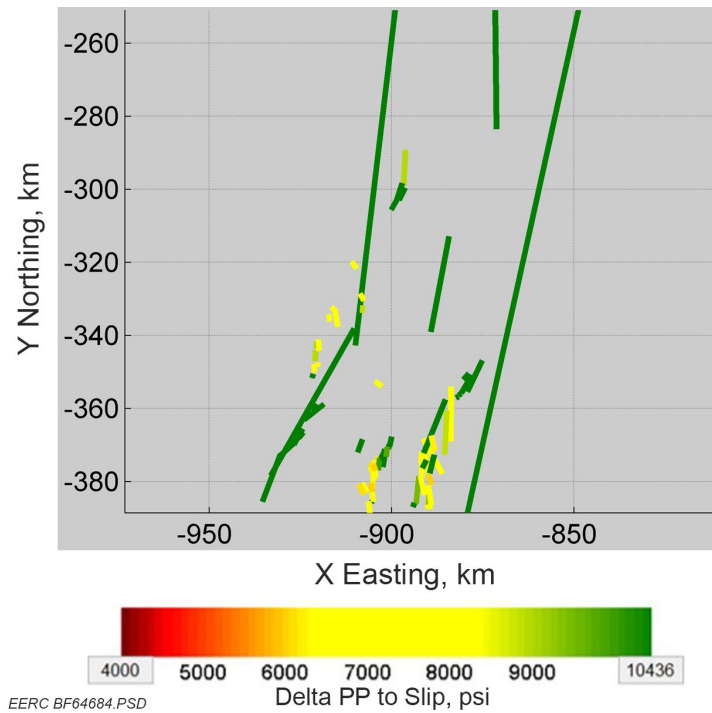


Figure 33. Greater Green River deterministic FSP model geomechanical critical stress analysis results. Green values indicate the fault is more stable vs. yellow and orange values which are less stable given geomechanical data inputs and assumptions. See Figure 25 for area of interest.

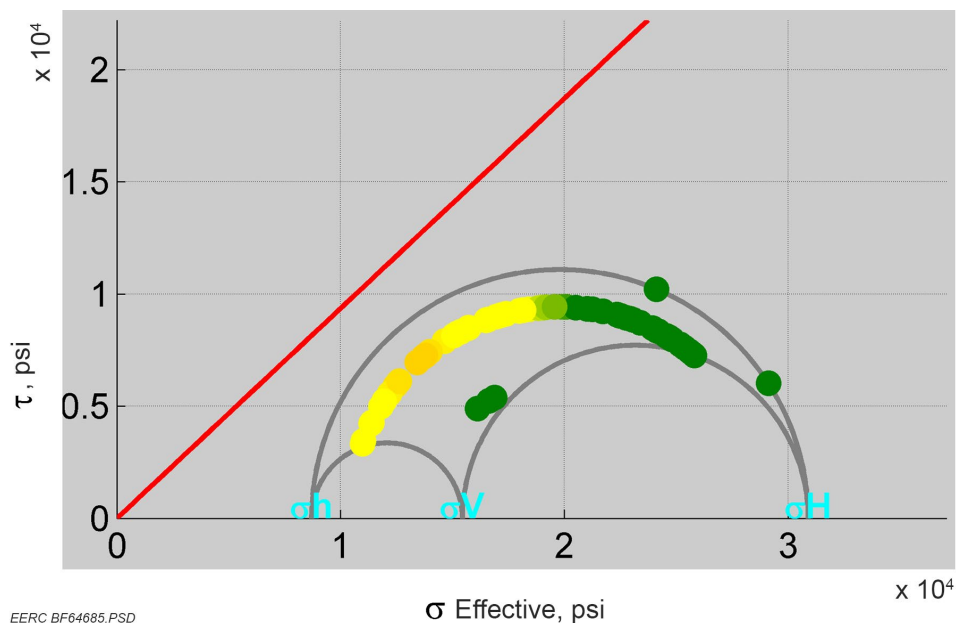


Figure 34. Greater Green River deterministic Mohr–Coulomb analysis of faults. The red line on the left indicates the edge of the fault failure envelope. Green dots indicate faults that are more stable vs. yellow and orange dots that are less stable.

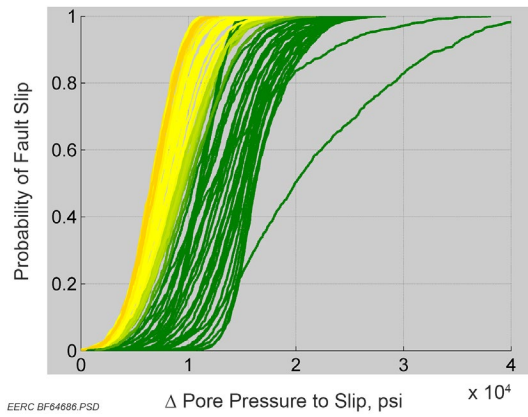


Figure 35. Greater Green River probability of fault slip assuming variability in inputs depicted in Figure 36. The x-axis scale is 10^4 psi.

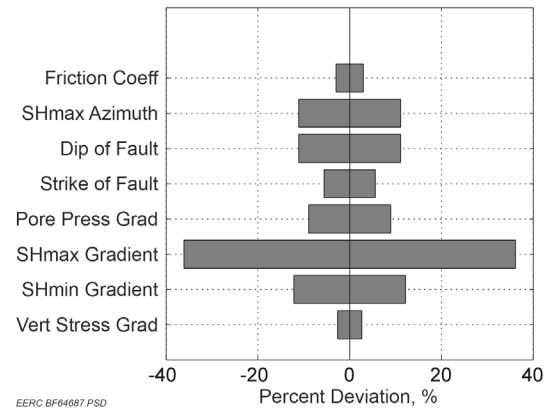


Figure 36. Greater Green River tornado plot showing percent variability in base case parameter inputs for geomechanics sensitivity analysis.

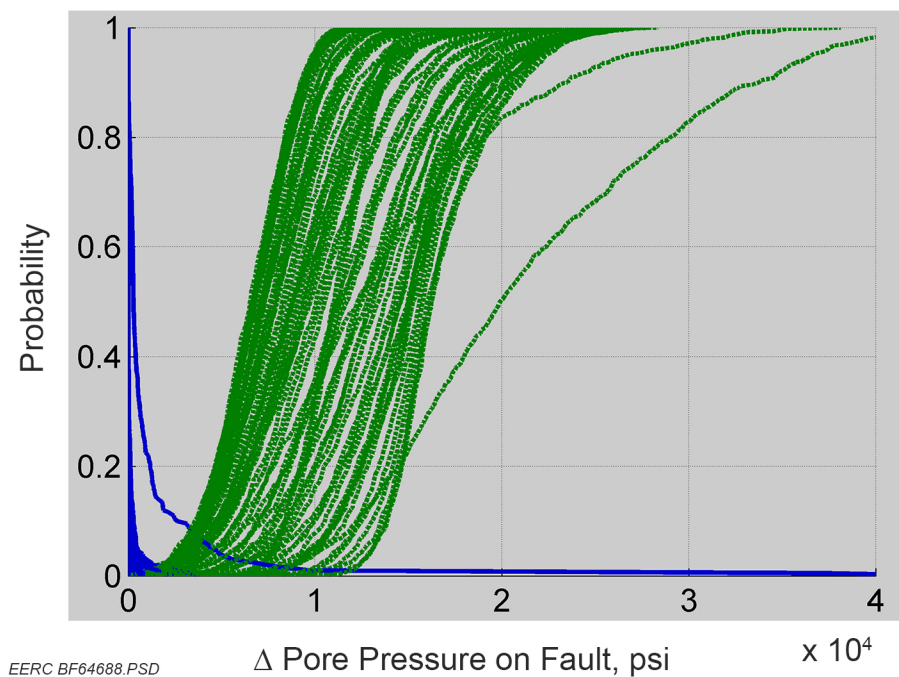


Figure 37. Probability distribution of pressure exceedance on all faults due to hydrological (CO_2 injection) factors in blue vs. pressure needed to slip each fault due to geomechanical factors in green after 20 years of CO_2 injection in the Greater Green River stress focus area.

A geomechanical sensitivity analysis was carried out to determine the probability of slip for each fault reflected in Figures 32–34 and to determine which input parameters (Table 5) are most sensitive to fault slippage. Data input ranges are captured in Table 6 and illustrated in Figure 36. Based on model inputs, faults that are most susceptible to slip (orange faults) have a 10% chance

of slipping with ~4000 psi of differential stress and a 90% chance of slipping with ~9000 psi of differential stress (Figure 35). Table 8 summarizes ranked results of the geomechanical fault slip sensitivity analysis for the Greater Green River stress study area.

**Table 8. Greater Green River Stress Focus Area FSP
Geomechanical Model Sensitivity Analysis Results by Sorted Rank**

Sorted Rank	Base Case Input Parameters
1	Maximum horizontal stress azimuth
2	Maximum horizontal stress gradient
3	Fault strike
4	Minimum horizontal stress gradient
5	Fault dip
6	Pore pressure gradient
7	Vertical stress gradient
8	Friction coefficient

Figure 37 depicts the probability of pressure exceedance (e.g., pressure increase at the fault face) on all faults due to hydrological (CO₂ injection) factors in blue versus the pressure needed to slip each fault due to geomechanical factors in green. The width of each probability curve family (geomechanical vs. hydrological) reflects overall uncertainty for each factor. Results indicate that there is a 10% chance that one fault has achieved a maximum ~2000 psi pressure response due to hydrological factors (blue) and a 90% chance that one fault requires a pressure of at least ~9000 psi to slip due to geomechanical factors (green). The probability distributions reflect the modeled project after 20 years of CO₂ injection.

The main results of geomechanical and hydrological deterministic and probabilistic critical stress analysis of the basement faults within the Greater Green River stress focus FSP study area include the following:

- Pore pressure to slip each fault under given geomechanical inputs is higher (1000~25,000 psi) than pore pressure increases due to hydrological (CO₂ injection) inputs for each scenario.
- Uncertainties due to geomechanical input data are larger (i.e., wider, or more influential) than uncertainties due to hydrological (CO₂ injection) input data (Figure 37).
- Given the base case CO₂ injection rate of 1 MTPA per well, the potential to slip faults is not determined by injection well location or the number of injection wells (hydrological input or human-controlled factors); however, it is determined predominantly by geomechanical factors maximum horizontal stress azimuth, maximum horizontal stress gradient, and fault strike (natural factors).
- Increased CO₂ injection rates above base case values used in the model may impact results.

South Central Alberta Stress Focus Area (Alberta, Canada)

Figure 38 shows the 13 modeled basement fault segments and stress data locations along with the maximum horizontal stress direction assumed for the model. The range in azimuths for the basement faults on the west are relatively consistent, which reflects the dominant and most recent Laramide orogeny thick-skinned tectonic deformation event (Schwartz et al., 2023) that impacted this region. The northeast–southwest-striking faults on the east represent the Virgin River Tectonic Zone that is part of the Snowbird Tectonic Zone which separates the Rae and Hearne tectonic domains (Figure 11). The Virgin River and Snowbird fault systems are interpreted as shear zones. Summarized stress calibration data and injection well locations are labeled sequentially, W1, W2, etc. Figures 39–43 summarize the geomechanical and hydrological critical stress analysis of basement faults within the study area.

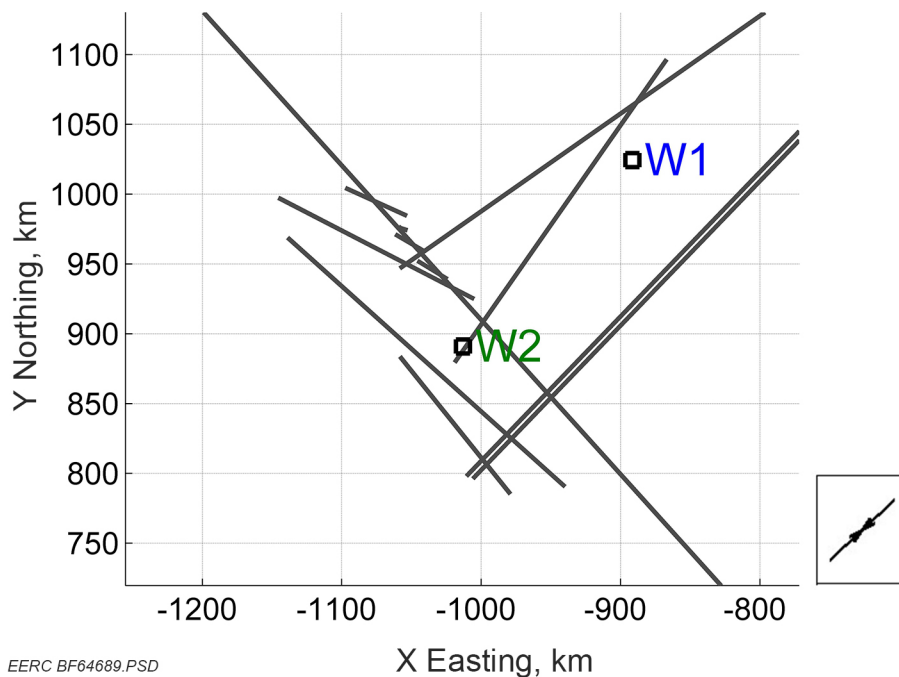


Figure 38. South Central Alberta stress focus area FSP model input faults, stress data, and injection well locations. The maximum horizontal stress direction is northeast–southwest for the modeled area. See Figure 25 for area of interest.

Figures 39 and 40 summarize the deterministic Mohr–Coulomb critical stress analysis of mapped faults, using the FSP tool. Green indicates faults that are more stable (higher effective stress to failure), while the red and orange indicate faults that are less stable (lower effective stress to failure) given geomechanical data inputs and assumptions.

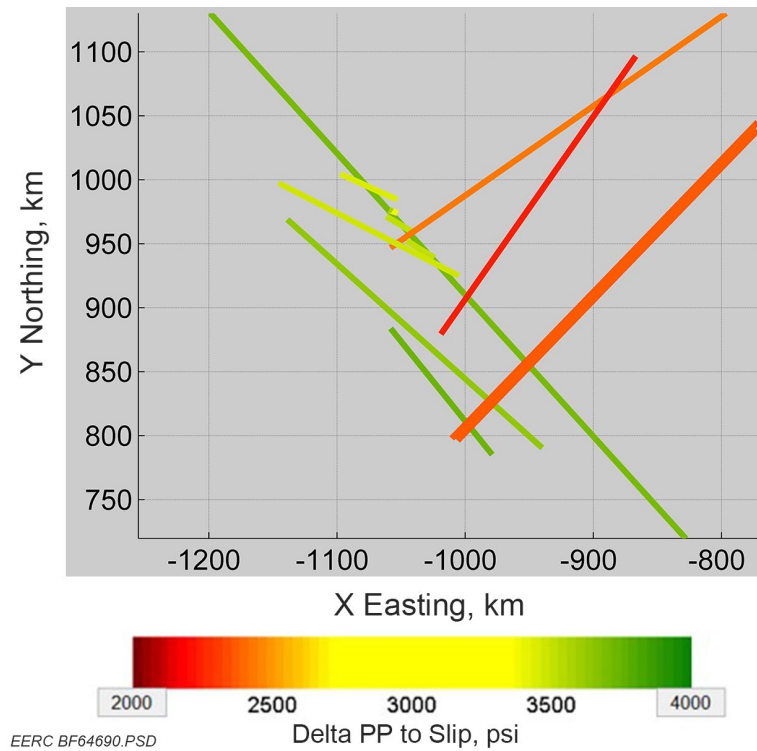


Figure 39. South Central Alberta deterministic FSP model geomechanical critical stress analysis results. Green values indicate the fault is more stable vs. red values which indicate the fault is less stable given geomechanical data inputs and assumptions. See Figure 25 for area of interest.

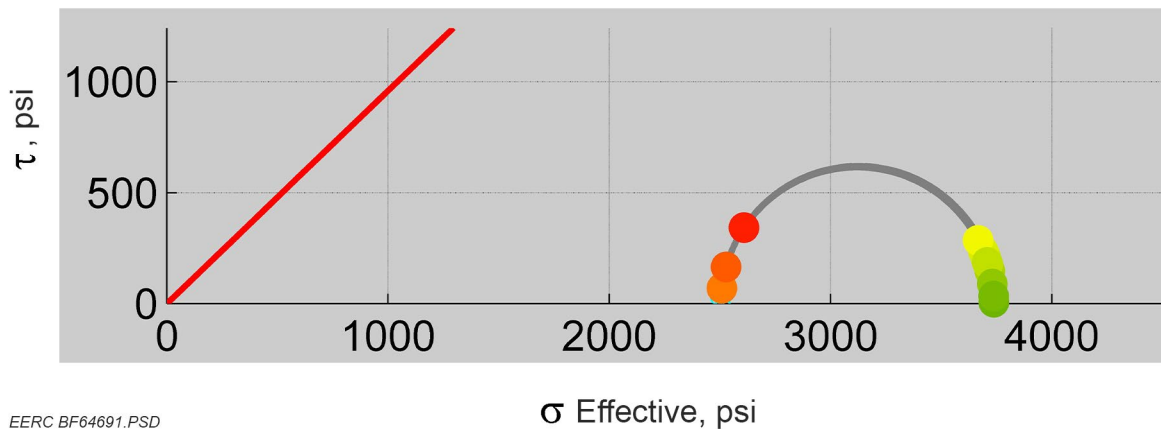


Figure 40. South Central Alberta deterministic Mohr-Coulomb analysis of faults. The red line on left indicates the edge of the fault failure envelope. Green and yellow dots indicate faults that are more stable (higher effective stress to failure) vs. two superimposed red dots which indicate faults that are less stable (lower effective stress to failure).

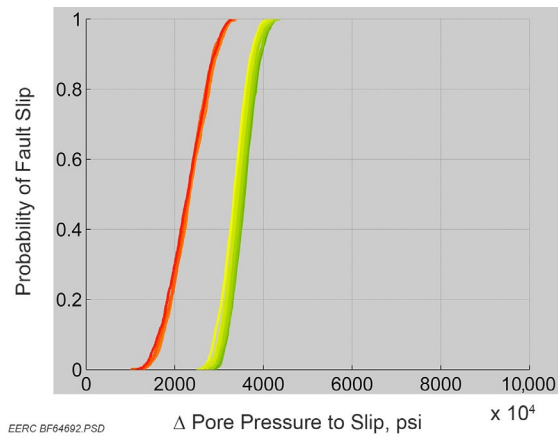


Figure 41. South Central Alberta probability of fault slip assuming variability in inputs depicted in Figure 42.

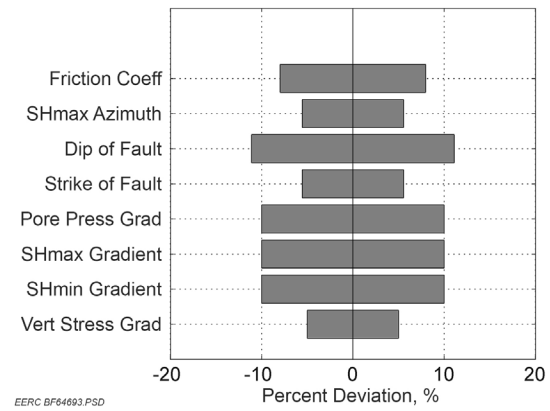


Figure 42. South Central Alberta tornado plot showing percent variability in base case parameter inputs for geomechanics sensitivity analysis.

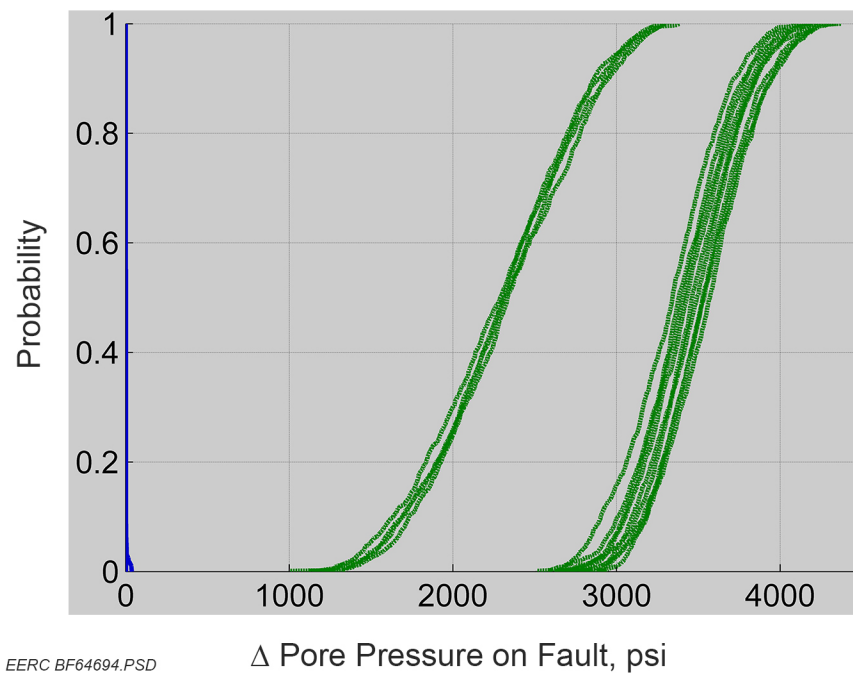


Figure 43. Probability distribution of pressure exceedance on all faults due to hydrological (CO₂ injection) factors in blue vs. pressure needed to slip each fault due to geomechanical factors in green after 20 years of CO₂ injection in the South Central Alberta stress focus area.

A geomechanical sensitivity analysis was carried out to determine the probability of slip for each fault reflected in Figures 38–41 and to determine which input parameters (Table 5) are most sensitive to fault slippage. Data input ranges are captured in Table 6 and illustrated in Figure 42. Based on the model inputs, faults that are most susceptible to slip (red faults) have a 10% chance of slipping with ~1900 psi of differential stress and a 90% chance of slipping with

~3000 psi of differential stress (Figure 43). Table 9 summarizes ranked results of the geomechanical fault slip sensitivity analysis for the South Central Alberta stress study area.

**Table 9. South Central Alberta Stress Focus Area FSP
Geomechanical Model Sensitivity Analysis Results by Sorted Rank**

Sorted Rank	Base Case Input Parameters
1	Pore pressure gradient
2	Vertical stress gradient
3	Minimum horizontal stress gradient
4	Maximum horizontal stress gradient
5	Fault strike
6	Maximum horizontal stress azimuth
7	Fault dip
8	Friction coefficient

The main results of geomechanical and hydrological deterministic and probabilistic critical stress analysis of the basement faults within the South Central Alberta stress focus FSP study area include the following:

- Pore pressure to slip each fault under given geomechanical inputs is higher (1000~1500 psi) than pore pressure increases due to hydrological (CO₂ injection) inputs for each scenario.
- Uncertainties due to geomechanical input data are larger (i.e., wider, or more influential) than uncertainties due to hydrological (CO₂ injection) input data (Figure 43).
- Given the base case CO₂ injection rate of 1 MTPA per well, the potential to slip faults is not determined by injection well location or the number of injection wells (hydrological input or human-controlled factors); however, it is determined predominantly by geomechanical factors pore pressure gradient, vertical stress gradient, and minimum horizontal stress gradient (natural factors).
- Increased CO₂ injection rates above base case values used in the model may impact results.

Northern Cook Inlet Stress Focus Area (Nicolai Creek Field, Alaska, USA)

Figure 44 shows the two modeled basement fault segments and stress data locations. The range in azimuths for the basement faults across the area is relatively consistent, which reflects the dominant and active tectonics that impact this region. Summarized stress calibration data and injection well locations are labeled sequentially, W1, W2, etc. Figures 45–47 summarize the geomechanical and hydrological critical stress analysis of basement faults within the study area. Two pore pressure scenarios were modeled – Case 1, which assumes an in situ (pre-hydrocarbon production) pore pressure gradient of 0.71 psi/foot and Case 2, which assumes a depleted reservoir

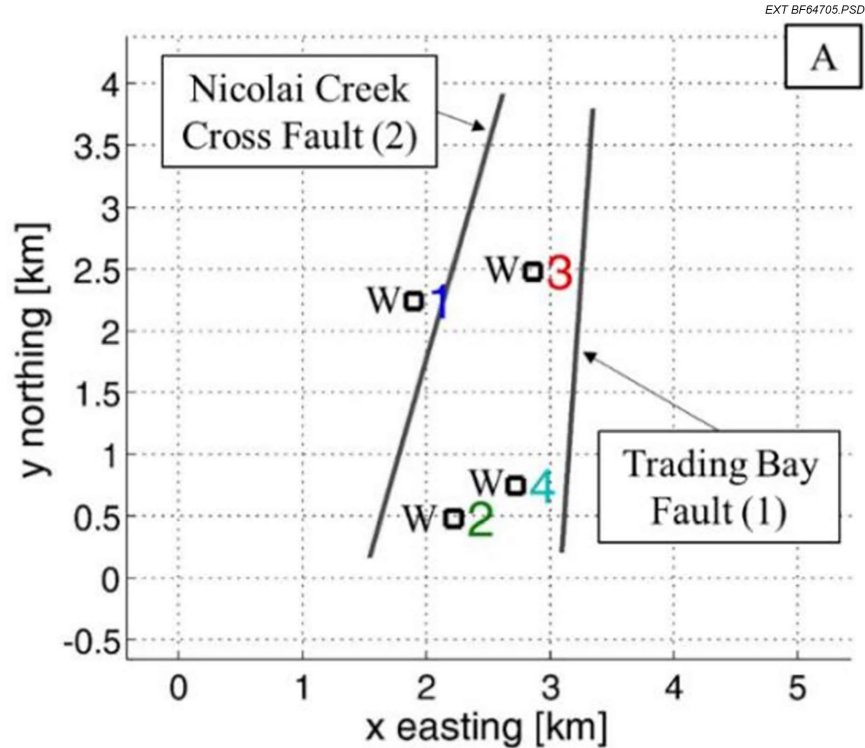


Figure 44. Northern Cook Inlet stress focus area (Nicolai Creek Field) FSP model input faults and stress data locations (Pantaleone, 2020). The maximum horizontal stress azimuth is 16 degrees for the modeled area. See Figure 25 for area of interest.

with a hydrostatic pore pressure gradient of 0.43 psi/foot (Table 7). Given the legacy oil and gas production from the field, Scenario 2 is more consistent with actual subsurface stress conditions.

Figure 45 summarizes the deterministic Mohr–Coulomb critical stress analysis of mapped faults using the FSP tool. Green indicates faults that are more stable (higher effective stress to failure), while orange and yellow indicate faults that are less stable (lower effective stress to failure) given an increase in pressure resulting from CO₂ injection. Two pore pressure scenarios were modeled: Case 1 assumes an original elevated overpressure gradient of 0.71 psi/foot and Case 2 assumes a hydrostatic gradient of 0.43 psi/foot related to a depleted hydrocarbon-bearing zone in the Nicolai Creek Field.

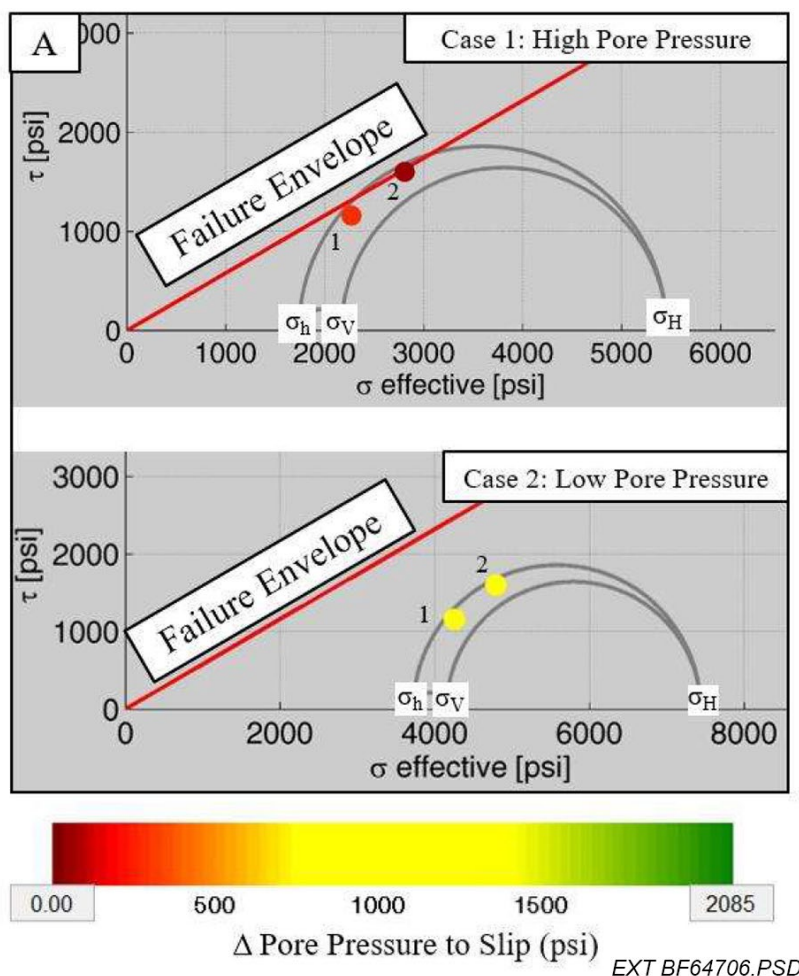


Figure 45. Northern Cook Inlet deterministic FSP model geomechanical critical stress analysis results (Pantaleone, 2020). The red line on the left indicates the edge of the fault failure envelope. Yellow dots indicate faults that are more stable vs. red dots which indicate faults that are less stable.

A geomechanical sensitivity analysis was carried out to determine the probability of slip for each fault reflected in Figures 44 - 46 and to determine which input parameters (Table 5) are most sensitive to fault slippage. Data input ranges are captured in Table 6 and illustrated in Figure 47. Based on the model inputs and assuming the high pore pressure gradient scenario, the dark red fault is most susceptible to slip, with a 20% chance of slipping with ~100 psi of differential stress and a 90% chance of slipping with ~800 psi of differential stress (Figure 46, Case 1), while the low (hydrostatic gradient) pore pressure gradient scenario reflects much more stable faults (Figure 46, Case 2). The two modeled faults in the low pore pressure scenario have a 10% chance of slip with ~2000 psi of differential stress and a 90% chance of slip with ~2800 psi of differential stress (Figure 46, Case 2). A ranked sensitivity analysis summary of base case geomechanical input criteria impacting fault slip for the Nicolai Creek Field was not reported.

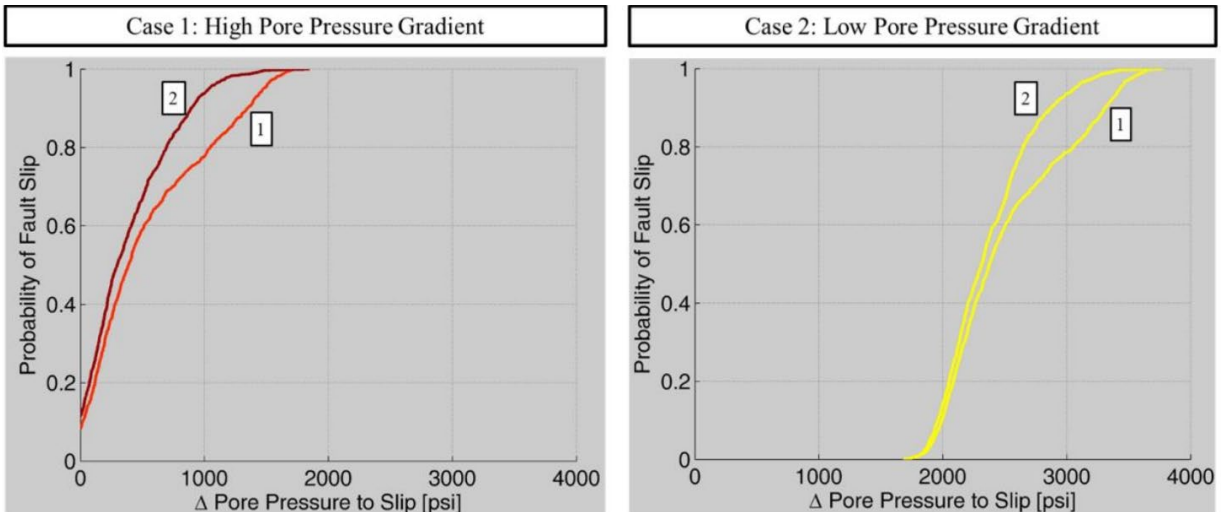


Figure 46. The probability of geomechanical fault slip as a function of pore pressure increases on each fault segment for Case 1 on left (overpressure) and Case 2 on right (hydrostatic pore pressure) for the northern Cook Inlet (Pantaleone, 2020).

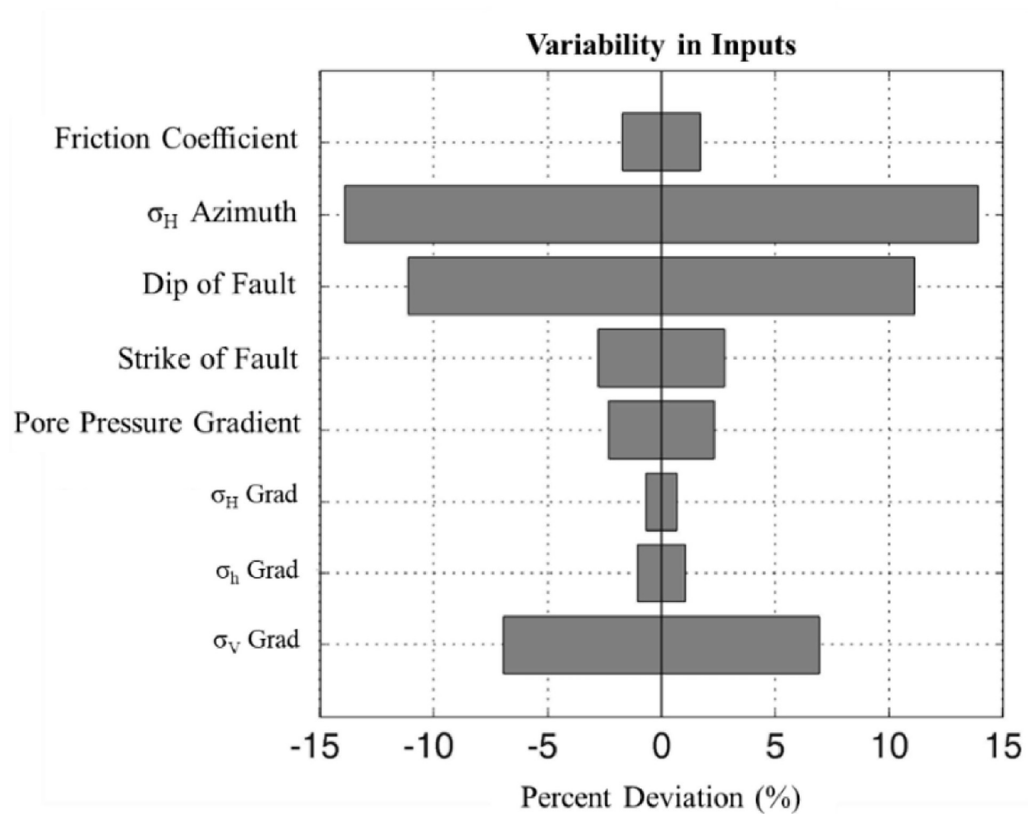


Figure 47. Northern Cook Inlet tornado plot showing percent variability in geomechanical base case parameter inputs for sensitivity analysis (Pantaleone, 2020).

Figure 48 depicts the probability of pressure exceedance (e.g., pressure increase at the fault face) on the two modeled faults due to hydrological (CO₂ injection) factors. The fault slip probability curves from Figure 46 are depicted and represent the pressure increase value after 30 years of CO₂ injection (blue vertical curve). In Case 1 (high pore pressure gradient scenario, 0.71 psi/foot), Fault 1 has a 20% cumulative probability of fault slip after 30 years of CO₂ injection and Fault 2 has a 27% cumulative probability of fault slip. In Case 2 (hydrostatic pore pressure gradient scenario, 0.43 psi/foot), both faults have a 0% cumulative probability of fault slip because the fault probability curve is at a higher pressure and does not intercept with the pressure exceedance curve.

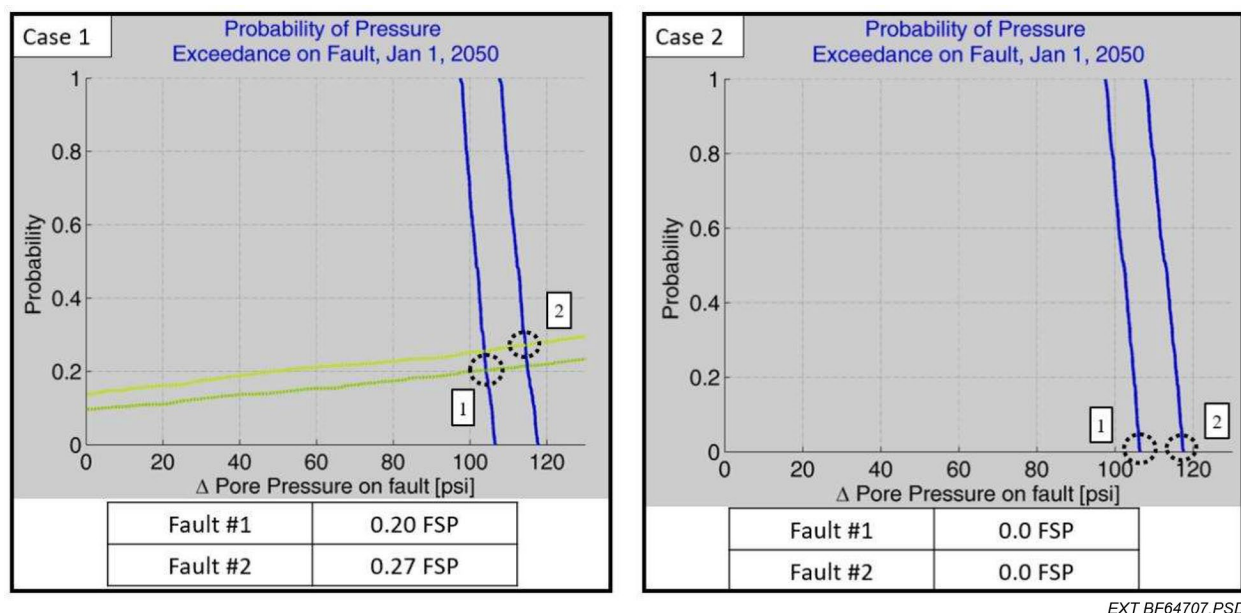


Figure 48. Northern Cook Inlet probability distribution of pressure exceedance for faults (light green colors) after 30 years of CO₂ injection due to hydrological factors (Pantaleone, 2020). Blue lines represent pressure increase for each fault after 30 years of CO₂ injection. Case 1 assumes an elevated 0.71-psi/foot pore pressure gradient, while Case 2 assumes normal pressure gradient of 0.43 psi/foot.

Main results of geomechanical and hydrological deterministic and probabilistic critical stress analysis of the basement faults within the northern Cook Inlet (Nicolli Creek Field) stress focus FSP study area are as follows:

- Pore pressure to slip each fault under given geomechanical inputs is higher (~0–1700 psi for the overpressured case vs. ~1900–3600 psi for the normally pressured case) than pore pressure increases due to hydrological (CO₂ injection) inputs for each scenario.
- Uncertainties due to geomechanical input data are larger (i.e., wider, or more influential) than uncertainties due to hydrological (CO₂ injection) input data (Figures 46 and 48).

- For the depleted Case 2 which more accurately reflects present-day conditions and given the base case CO₂ injection rate of 2.32 MTPA for each well, the necessary pore pressure to slip faults is not determined by injection well location or number of injection wells (hydrological input or human-controlled factors); however, it is determined predominantly by geomechanical or natural factors.
- Increased CO₂ injection rates above base case values used in the model may impact results.

GEOMECHANICS OBSERVATIONS OF SECONDARY STRESS FOCUS AREAS

As previously discussed, the remaining four identified stress focus areas were either devoid or had minimal stress calibration data available that would allow critical stress analysis FSP modeling to be carried out. Based on results of the FSP modeling carried out across the four high-graded stress focus areas, general observations can be made that will be important to consider in the future, should stress data become available for detailed analyses.

Alberta Central and Alberta South Stress Focus Areas

The stress focus areas (Figure 19) located in Alberta, Canada, are situated in the present-day tectonic foredeep on the east side of the Laramide-aged Canadian Rocky Mountains, which comprises the Alberta sedimentary basin. The Laramide tectonic event is associated with thick-skinned deformation, which has impacted basement. The region is very active with existing and planned carbon storage industry activity (Figure 20). The stress focus areas are all situated in the deepest part of the foredeep, and the western margins of the areas are situated geographically close to the Laramide deformation front, which has experienced recent seismic activity (Figure 21). Of particular interest is the Alberta South Central stress focus area where the Virgin River and Snowbird Tectonic Zone transects the area in a general east–northeast–west–southwest-striking direction, creating complex faulting in the subsurface. Additionally, all three stress focus areas in Alberta, Canada, were encompassed by the geologically recent glacial event (~18,000 ma), which has elevated stresses that persist in the subsurface as discussed above. The present-day stress regime across the foredeep region is largely strike-slip, which suggests that the maximum horizontal stress is greater than the vertical stress and the minimum horizontal stress. This is important because given a constant CO₂ injection rate, fault stability will tend to be controlled by both the fault azimuth with respect to the maximum horizontal stress direction and the maximum horizontal stress gradient. Accurate mapping of faults along with acquisition of stress calibration data will be necessary to confidently predict the risk of fault slip in site-specific areas of interest.

Powder River and Wind River Stress Focus Areas

The two stress focus areas (Figure 19) located in Wyoming, USA, are situated within and adjacent to the Laramide-aged Rocky Mountains. The Laramide tectonic event is associated with thick-skinned deformation, which has impacted basement. The Wind River area is situated southwest of the Powder River area and has experienced the impact of Laramide-aged tectonism to a greater extent than the Powder River area. Both areas are very active regarding existing and

planned carbon storage activities, with the main present-day industry focused on CO₂ injection related to EOR of existing oil fields situated across both areas and including the Greater Green River stress focus area to the southwest. Both areas including the Greater Green River area are situated far south of the maximum extent of the ~18,000 ma glacial event, which manifests an overall lower present-day stress regime, e.g., normal stress regime is dominant throughout the area, but strike-slip regimes are also present because of the proximity of the region to the Laramide-aged tectonic event.

SITE-SPECIFIC WORKFLOW – GEOMECHANICS ANALYSIS OF FAULTS

For areas where a site-specific analysis of existing faults and associated fractures is required to determine the likelihood of slippage in response to increases in pore pressure resulting from CO₂ or other fluid injection, the following is a recommended and scalable geological static approach, as the existence and nature of faults and fractures in the subsurface are controlled by tectonic and structural history, subsurface stress, stratigraphy, and lithology:

- Carry out regional assessment of tectonic regime based on available literature, legacy studies, etc., placing the study area within the context of the tectonic framework.
- Carry out a 3D and/or 2D seismic interpretation and integration of available well control to interpret faults and fault architecture that leads to a kinematically correct structural framework (Bond and others, 2007; Krantz and Neely, 2016). Assessing the distribution and orientation of faults relative to the stress field is critical for characterizing the hazard of fault reactivation and managing possible induced seismicity (Zoback, 2012; Ellsworth, 2013; Underground Injection Control National Technical Workgroup, 2015; Huarng and others, 2017; Hennings and others, 2019)
- Develop a constrained static geomechanical model to analyze rock deformation and behavior, based on static Young's modulus, Poisson's ratio, friction angle, and unconfined compressive strength (UCS) lab-derived rock analysis data. Use the UCS data to constrain SH_{max} during the stress polygon analysis (Moos and Zoback, 1990). When calibration data are not available, consider a range of reasonable data ranges based on offset data, analogs, and knowledge of stratigraphy and lithology.
- Consider mechanical stratigraphy (Ferrill and others, 2017; Bradley and Mostafavi, 2021) relationships, based on the geomechanics rock strength mechanical earth model, so interpretations of preferential zones to fracturing can be determined.
- Use stress and strain values derived from 3D kinematic modeling and/or geomechanical modeling steps to develop proxies for fracture intensity and orientation. If warranted, prepare a discrete fracture network (DFN) of the major fracture systems using appreciable shear deformation (Zoback, 2010; Lei and others, 2017; Dershowitz and others, 2004). Integrate with direct borehole measurements such as formation microimager (FMI) image logs (or similar wellbore data) interpretations or other underground measurements to constrain the fracture model. Develop realistic and data-constrained multiple scenarios.

- Carry out fault analysis to determine the likelihood of concerns with fault juxtaposition between the candidate CO₂ injection zone and permeable zones (Grant, 2019; Allan, 1989; Clarke and others, 2005); use results to risk and rank candidate CO₂ zones and regions.
- Carry out a static critical stress and risk analysis of candidate faults/associated fracture sets and orientations that may fail in response to elevated pore pressure in response to CO₂ injection, given the dominant SH_{max} direction, Sh_{min}, SH_{max}, and other pertinent geomechanics calibration values. Faults that are oriented more favorably for slip in the stress field tend to be more permeable because of dilation (Barton and others, 1995).
- Calibrate results with available data such as the North America stress map, microseismic data, induced seismicity events, and regional structure mapping and analyses.
- Finalize interpretation and consider uncertainty and the range of outcomes.

This method can be adapted for different data types and availability and for addressing specific technical concerns. Results from this recommended approach can also be imported into dynamic simulation models for additional insight and analysis.

KEY MESSAGES – CO₂ STORAGE IN BASAL RESERVOIRS

- Faulting and fracturing associated with reactivated basement faults in tectonically active regions can be common in basal reservoirs, particularly the geomechanically stronger intervals, leading to a higher risk of fault slippage and related induced seismicity in response to fluid injection (CO₂, produced water disposal, fracture fluids, etc.).
- In these examples, geomechanical factors versus hydrological factors are generally more impactful to mitigating the risk of fault slip in basal reservoir carbon storage areas. Robust and well-calibrated geomechanical models are necessary to understand these factors and to reduce uncertainty of results.
- The critical technical factors to understand and reduce uncertainty of geomechanical modeling results include pore pressure gradient, vertical stress gradient, maximum horizontal stress gradient, minimum horizontal stress gradient, maximum horizontal stress azimuth, fault dip, fault strike, and fault friction coefficient. Although these factors are not prioritized in order of importance, within the PCOR region, the most important factors vary by geological region, demonstrating the importance of accessing robust and high-quality data and carrying out site-specific geological and geomechanical evaluations.
- Because of the proximity of basal reservoirs to the stressed basement and crust, stress transfer can take place along basement-rooted faults that extend into the overburden, particularly in PCOR basins that have seen recent tectonism. This phenomenon is recognized and described in the literature, but it is difficult to model. As a result of the stress transfer, these reactivated faults can therefore be hydraulically connected to shallower CO₂ injection zones.

- Understanding the dominant fault regime is important for robust critical stress analysis evaluations and characterizing the change of fault slip in response to CO₂ injection.
- Appropriate and robust wellbore and laboratory-derived stress data from core and calibrated integrated mechanical earth model interpretations are necessary to carry out geomechanical critical stress analysis of faults and to reduce uncertainty. However, unless core has been taken of a fault, rock strength laboratory results are only proxies for fault rock properties.
- CO₂ injection can cause changes in pore pressure that can cause induced seismicity. The likelihood of higher magnitude seismicity increases anytime injection is hydraulically connected to optimally oriented basement faults.
- Given results of the static geomechanical characterization for each stress focus area, decreased CO₂ injection rates along with careful selection of injection well locations versus basement fault locations are effective methods to mitigate the risk of fault slip in basal reservoir injection zones.
- High-quality 3D and 2D seismic data, integrated with available well control and potential fields (gravity and magnetics) data, are a recommended approach to characterize basement faults that may prove critical to the design and location of a carbon storage sites and associated injection wells.
- More research is required in thermally induced stress effects due to cooler CO₂ being injected into storage reservoirs, which is generally agreed in the literature to reduce fracture gradient of the storage reservoir or confining zone, potentially reducing CO₂ storage capacity (Andrianov and others, 2023; Goodrazi, 2015). Also, there are research results showing the opposite phenomena such as increasing CO₂ injectivity (Jiang and others, 2017). To properly assess the impact of thermally induced stress in response to CO₂ injection in site-specific areas, advanced dynamic geomechanical modeling coupled with temperature and pressure is required.

REFERENCES

- Adler, F.J., 1987, Mid-Continent COSUNA (Correlation of Stratigraphic Units of North America): American Association of Petroleum Geologists, <https://store.aapg.org/>.
- Alberta Geological Survey, 2023, Alberta Energy Regulator, <https://geology-ags-aer.opendata.arcgis.com/> (accessed August 2023).
- Allan, U.S., 1989, Model for hydrocarbon migration and entrapment within faulted structures: AAPG Bulletin, v. 73, p. 803–811.
- Anderson, F.J., 2016, North Dakota earthquake catalog (1870–2015): North Dakota Geological Survey MS-93.
- Anderson, E.M., 1951, The dynamics of faulting and dyke formation with applications to Britain: Edinburgh and London, Oliver, and Boyd, 206 p.

- Andrianov, N., Geological Survey of Denmark, and Greenland (GUES), Amour, F., Hajiabadi, R., Nick, H.M., and Haspang, M.P., 2023, Coupled CO₂ injection well flow model to assess thermal stresses under geomechanical uncertainty: Society of Petroleum Engineers, doi: 10.2118/212235-MS.
- Angelier, J., 1979, Determination of the mean principal directions of stresses for a given fault population: *Tectonophysics*, v. 56, no. 3–4, p. T17–T26, doi:10.1016/0040-1951(79)90081-7.
- Ballard, W., Bluemle, J., and Gerhard, L., 1983, Northern Rockies and Williston Basin COSUNA (Correlation of Stratigraphic Units of North America): American Association of Petroleum Geologists.
- Barton, C.A., Zoback, M.D., and Moos, D., 1995, Fluid flow along potentially active faults in crystalline rock: *Geology*, v. 23, no. 8, p. 683–686, doi:10.1130/0091-7613(1995)023<0683.
- Bartos, T.T., Galloway, D.L., Hallberg, L.L., Dechesne, M., Diehl, S.F., and Davidson, S.L., 2021, Geologic and hydrogeologic characteristics of the White River Formation, Lance Formation, and Fox Hills Sandstone, northern greater Denver Basin, southeastern Laramie County, Wyoming: U.S. Geological Survey Scientific Investigations Report 2021–5020, 219 p., 1 pl., <https://doi.org/10.3133/sir20215020> (accessed August 2023).
- Bayley, R.W., and Muehlberger, W.R., 1968, Basement rock map of the US, exclusive of AK and HI: U.S. Geological Survey, https://ngmdb.usgs.gov/Prodesc/proddesc_66043.htm (accessed August 2023).
- Bergstrom, D.J., and Morey, G.B., 1985, Northern Mid-Continent COSUNA (Correlation of Stratigraphic Units of North America): American Association of Petroleum Geologists.
- Bond, C.E., Gibbs, A.D., Shipton, Z.K. and Jones, S., 2007, What do you think this is? “conceptual uncertainty in geoscience interpretation: *GSA Today*, v. 17, no. 11, doi: 10.1130/GSAT01711A.1.
- Bradley, R., and Mostafavi, V., 2021, Mechanical stratigraphy modeling, the foundation of unconventional geomechanical analysis, *in* Unconventional Resources Technology Conference, July 2021, URTeC: 5153, doi: 10.15530/urtec-2021-5153.
- Brown, D.L., and Brown, D.L., 1987, Wrench-style deformation and paleostructural influence on sedimentation in and around a cratonic basin, in Longman, W., ed., Williston Basin— anatomy of a cratonic oil province: 1987 Rocky Mountain Association of Geologists Symposium, p. 433–440.
- Burberry, C.M., Swiatlowski, J.L., Searls M.L., and Filina, I., 2018, Joint and lineament patterns across the midcontinent indicate repeated reactivation of basement-involved faults: *Geosciences*, v. 8, p. 215.

- Byerlee, J.D., 1967, Frictional characteristics of granite under high confining pressure: *Journal of Geophysical Research*, v. 72, no. 14, p. 3639–3848.
- Carlson, C.G., and Anderson, S.B., 1965, Sedimentary and tectonic history of the ND part of Williston Basin: *American Association of Petroleum Geologists Bulletin*, v. 49, no. 11, p. 1833–1846.
- Castillo, D.A., and Zoback, M.D., 1994, Systematic variations in stress state in the southern San Joaquin Valley—inferences based on well-bore data and contemporary seismicity: *American Association of Petroleum Geologists Bulletin*, v. 78, no. 8, p. 1257–1275, doi:10.1306/A25FEAC7-171B-11D7-8645000102C1865D.
- Chalaturnyk, R.J., 2007, Geomechanical characterization of the Weyburn Field for geological storage of CO₂: *American Rock Mechanics Association, Proceedings*, arma-07-198.
- Chorlton, L.B., 2007, Generalized geology of the world: bedrock domains and major faults in GIS format—a small-scale world geology map with an extended geological attribute database: *Geological Survey of Canada Open File 5529*, 48 p., 1 CD ROM, <https://doi.org/10.4095/223767> (accessed August 2023).
- Cipolla, C.L., Liu, D., and Kyte, D.G., 1994, Practical application of in situ stress profiles: *Society of Petroleum Engineers, SPE 28607*.
- Clarke, S.M., Burley, S.D., and Williams, G.D., 2005, A three-dimensional approach to fault seal analysis—fault-block juxtaposition and argillaceous smear modeling: *Basin Research*, v. 17, p. 269–288, doi: 10.1111/j.1365-2117.2005.00263.x.
- Cui, Y., Miller, D., Schiarizza, P., and Diakow, L.J., 2017, British Columbia digital geology: British Columbia Ministry of Energy, Mines, and Petroleum Resources, British Columbia Geological Survey Open File 2017-8, 9 p., data version 2019-12-19, www2.gov.bc.ca/gov/content/industry/mineral-exploration-mining/59british-columbia-geological-survey/geology/bcdigitalgeology (accessed August 2023).
- Dershowitz, W.S., LaPointe, P.R., and Doe, T.W., 2004, Advances in discrete fracture network modeling: *Proceedings of the US EPA/NGWA fractured rock conference*, Portland, Oregon, p. 882–894.
- Dicken, C.L., Pimley, S.G., and Cannon, W.F., 2001, Precambrian basement map of the northern midcontinent, U.S.A.—a digital representation of the 1990 P.K. Sims map: *U.S. Geological Survey Open-File Report 01-021*, <https://doi.org/10.3133/ofr0121> (accessed August 2023).
- Domrois, S.L., 2013, The Midcontinent exposed—Precambrian basement topography, and fault and fold zones, within the cratonic platform of the United States: M.S. Thesis, Urbana, Illinois.
- Ekpo, E., Eaton, D., and Weir, R., 2017, Basement tectonics and fault reactivation in Alberta based on seismic and potential field data: *Geophysics*, December 20, DOI: 10.5772/intechopen.72766.

- Ellsworth, W.L., 2013, Injection-induced earthquakes, *Science* 341, no. 6142, 1225942, doi: 10.1126/science.1225942.
- Ferrill, D.A., Morris, A.P., McGinnis, R.N, Smart, K.J., Wiggington, S.S. and Hill, N.J., Mechanical stratigraphy and normal faulting, *Journal of Structural Geology*, vol. 94, p. 275–302.
- Filina, I., Guthrie, K., Searly, M., and Burberry, C.M, 2018, Seismicity in Nebraska and adjacent states—the historical perspective and current trends: *The Mountain Geologist*, v. 55, no. 4, p. 217–229, December.
- Garrrity, C.P., and Soller, D.R., 2005, Database of the geologic map of North America—adapted from the map by J.C. Reed, Jr. and others, 2005: U.S. Geological Survey data series 424, <https://pubs.er.usgs.gov/publication/ds424> (accessed August 2023).
- Gerhard, L.C., Fischer, D.W., and Anderson, S.B., 1990, Petroleum geology of the Williston Basin, *in* Leighton, M.W., Kolata, D.R., Oltz, D.F., and Eidel, J.J., eds., *Interior cratonic basins: American Association of Petroleum Geologists Memoir 51*, chapter 29.
- Gifford, N.J., Malone, S.J., and Mueller, P.A., 2020, The medicine hat block and the early Paleoprotozoic assembly of western Laurentia: *Geosciences*, v. 10, no. 271, doi:10.3390/geosciences10070271.
- Global CCS Institute, 2023, Facilities database, <https://co2re.co/FacilityData> (accessed March 2023).
- Goodrazi, S., Settari, A. Zoback, M.D., and Keith, D.W., 2015, Optimization of a CO₂ storage project based on thermal, geomechanical and induced fracturing effects: *Journal of Science and Engineering*, v. 134, p. 49–59.
- Grant, N., 2019, Stochastic modelling of fault gouge zones: implications for fault seal analysis: *Geological Society, London, Special Publications*, v. 496, p. 163–197, <https://doi.org/10.1144/SP496-2018-135>.
- Gregersen, L.S., and Shellenbaum, D.P., 2016, Top mesozoic unconformity subcrop map, Cook Inlet Basin, Alaska: Alaska Division of Geological & Geophysical Surveys Report of Investigation 2016-4, 1 sheet, scale 1:500,000, <https://doi.org/10.14509/29658>.
- Guthrie, K., 2018, Analysis of subsurface faults in Nebraska from earthquakes and potential fields: Undergraduate thesis, University of Nebraska-Lincoln, 72 p., data not used.
- Hasterok, D., Halpin, J., Hand, M., Collins, A., Kreemer, C., Gard, M.G., and Glorie, S., 2022, New maps of global geologic provinces and tectonic plates (revised): *Earth Science Reviews*, preprint available (EarthArXiv) <https://doi.org/10.31223/X5TD1C>.
- Heck, T.J., 1988, Precambrian structure map of North Dakota: North Dakota Geological Survey misc. map no. 30.

- Heidbach, O., Rajabi, M., Cui, X., Fuchs, K., Muller, B., Reindecker, J., Reiter, K., Tingay, M., Wenzel, F., Xie, F., Ziegler, M.O., Zoback, M-L., and Zoback, M., 2018, The world stress map database release 2016—crustal stress pattern across scales: *Tectonophysics*, v. 744, p. 484–498, doi:10.1016/j.tecto. 2018.07.007.
- Hennings, P.H., Lund Snee, J.-E, Osmond, J.L., DeShon, H.R., Dommissie, R., Horne, E. Lemons, C., and Zoback, M.D. 2019, *Bulletin of the Seismological Society of America*, doi: 10.1785/0120190017.
- Hoffman, P., 1989, Tectonic domains for the basement of the Western Canada Sedimentary Basin, based largely on interpretation of potential field data and Upb geochronology of selected samples of basement, Figure 4.1, <https://ags.aer.ca/atlas-the-western-canada-sedimentary-basin/chapter-4-potential-fields-and-basement-structure> (accessed August 2023).
- Huang, Y., W. L. Ellsworth, and G. C. Beroza (2017). Stress drops of induced and tectonic earthquakes in the central United States are indistinguishable, *Sci. Adv.* 3, no. 8, e1700772, doi: 10.1126/sciadv.1700772
- Jacoby, W.R., 1970, Instability in the upper mantle and global plate movements: *Geology*, v. 75, no. 29.
- Jaeger, J.C., Cook, N.G.W., and Zimmerman, R.W., 2009, *Fundamentals of rock mechanics*: John Wiley & Sons, 488 p.
- Jiang, T., Pekot, L.J., Jin, L., Peck, W.D., Gorecki, C.D., and Worth, K., 2017, Numerical modeling of the Aquistore CO₂ storage project: *Energy Procedia*, v. 114, p. 4886–4895. doi: 10.1016/j.egypro.2017.03.1630.
- Kent, H., Couch, E., and Knepp, R., 1988, Central and southern Rockies COSUNA (Correlation of Stratigraphic Units of North America): American Association of Petroleum Geologists.
- Krantz, B. and Neely, T. 2016, Subsurface Structural Interpretation: The Significance of 3-D Structural Frameworks *in* B. Krantz, C. Ormand, and B. Freeman, eds., 3-D structural interpretation: Earth, mind, and machine: AAPG Memoir 111, p. 91–109.
- LeFever, J.A., LeFever, R.D., and Nordeng, S.H., 2011, Revised nomenclature for the Bakken Formation (Mississippian–Devonian), North Dakota, *in* Robinson, J.W., LeFever, J.A., and Gaswirth, S.B. [eds.], *The Bakken–Three Forks petroleum system in the Williston Basin: Rocky Mountain Association of Geologists Guidebook*, p. 11–26.
- Lei, Q., Latham, J.-P., and Tsang, C.-F., 2017, The use of discrete fracture networks for modelling coupled geomechanical and hydrological behaviour of fractured rocks: *Computers and Geotechnics*, v. 85, p. 151–176.
- Levandowski, W.B., Herrmann, R.B., Briggs, R.W., Boyd, O.S., and Gold, R.D., 2022, An updated stress map of the continental U.S. reveals heterogeneous intraplate stress: U.S. Geological Survey data release, <https://doi.org/10.5066/P9BA1104>.

- Lund, K., Box, S.E., Holm-Denoma, C.S., San Juan, C.A., Blakely, R.J., Saltus, R.W., Anderson, E.D., and DeWitt, E.H., 2015, Basement domain map of the conterminous United States and Alaska: U.S. Geological Survey Data Series 898, 41 p., <https://dx.doi.org/10.3133/ds898> (accessed August 2023).
- Lund-Snee, J.-E., 2020, State of stress in North America—seismicity, tectonics, and unconventional energy development: Doctoral dissertation, Department of Geophysics, Stanford University, March 2020.
- Lund-Snee, J.-E., and Zoback, M.D., 2020, Multiscale variations of the crustal stress field throughout North America: *Nature Communications*, v. 11, p. 1951, doi:10. 1038/s41467-020-15841-5.
- Lund-Snee, J.-E., and Zoback, M., 2022, State of stress in area of active unconventional oil and gas development in North America, *AAPG Bulletin*, v. 106, no. 2 (February 2022), pp. 355–385.
- Lund-Snee, J.-E., and Zoback, M.D., 2018, State of stress in the Permian Basin, Texas, and New Mexico—implications for induced seismicity: *Leading Edge*, v. 37, no. 2, p. 127–134, doi:10.1190/tle37020127.1.
- Manitoba Geological Survey, 2023, Geoscientific maps gallery, https://rdmaps.gov.mb.ca/Html5Viewer/index.html?viewer=MapGallery_Geology.MapGallery (accessed August 2023).
- Marshak, S., Domrois, S. Abert, C., and Larson, T., 2016, DEM of the Great Unconformity, USA, cratonic platform, <https://databank.illinois.edu/datasets/IDB-7546972> (accessed August 2023).
- Marshak, S., Domrois, S., Abert, C., Larson, T., Pavlis, G., Hamburger, M., Yang, X., Gilbert, H., and Chen C., 2017, The basement revealed—tectonic insight from a digital elevation model of the Great Unconformity, USA, cratonic platform: *Geology*, May 2017, v. 45, no. 5, p. 391–394.
- McCormick, K.A., 2010, Precambrian basement terrane of South Dakota: Department of Environmental and Natural Resources, South Dakota Geological Survey Bulletin 41.
- Miller, M.B., 2023, Structural geology notes, <https://pages.uoregon.edu/millerm/faults.html> (accessed August 2023).
- Miskimins, J.L., Hurley, N.F. and Graves, R.M., 3D stress characterization from hydraulic fracture and borehole breakout data in a faulted anticline, Wyoming: *Society of Petroleum Engineers*, SPE 71341.
- Moos, D., and Zoback, M.D., 1990, Utilization of observations of wellbore failure to constrain the orientation and magnitude of crustal stresses—application to continental, Deep Sea Drilling Project, and Ocean Drilling Program boreholes: *Journal of Geophysical Research*, v. 95, p. 9305–9325.

- Mossop, G.D., and Shetsen, I., compilers, 1994, Geological atlas of the Western Canada Sedimentary Basin from Price and others, 1984: Canadian Society of Petroleum Geologists and Alberta Research Council, ISBN 0-920230-53-9.
- Muehlberger, W.R., 1996, Tectonic map of North America: American Association of Petroleum Geologists, 4 plates.
- Nakamura, K., and Uyeda, S., 1980, Stress gradient in arc-back arc regions and plate subduction: *Journal of Geophysical Research*, v. 85, p. 6419–6428.
- North Dakota Division of Mineral Resources, 2023, Class VI – geologic sequestration well permits, www.dmr.nd.gov/dmr/oilgas/ClassVI (accessed August 2023).
- Nunn, J.A., 1985, State of stress in the northern Gulf Coast: *Geology*, v. 13, p. 429–432, doi:10.1130/0091-7613(1985)13<429: SOSITN>2.0.CO;2.
- Orowan, E., 1964, Continental drift and the origin of mountains: *Science*, v. 146, no. 3647, p. 1003–1010, doi:10.1126/science.146.3647.1003.
- Ozkan, A., 2001, Diagenesis and porosity evolution of the flathead sandstone (Middle Cambrian), Wyoming and Montana, Master of Science Thesis, University of Texas at Austin, 189 p.
- Pantaleone, S., 2020, Integrated analysis of carbon sequestration potential and risks of fault slip in the Cook Inlet Basin, Alaska: M.S. thesis, University of Alaska Anchorage, May 2020.
- Peska, P., and Zoback, M.D., 1995, Compressive and tensile failure of inclined well bores and determination of in situ stress and rock strength: *Journal of Geophysical Research: Solid Earth*, v. 100, no. B7, p. 12791–12811, doi:10.1029/95JB00319.
- Richardson, R.M., 1992, Ridge forces, absolute plate motions, and the intraplate stress field: *Journal of Geophysical Research*, v. 97, no. B8, p. 11,739–11,748, doi:10.1029/91JB00475.
- Robertson, E.P., 2022, CO₂ enhanced oil recovery in Wyoming—2020 update: Enhanced Oil Recovery Institute Bulletin, no. 2202/2022, Casper, Wyoming, Enhanced Oil Recovery Institute.
- Ross, G., and Villeneuve, M., 2003, Provenance of the Mesoproterozoic (1.45 Ga) Belt basin (western North America)—another piece in the pre-Rodinia paleogeographic puzzle: *Geological Society of America Bulletin*, v. 115, 10.1130/B25209.1.
- Saskatchewan Ministry of Energy and Resources, 2023, <https://gisappl.saskatchewan.ca/Html5Ext/index.html?viewer=GeoAtlas> (accessed August 2023).
- Schaff, R.G., and Gilbert, W.G., 1987, Southern Alaska COSUNA (Correlation of Stratigraphic Units of North America), American Association of Petroleum Geologists.

- Schwartz, J.J., Lackey, J.S., Miranda, E.A., Klepeis, K.A., Mora-Klepeis, G., Robles, F. and Klepeis, J.D., Magmatic surge requires two-stage model for the Laramide orogeny. *Nature Communications* 14, 3841 (2023). <https://doi.org/10.1038/s41467-023-39473-7>.
- Shaver, R.H., 1985, *Midwestern Basins and Arches COSUNA (Correlation of Stratigraphic Units of North America)*, American Association of Petroleum Geologists.
- Shultz, S., 2019, Late Mesozoic reactivation of the Snowbird tectonic zone and the resulting effects on the stratigraphic architecture of the Viking Formation: Canadian Society of Petroleum Geologists Structural Division Luncheon, December 2019.
- Simpson, R.W., 1997, Quantifying Anderson's fault types: *Journal of Geophysical Research*, v. 102, no. B8, p. 17909–17919, doi:10.1029/97JB01274.
- Sims, P.K., and Peterman, Z.E., 1986, Early Proterozoic central plains orogen—a major buried structure in the north-central United States: *Geology*, v. 14, p. 488–491.
- Sims, P.K., O'Neil, J.M., Bankey, V., and Anderson, E.D., 2004, Precambrian basement geologic map of Montana – an interpretation of aeromagnetic models: *Scientific investigations map* 2829, v 1.0.
- Sims, P.K., Saltus, R.W., and Anderson, E.D., 2008, Precambrian basement structure of the continental United States – an interpretation of geologic and aeromagnetic data: *U.S. Geological Survey scientific investigations map* 3012.
- Stein, S., Cloetingh, S.A., Sleep, N.H., and Wortel, R., 1989, Passive margin earthquakes, stresses and rheology, *in* *Earthquakes at north-Atlantic passive margins—neotectonics and postglacial rebound*, v. 266: Dordrecht, Springer Netherlands, p. 231–259, doi:10.1007/978-94-009-2311-9_14.
- Stein, S., Sleep, N.H., Geller, R.J., Wang, S., and Kroeger, G.C., 1979, Earthquakes along the passive margin of eastern Canada: *Geophysical Research Letters*, v. 6, no. 7, p. 537–540, doi:10.1029/GL006i007p00537.
- Stewart, I.S., Sauber, J., and Rose, J., 2000, Glacio-seismotectonics—ice sheets, crustal deformation, and seismicity: *Quaternary Science Reviews*, v. 19, nos. 14–15, p. 1367–1389, doi: 10.1016/S0277-3791(00)00094-9.
- University of Koeln, 2022, This feature layers shows the global extent of ice sheets at the last glacial maximum (LGM) approximately 18,000 years before present, www.uni-koeln.de/ (assessed August 2023).
- Underground Injection Control National Technical Workgroup (2015), *Minimizing and Managing Potential Impacts of Injection-Induced Seismicity from Class II Disposal Wells: Practical Approaches*: February 2015, U.S. Environmental Protection Agency, Washington, D.C.

- U.S. Environmental Protection Agency, 2023a, Facility Level Information on Greenhouse gases Tool (FLIGHT) database, <https://ghgdata.epa.gov/ghgp/main.do#/facility> (accessed August 2023).
- U.S. Environmental Protection Agency, 2023b, Subpart RR, geologic sequestration of carbon dioxide, www.epa.gov/ghgreporting/subpart-rr-geologic-sequestration-carbon-dioxide (accessed August 2023).
- U.S. Geological Survey, 2021a, Earthquake hazards program and catalog, <https://earthquake.usgs.gov/earthquakes/search/> (accessed August 2023).
- U.S. Geological Survey, 2021b, Earthquake intensity scale, modified Mercalli intensity (MMI) scale, www.usgs.gov/media/images/earthquake-intensity-scale (accessed August 2023).
- U.S. Geological Survey, 2023, U.S. quaternary faults: Golden, Colorado, U.S. Geological Society Geologic Hazards Science Center, <https://usgs.maps.arcgis.com/apps/webappviewer/index.html?id=5a6038b3a1684561a9b0aadf88412fcf> (accessed August 2023).
- Villarrasa, V., and Carrera, J., 2015, Geologic carbon storage is unlikely to trigger large earthquakes and reactivate faults through which CO₂ could leak, *Proceedings of the National Academy of Sciences of the United States of America* (PNAS): v. 112, no. 19, p. 5913–5943,
- Walker, J.D., and Geissman, J.W., compilers, 2022, *Geologic time scale v. 6.0*: Geological Society of America, <https://doi.org/10.1130/2022.CTS006C>.
- Walsh, F.R., Zoback, M.D., Lele, S.P., Pais, D., Weingarten, M., and Tyrell, T., 2018, FSP 2.0—a program for probabilistic estimation of fault slip potential resulting from fluid injection: User guide from the Stanford Center for Induced and Triggered Seismicity, SCITS.Stanford.edu/software (accessed August 2023).
- Weides, S., Moeck, I., Majorowicz, J., and Grobe, M., 2014, The Cambrian Basal Sandstone Unit in central Alberta – an investigation of temperature distribution, petrography and hydraulic and geomechanical properties of a deep saline aquifer: *Canadian Journal of Earth Sciences*, July 2014, DOI: 10.1139/cjes-2014-0011.
- Wheeler, J.O., Hoffman, P.F., Card, K.D., Davidson, A., Sanford, B.V., Okulitch, A.V., and Roest, W.R., compilers, 1997, *Geological map of Canada*: Geological Survey of Canada, map D1860A.
- Whitmeyer, S.J., and Karlstrom, K.E., 2007, Tectonic model for Proterozoic growth of North America: *Geosphere*, August 2007, v. 3. no. 4., p. 220–259.
- Wyoming Department of Environmental Quality, 2023, Class VI permit applications, <https://deq.wyoming.gov/water-quality/groundwater/uic/class-vi/> (accessed August 2023).

- Wyoming State Geological Survey, 2022, Precambrian basement map of Wyoming—structural configuration: Wyoming State Geological Survey Open File Report 2022-5, 8 p., 1 pl., scale 1:500,000.
- Yukon Geological Survey – Government of Yukon, 2020, Geological terranes ArcGIS feature class downloadable dataset (GeoYukon Web Service), Website: <https://yukon.maps.arcgis.com/home/item.html?id=4d2a6fa758284818be7b3eb2017260a6> (accessed August 2023), Citation Reference: 723f6998-058e-11dc-8314-0800200c9a66.
- Zoback, M.L., 1992, First- and second-order patterns of stress in the lithosphere—the World Stress Map Project: *Journal of Geophysical Research*, v. 97 no. B8, p. 11703–11728, doi:10.1029/92JB00132.
- Zoback, M.D., 2010, *Reservoir geomechanics*: New York, New York, Cambridge University Press, doi:10.1017/CBO9780511586477.
- Zoback, M.D., 2012, Managing the seismic risk posted by wastewater disposal, *Earth* 57, no. 4, 38.
- Zoback, M.D., and Gorelick, S.M., 2012, Earthquake triggering and large-scale geologic storage of carbon dioxide, *Proceedings of the National Academy of Sciences of the United States of America (PNAS)*: v. 109, no. 26, <https://doi.org/10.1073/pnas.1202473109>.
- Zoback, M.L., and Zoback, M.D., 1980, State of stress in the conterminous United States: *Journal of Geophysical Research*, v. 85, no. B11, p. 6113–6156, doi: JB085iB11p06113.
- Zoback, M.L., and Zoback, M.D., 1989, Tectonic stress field of the continental United States, chapter 24, *in* Pakiser, L.C., and Mooney, W.D., eds., *Geophysical framework of the continental United States*: Boulder, Colorado, Geological Society of America Memoir 172, p. 523–540, doi: 10.1130/MEM172-p523.

APPENDIX A

PCOR REGION INDUSTRY CARBON CAPTURE AND STORAGE PROJECTS

PCOR REGION INDUSTRY CARBON CAPTURE AND STORAGE PROJECTS

The Plains CO₂ Reduction (PCOR) region industry carbon capture and storage (CCS) projects have been compiled and are captured in Table A-1. Information includes stress focus area, project status, location, facility type (source, sink, or combination source and sink), primary industry, CO₂ target type, and facility capacity, if known.

Table A-1. PCOR Region Industry CCS Projects, listed alphabetically

Facility Name	Stress Study Area	Status	Country	State/ Province	Facility Type	Industry	CO ₂ Target	Facility Capacity, MTPA
Aberdeen Biorefinery CCS		Advanced development	USA	SD	Source	Ethanol production	Saline	0.143
ACTL with Nutrien CO ₂ Stream	Alberta South Central	Operational	Canada	AB	Source	Fertilizer production	Enhanced oil recovery (EOR)	0.3
ACTL with NW Redwater Sturgeon Refinery CO ₂	Alberta South Central	Operational	Canada	AB	Source	Oil and gas processing	EOR	1.6
ADM CCS		Advanced development	USA	NE	Source	Ethanol production	Saline	
ADM CCS2		Advanced development	USA	IL	Sink	Ethanol production	Saline	1.2
ADM Corn Processing		Advanced development	USA	IA	Source	Ethanol production	Saline	
ADM Corn Processing		Advanced development	USA	IL	Source	Ethanol production	Saline	
Alberta Carbon Grid	Alberta South Central	Early development	Canada	AB	Sink	Oil and gas processing	Saline	
Aquistore CCS	Williston Basin	Operational	Canada	SK	Sink	Power generation	Saline	1
Athabasca Banks	Alberta Central	Early development	Canada	AB	Sink	Oil and gas processing	Saline	
Atkinson Biorefinery CCS		Advanced development	USA	IA	Source	Ethanol production	Saline	0.157
Atlas CCS	Alberta South Central	Early development	Canada	AB	Sink	Oil and gas processing	Saline	

Continued . . .

Table A-1. PCOR Region Industry CCS Projects, listed alphabetically (continued)

Facility Name	Stress Study Area	Status	Country	State/ Province	Facility Type	Industry	CO ₂ Target	Facility Capacity, MTPA
Battle River	Alberta South Central	Early development	Canada	AB	Sink	Oil and gas processing	Saline	
Bear Creek Gas-Processing Plant	Williston Basin	Early Development	USA	ND	Source	Oil and gas processing	Saline	0.02
Beaver Creek EOR	Wind River	Operational	USA	WY	Sink	Oil and gas processing	EOR	0.76
Bell Creek Pilot CCS	Powder River	Operational	USA	MT	Sink	Oil and gas processing	EOR	2.6
Big Sand Draw EOR	Wind River	Operational	USA	WY	Sink	Oil and gas processing	EOR	1.51
Big River Galva Biorefinery CCS		Advanced development	USA	IL	Source	Ethanol production	Saline	0.109
Big River United Energy		Advanced Development	USA	IA	Source	Ethanol production	Saline	
Big River W. Burlington CCS		Advanced development	USA	IA	Source	Ethanol production	Saline	
Blue Flint Ethanol and CCS	Williston Basin	Advanced development	USA	ND	Source and sink	Ethanol production	Saline	0.2
Boundary Dam Coal Power Plant	Williston Basin	Operational	Canada	SK	Source	Power Generation	Saline	1
Bow River	Alberta South Central	Early development	Canada	AB	Sink	Oil and gas processing	Saline	
Brazeau	Alberta South Central	Early development	Canada	AB	Sink	Oil and gas processing	Saline	
Brine Extraction Storage Test (BEST)	Williston Basin	Completed	USA	ND	Sink	CCS technology research and development (R&D)	Saline	0
Cargill Ft. Dodge		Advanced development	USA	IA	Source	Ethanol production	Saline	
Caroline CCS Power Complex	Alberta South Central	Early development	Canada	AB	Sink	Power generation	Depleted oil and gas zone	3
Casselton Biorefinery CCS		Advanced development	USA	ND	Source	Ethanol production	Saline	0.501

Continued . . .

Table A-1. PCOR Region Industry CCS Projects, listed alphabetically (continued)

Facility Name	Stress Study Area	Status	Country	State/ Province	Facility Type	Industry	CO ₂ Target	Facility Capacity, MTPA
Cedar Creek Anticline EOR		Early development	USA	MT	Sink	Oil and gas processing	EOR	7
Central Alberta	Alberta South Central	Early development	Canada	AB	Sink	Oil and gas processing	Saline	
Central City Biorefinery CCS		Advanced development	USA	NE	Source	Ethanol production	Saline	0.332
Cerilon Gas-to-Liquids Plant	Williston Basin	Early development	USA	ND	Source	Oil and gas processing	Saline	2
Clear Horizon	Alberta South	Early development	Canada	AB	Sink	Oil and gas processing	Saline	
CMC Research Institute (CMCRI)	Alberta South Central	Completed	Canada	AB	Sink	CCS technology R&D	Post-combustion	0
Coal Creek Station	Williston Basin	Early development	USA	ND	Source and sink	Power generation	Saline	10
Cutbank Field CO ₂ Field Laboratory	Alberta South	Advanced development	USA	MT	Sink	CCS technology R&D	Saline	0
Dave Johnston Plant CCS	Powder River	Early development	USA	WY	Sink	Power generation	EOR	0
Deep Lignite Seam CCS Field Test	Williston Basin	Completed	USA	ND	Sink	CCS technology R&D	Coal	0.002
Derricks Lake Gas Processing Plant	Williston Basin	Early development	USA	ND	Source	Oil and gas processing	Saline	0.05
Dry Fork CCS	Powder River	Early development	USA	WY	Source and sink	Power generation	Saline	3.3
Elkhorn Valley Ethanol CCS		Advanced development	USA	NE	Source	Ethanol production	Saline	0.152
Enchant EOR	Alberta South	Operational	Canada	AB	Sink	Oil and gas processing	EOR	0.012
EOR Fields for ACTL	Alberta South Central	Operational	Canada	AB	Sink	Oil and gas processing	EOR	
Flint Hills Shell Rock		Advanced development	USA	IA	Source	Ethanol production	Saline	

Continued . . .

Table A-1. PCOR Region Industry CCS Projects, listed alphabetically (continued)

Facility Name	Stress Study Area	Status	Country	State/ Province	Facility Type	Industry	CO ₂ Target	Facility Capacity, MTPA
Fort Nelson Feasibility Project		Completed	Canada	BC	Sink	CCS technology R&D	Saline	0
Garden Creek Gas Processing Plant	Williston Basin	Early development	USA	ND	Source	Oil and gas processing	Saline	0.071
Gerald Gentlemen Station CCS		Advanced development	USA	NE	Source and sink	Power generation	Saline	4.3
Goldfield Biorefinery CCS		Advanced development	USA	IA	Source	Ethanol production	Saline	0.215
Grand Junction Biorefinery CCS		Advanced development	USA	IA	Source	Ethanol production	Saline	0.343
Grand Prairie CCS	Alberta Central	Early development	Canada	AB	Sink	Oil and gas processing	Saline	
Grand Prairie Net Zero	Alberta Central	Early development	Canada	AB	Sink	Oil and gas processing	Saline	
Granite Falls Biorefinery CCS		Advanced development	USA	MN	Source	Ethanol production	Saline	0.18
Grasslands Gas-Processing Plant	Williston Basin	Early development	USA	ND	Source	Oil and gas processing	Saline	0.063
Great Plains Synfuel Plant	Williston Basin	Operational	USA	ND	Source	Synthetic natural gas	EOR	3
Greenview Region	Alberta Central	Early development	Canada	AB	Sink	Oil and gas processing	Saline	
Grieve EOR	Wind River	Operational	USA	WY	Sink	Oil and gas processing	EOR	0.19
Heron Lake Biorefinery CCS		Advanced development	USA	MN	Source	Ethanol production	Saline	0.186
Horizon Oil Sands CCS		Operational	Canada	AB	Source and sink	Oil and gas processing	Saline	0.438
Huron Biorefinery CCS		Advanced development	USA	SD	Source	Ethanol production	Saline	0.086
Husky Energy Lashburn and Tangleflags CCS		Operational	Canada	SK	Sink	Ethanol production	EOR	0.091

Continued . . .

Table A-1. PCOR Region Industry CCS Projects, listed alphabetically (continued)

Facility Name	Stress Study Area	Status	Country	State/ Province	Facility Type	Industry	CO ₂ Target	Facility Capacity, MTPA
Illinois Clean Fuels Project		Early development	USA	IL	Sink	Fuel production	Saline	8.125
Integrated Midcontinent Stacked CCS Hub		Advanced development	USA	NE	Sink	Ethanol production	Saline	1.7
Kevin Dome CCS	Alberta South	Completed	USA	MT	Sink	CCS technology R&D	Saline	0
Lamberton Biorefinery CCS		Advanced development	USA	MN	Source	Ethanol production	Saline	0.157
Lawler Biorefinery CCS		Advanced development	USA	IA	Source	Ethanol production	Saline	0.572
LINC Energy EOR	Powder River	Operational	USA	WY	Sink	Oil and gas processing	Saline	0.223
Lloydminster EOR		Operational	Canada	SK	Sink	Ethanol production	EOR	0.091
Lonesome Creek Gas-Processing Plant	Williston Basin	Early development	USA	ND	Source	Oil and gas processing	Saline	0.041
Lost Cabin Gas Plant		Operational	USA	WY	Source	Oil and gas processing	EOR	0.57
Lost Soldier (Baroil) EOR	Greater Green River	Operational	USA	WY	Sink	Oil and gas processing	EOR	1.99
Marcus Biorefinery CCS		Advanced development	USA	IA	Source	Ethanol production	Saline	0.458
Maskwa	Alberta Central	Early development	Canada	AB	Sink	Oil and gas processing	Saline	
Mason City Biorefinery CCS		Advanced development	USA	IA	Source	Ethanol production	Saline	0.343
Meadowbrook	Alberta South Central	Early development	Canada	AB	Sink	Oil and gas processing	Saline	
Merrill Biorefinery CCS		Advanced development	USA	IA	Source	Ethanol production	Saline	0.157
Mina Biorefinery CCS		Advanced development	USA	MN	Source	Ethanol production	Saline	0.4

Continued . . .

Table A-1. PCOR Region Industry CCS Projects, listed alphabetically (continued)

Facility Name	Stress Study Area	Status	Country	State/ Province	Facility Type	Industry	CO ₂ Target	Facility Capacity, MTPA
Nauticol Energy Blue Methanol	Alberta Central	Early development	Canada	AB	Source and sink	Methanol production	Saline	1
Nevada Biorefinery CCS		Advanced development	USA	IA	Source	Ethanol production	Saline	0.257
North Drumheller	Alberta South Central	Early development	Canada	AB	Sink	Oil and gas processing	Saline	
NW McGregor Field Validation Test	Williston Basin	Completed	USA	ND	Sink	CCS technology R&D	EOR	0
Oil Sands Pathways	Alberta South Central	Early development	Canada	AB	Sink	Oil and gas processing	Saline	
Onida Biorefinery CCS		Advanced development	USA	SD	Source	Ethanol production	Saline	0.229
Opal Carbon	Alberta Central	Early development	Canada	AB	Sink	Oil and gas processing	Saline	
Open Access Wabamun	Alberta South Central	Early development	Canada	AB	Sink	Oil and gas processing	Saline	
Origins	Alberta South Central	Early development	Canada	AB	Sink	Oil and gas processing	Saline	
Otter Tail Biorefinery CCS		Advanced development	USA	MN	Source	Ethanol Production	Saline	0.172
Painter Reservoir CCS1	Greater Green River	Advanced development	USA	WY	Source and sink	Oil and gas processing	Saline	0.375
Patrick Draw (Monell) EOR	Greater Green River	Operational	USA	WY	Sink	Oil and gas processing	EOR	3.79
Pembina Cardium CO ₂ Monitoring Pilot	Alberta South Central	Completed	Canada	AB	Sink	Oil and gas processing	EOR	0.023
Pikes Peak South		Completed	Canada	SK	Sink	CCS technology R&D	Post-combustion	
Pincher Creek	Alberta South	Early development	Canada	AB	Sink	Oil and gas processing	Saline	
Plainview Biorefinery CCS		Advanced development	USA	NE	Source	Ethanol production	Saline	0.315

Continued . . .

Table A-1. PCOR Region Industry CCS Projects, listed alphabetically (continued)

Facility Name	Stress Study Area	Status	Country	State/ Province	Facility Type	Industry	CO ₂ Target	Facility Capacity, MTPA
Pleasant Prairie Power Plant Field Pilot		Completed	USA	WI	Source and sink	Power generation	Post-combustion	0
Poet Biorefining Aston		Advanced development	USA	IA	Source	Ethanol production	Saline	
Polaris CCS	Alberta South Central	Early development	Canada	AB	Source	Hydrogen production	Saline	0.75
Prairie Rose CCS	Williston Basin	Early development	USA	ND	Sink	Oil and gas processing	Saline	6.12
Project Tundra	Williston Basin	Advanced development	USA	ND	Source and sink	Power generation	Saline	3.6
Quad City Corn Processing		Advanced development	USA	IA	Source	Ethanol production	Saline	
Quest CCS	Alberta South Central	Operational	Canada	AB	Sink	Hydrogen production	Saline	1.1
Ram River	Alberta South Central	Early development	Canada	AB	Sink	Oil and gas processing	Saline	
Red Trail Energy		Operational	USA	ND	Source and sink	Ethanol production	Saline	0.18
Redfield Biorefinery CCS		Advanced development	USA	SD	Source	Ethanol production	Saline	0.172
Riley Ridge Processing Plant		Operational	USA	WY	Source	Oil and gas processing	Depleted O&G Zone	2
Rocky Mountain	Alberta Central	Early development	Canada	AB	Sink	Oil and gas processing	Saline	
Rolling Hills	Alberta South Central	Early development	Canada	AB	Sink	Oil and gas processing	Saline	
Roughrider Carbon Storage Hub	Williston Basin	Early development	USA	ND	Sink	Oil and gas processing	Saline	2.331
Salt Creek Oil Field EOR	Powder River	Operational	USA	WY	Sink	Oil and gas processing	EOR	13.2
Saskatchewan NET Power Plant	Williston Basin	Early development	Canada	SK	Source and sink	Power Generation	Saline	0

Continued . . .

Table A-1. PCOR Region Industry CCS Projects, listed alphabetically (continued)

Facility Name	Stress Study Area	Status	Country	State/ Province	Facility Type	Industry	CO ₂ Target	Facility Capacity, MTPA
Shand CCS Test Facility	Williston Basin	Operational	Canada	SK	Source and sink	Power generation	Post-combustion	0
Shenandoah Biorefinery CCS		Advanced development	USA	IA	Source	Ethanol production	Saline	0.235
Shute Creek Gas Processing / La Barge Field	Greater Green River	Operational	USA	WY	Source and sink	Oil and gas processing	EOR	7.5
Sioux Center Biorefinery CCS		Advanced development	USA	IA	Source	Ethanol production	Saline	0.186
Siouxland Ethanol		Advanced development	USA	NE	Source	Ethanol production	Saline	
Stateline Gas Processing Plant	Williston Basin	Early development	USA	ND	Source	Oil and gas processing	Saline	0.085
Steamboat Rock Biorefinery CCS		Advanced development	USA	IA	Source	Ethanol production	Saline	0.229
Summit Carbon Solutions	Williston Basin	Advanced development	USA	ND	Sink	Ethanol production	Saline	12
Superior Biorefinery CCS		Advanced development	USA	IA	Source	Ethanol Production	Saline	0.172
Sweetwater CO ₂ Storage Hub	Greater Green River	Advanced development	USA	WY	Sink	Oil and gas processing	Saline	5
Tallgrass CCS		Advanced development	USA	WY	Sink	Ethanol production	Saline	0.23
Terrestrial Field Validation Test		Completed	USA	SD	Sink	CCS technology R&D	Soil	0
Tourmaline Clearwater	Alberta Central	Early development	Canada	AB	Sink	Oil and gas processing	Saline	
Valero Albert City Plant		Advanced development	USA	IA	Source	Ethanol production	Saline	
Valero Ft. Dodge		Advanced development	USA	IA	Source	Ethanol production	Saline	
Valero Hartley Plant		Advanced development	USA	IA	Source	Ethanol production	Saline	

Continued . . .

Table A-1. PCOR Region Industry CCS Projects, listed alphabetically (continued)

Facility Name	Stress Study Area	Status	Country	State/ Province	Facility Type	Industry	CO ₂ Target	Facility Capacity, MTPA
Valero Lakota Ethanol CCS		Advanced development	USA	IA	Source	Ethanol production	Saline	0.35
Valero Renewable Fuels		Advanced development	USA	SD	Source	Ethanol production	Saline	
Valero Renewable Fuels		Advanced development	USA	IA	Source	Ethanol production	Saline	
Valero Renewable Fuels Albion Plant		Advanced development	USA	NE	Source	Ethanol production	Saline	
Valero Welcome Plant CCS		Advanced development	USA	MN	Source	Ethanol production	Saline	0.343
VeloxoTherm Capture Process Test		Advanced development	Canada	SK	Sink	Oil and gas processing	EOR	0.011
Watertown Biorefinery CCS		Advanced development	USA	SD	Source	Ethanol production	Saline	0.372
Wentworth Biorefinery CCS		Advanced development	USA	SD	Source	Ethanol production	Saline	0.257
Wertz (Baroil) EOR	Greater Green River	Operational	USA	WY	Sink	Oil and gas processing	EOR	1.51
Weyburn–Midale Field EOR	Williston Basin	Operational	USA	SK	Sink	Power generation	EOR	2.8
Wood River Biorefinery CCS		Advanced development	USA	NE	Source	Ethanol production	Saline	0.346
World Midstream	Alberta South Central	Early development	Canada	AB	Sink	Oil and gas processing	Saline	
WY Integrated Test Center	Powder River	Completed	USA	WY	Sink	CCS technology R&D	Post-combustion	0
York Biorefinery CCS		Advanced development	USA	NE	Source	Ethanol production	Saline	0.143
Zama Field Validation Test		Completed	Canada	AB	Sink	CCS technology R&D	Saline	0.005